

Explicit partitioning strategies for the interaction between a fluid and a multilayered poroelastic structure: an operator-splitting approach

M. Bukač^{a,*}, P. Zunino^b, I. Yotov^a

^a*Department of Mathematics, University of Pittsburgh, Pittsburgh, PA 15260, USA*

^b*Department of Mechanical Engineering & Materials Science, University of Pittsburgh, Pittsburgh, PA 15261, USA*

Abstract

We study the interaction between an incompressible, viscous, Newtonian fluid and a multilayered structure, which consists of a thin elastic layer and a thick poroelastic material. The thin layer is modeled using the linearly elastic Koiter membrane model, while the thick poroelastic layer is modeled as a Biot system. The objective of this work is to investigate how the poroelastic phenomena affect the characteristic features of blood flow in arteries, such as propagation of pressure waves. We develop a loosely coupled fluid-structure interaction finite element solver based on the Lie operator splitting scheme. We prove a conditional stability of the scheme and derive error estimates. Theoretical results are supported with numerical examples.

Keywords: Fluid-structure interaction, multilayered structure, poroelasticity, operator-splitting scheme

1. Introduction

We study the interaction between an incompressible viscous, Newtonian fluid and a multilayered poroelastic structure. The need of a multilayered description of the wall is suggested by results of *in vivo* measurements of arterial wall motion [16, 17], which indicate that the inner parts of the vessel wall (intima-media complex) exhibit a larger longitudinal displacement than the outer part of the vessel wall (adventitia), introducing the presence of substantial shear strain and shear stress within the wall. Keeping in mind the general and ambitious aim of improving the understanding of arterial mechanical properties, we also introduce poroelastic effects in FSI simulations. The material properties of arteries have been widely studied [1, 7, 23, 30, 51, 44, 12]. Pseudo-elastic [52, 23], viscoelastic [1, 12, 7] and nonlinear material models represent well known examples. To our knowledge, only a few of them have been deeply analyzed in the time dependent domain, namely when coupled with the pulsation induced by heartbeat. These considerations also apply to poroelasticity, which is addressed here. Poroelasticity becomes particularly interesting when looking at the coupling of flow with mass transport. This is a significant potential application of our model, since mass transport provides nourishment, remove wastes, affects pathologies and allows to deliver drugs to arteries [42]. Poroelastic phenomena are interesting in different applications where soft biological tissues are involved. We mention for example cerebro-spinal flow [34], which also involves FSI, the study of hysteresis effects observed in the myocardial tissue [28, 27], as well as the modeling of lungs

*Corresponding author (+1 412 624 0177)

Email addresses: martinab@pitt.edu (M. Bukač), paz13@pitt.edu (P. Zunino), yotov@math.pitt.edu (I. Yotov)

as a continuum material [43]. Besides biological applications, this model can also be used in numerous other applications: geomechanics, ground-surface water flow, reservoir compaction and surface subsidence, seabed-wave interaction problem, etc.

While there exist many complex and detailed models for multilayered structures in different applications, the interaction between the fluid and a multilayered structure remains an area of active research. To our knowledge, the only theoretical result was presented in [38], where the authors proved existence of a solution to a fluid-two-layered-structure interaction problem, in which one layer is modeled as a thin (visco)elastic shell and the other layer as a linearly elastic structure. Several studies focused on numerical simulations. An interaction between the fluid and a two-layer anisotropic elastic structure was used in [47] to model the human right and left ventricles. Slightly different models were used in [31] to model fully coupled fluid-structure-soil interaction for cylindrical liquid-contained structures subjected to horizontal ground excitation. The work in [8] focused on studying velocity of acoustic waves excited in multilayered structures contacting with fluids. A fluid-multilayered structure interaction problem coupled with transport was studied in [14], with the purpose of investigating low-density lipoprotein transport within a multilayered arterial wall. However, none of these studies present a numerical scheme supported with numerical analysis.

In this work, we propose a model that captures interaction between a fluid and a multilayered structure, which consists of a thin elastic layer and a thick poroelastic layer. We assume that the thin layer represents a homogenized combination of the endothelium, tunica intima, and internal elastic lamina, and that the thick layer represents tunica media. The thin elastic layer is modeled using the linearly elastic Koiter membrane model, while the poroelastic medium is modeled using the Biot equations. The Biot system consists of an elastic skeleton and connecting pores filled with fluid. We assume that the elastic skeleton is homogeneous and isotropic, while the fluid in the pores is modeled using the Darcy equations. The Biot system is coupled to the fluid and the elastic membrane via the kinematic (no-slip and conservation of mass) and dynamic (conservation of momentum) boundary conditions. More precisely, we assume that the elastic membrane can not store fluid, but allows the flow through it in the normal direction. In the tangential direction, we prescribe the no-slip boundary condition. This assumption is reasonable in blood flow modeling, since it has been shown in [33] that predominant direction of intimal transport is the radial direction normal to the endothelial surface, for all ranges of relative intimal thickness.

The coupling between a fluid and a single layer poroelastic structure has been previously studied in [5, 46, 39, 49]. In particular, the work in [5] is based on the modeling and a numerical solution of the interaction between an incompressible, Newtonian fluid, described using the Navier Stokes equations, and a poroelastic structure modeled as a Biot system. The problem was solved using both a monolithic and a partitioned approach. The partitioned approach was based on the domain decomposition procedure, with the purpose of solving the Navier-Stokes equations separately from the Biot system. However, sub-iterations were needed between the two problems due to the instabilities associated with the “added mass effect”. Namely, in fluid-structure interaction problems, the “classical” loosely-coupled methods have been shown to be unconditionally unstable if the density of the structure is comparable to the density of the fluid [13], which is the case in hemodynamics applications. To resolve this problem, as an alternative to sub-iterations, several different splitting strategies have been proposed [9, 3, 21, 20, 41, 26]. In particular, the kinematically coupled β -scheme proposed in [9] is based on embedding the no-slip kinematic condition into the thin structure equations. Using the Lie operator splitting approach [25], the structure equations is split so that the structure inertia is treated together with the fluid as a Robin boundary condition, while the structure elastodynamics is treated separately. This method has been shown to be unconditionally stable, and therefore independent of

the fluid and structure densities [11].

Motivated by the kinematically coupled β -scheme, in this manuscript we propose a loosely-coupled finite element scheme based on the Lie operator splitting method. We use the operator splitting to separate the fluid problem (Navier-Stokes equations) from the Biot problem. The no-slip kinematic condition in the tangential direction is embedded into the membrane equations. Operator splitting is preformed so that the tangential component of the structure inertia is treated together with the fluid as a Robin boundary condition. Assuming the primal formulation for the Darcy equations, the continuity of the normal flux and the balance of normal components of stress between the Navier Stokes fluid and the fluid in the pores is treated in a similar way as in the partitioned algorithms for the Stokes-Darcy coupled problems [32, 45]. The membrane elastodynamics is embedded into the Biot system as a Robin boundary condition. In the contrast with domain decomposition methods proposed in [5], the operator splitting approach does not require sub-iterations between the fluid and the Biot problem, making our scheme more computationally efficient.

We prove a conditional stability of the proposed scheme, where the stability condition does not depend on the fluid and structure densities, but it is related to the decoupling of the Stokes-Darcy interaction problem. Furthermore, we derive the error estimates and prove the convergence of the scheme. The rates of convergence and the stability condition were validated numerically on a classical benchmark problem typically used to test the results of fluid-structure interaction algorithms. In the second numerical example, we investigate the effects of porosity to the structure displacement. Namely, we distinguish a high storativity and a high permeability case in the Darcy equations, and compare them to the results obtained using a purely elastic model. Depending on the regime, we observe a significantly different behavior of the coupled system.

The rest of the paper is organized as follows. In the following section we introduce the model equations and the coupling conditions. In Section 3 we propose a loosely-coupled scheme based on the operator-splitting approach. The weak formulation and stability of the scheme is presented in Section 4. In Section 5 we derive the error analysis of the scheme. Finally, the numerical results are presented in Section 6.

2. Description of the problem

Consider a bounded, deformable, two-dimensional domain $\Omega(t) = \Omega^f(t) \cup \Omega^p(t)$ of reference length L , which consists of two regions, $\Omega^f(t)$ and $\Omega^p(t)$, see Figure 1. We assume that the region $\Omega^f(t)$ has reference width $2R$, and is filled by an incompressible, viscous fluid. We denote the width of the second region $\Omega^p(t)$ by r_p , and assume that $\Omega^p(t)$ is occupied by a fully-saturated poroelastic matrix. The two regions are separated by a common interface $\Gamma(t)$. We assume that $\Gamma(t)$ has a mass,

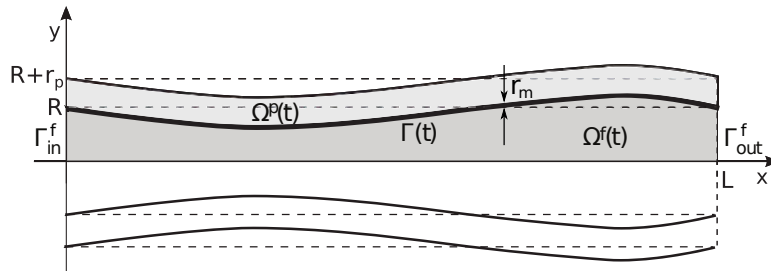


Figure 1: Deformed domains $\Omega^f(t) \cup \Omega^p(t)$.

and represent a thin, elastic structure. Namely, we assume that the thickness of the interface r_m is

“small” with respect to the radius of the fluid domain, $r_m \ll R$. Thus, the volume of the interface is negligible, so it acts as a membrane that can not store fluid, but allows the flow through it in the normal direction.

We are interested in simulating a pressure-driven flow through the deformable channel with a two-way coupling between the fluid, thin elastic interface, and poroelastic structure. Without loss of generality, we restrict the model to a two-dimensional (2D) geometrical model representing a deformable channel. We consider only the upper half of the fluid domain supplemented by a symmetry condition at the axis of symmetry. Thus, the reference fluid and structure domains in our problem (showed by dashed lines in Figure 1) are given, respectively, by

$$\begin{aligned}\hat{\Omega}^f &:= \{(x, y) \mid 0 < x < L, 0 < y < R\}, \\ \hat{\Omega}^p &:= \{(x, y) \mid 0 < x < L, R < y < R + r_p\},\end{aligned}$$

and the reference lateral boundary by $\hat{\Gamma} = \{(x, R) \mid 0 < x < L\}$. The inlet and outlet fluid boundaries are defined, respectively, as $\Gamma_{in}^f = \{(0, y) \mid 0 < y < R\}$ and $\Gamma_{out}^f = \{(L, y) \mid 0 < y < R\}$.

We model the flow using the Navier-Stokes equations for a viscous, incompressible, Newtonian fluid:

$$\rho_f \left(\frac{\partial \mathbf{v}}{\partial t} + \mathbf{v} \cdot \nabla \mathbf{v} \right) = \nabla \cdot \boldsymbol{\sigma}^f + \mathbf{g} \quad \text{in } \Omega^f(t) \times (0, T), \quad (2.1)$$

$$\nabla \cdot \mathbf{v} = 0 \quad \text{in } \Omega^f(t) \times (0, T), \quad (2.2)$$

where $\mathbf{v} = (v_x, v_y)$ is the fluid velocity, $\boldsymbol{\sigma}^f = -p_f \mathbf{I} + 2\mu_f \mathbf{D}(\mathbf{v})$ is the fluid stress tensor, p_f is the fluid pressure, ρ_f is the fluid density, μ_f is the fluid viscosity and $\mathbf{D}(\mathbf{v}) = (\nabla \mathbf{v} + (\nabla \mathbf{v})^\tau)/2$ is the rate-of-strain tensor. Denote the inlet and outlet fluid boundaries by Γ_{in}^f and Γ_{out}^f , respectively. At the inlet and outlet boundary we prescribe the normal stress:

$$\boldsymbol{\sigma}^f \mathbf{n}_{in} = -p_{in}(t) \mathbf{n}_{in} \quad \text{on } \Gamma_{in}^f \times (0, T), \quad (2.3)$$

$$\boldsymbol{\sigma}^f \mathbf{n}_{out} = 0 \quad \text{on } \Gamma_{out}^f \times (0, T), \quad (2.4)$$

where $\mathbf{n}_{in}/\mathbf{n}_{out}$ are the outward normals to the inlet/outlet fluid boundaries, respectively. These boundary conditions are common in blood flow modeling [2, 37, 40] even though they are not physiologically optimal since the flow distribution and pressure field in the modeled domain are often unknown [50]. Along the middle line of the channel $\Gamma_0^f = \{(x, 0) \mid 0 < x < L\}$ we impose the symmetry conditions:

$$\frac{\partial v_x}{\partial y} = 0, \quad v_y = 0 \quad \text{on } \Gamma_0^f \times (0, T). \quad (2.5)$$

The lateral boundary represents a deformable, thin elastic wall, whose dynamics is modeled by the linearly elastic Koiter membrane model, given in the Lagrangian formulation by:

$$\rho_m r_m \frac{\partial^2 \hat{\eta}_x}{\partial t^2} - C_2 \frac{\partial \hat{\eta}_y}{\partial \hat{x}} - C_1 \frac{\partial^2 \hat{\eta}_x}{\partial \hat{x}^2} = \hat{f}_x \quad \text{on } \hat{\Gamma} \times (0, T), \quad (2.6)$$

$$\rho_m r_m \frac{\partial^2 \hat{\eta}_y}{\partial t^2} + C_0 \hat{\eta}_y + C_2 \frac{\partial \hat{\eta}_x}{\partial \hat{x}} = \hat{f}_y \quad \text{on } \hat{\Gamma} \times (0, T), \quad (2.7)$$

where $\hat{\boldsymbol{\eta}}(\hat{x}, t) = (\hat{\eta}_x(\hat{x}, t), \hat{\eta}_y(\hat{x}, t))$ denotes the axial and radial displacement, $\hat{\mathbf{f}} = (\hat{f}_x, \hat{f}_y)$ is a vector of surface density of the force applied to the membrane, ρ_m denotes the membrane density and

$$C_0 = \frac{r_m}{R^2} \left(\frac{2\mu_m \lambda_m}{\lambda_m + 2\mu_m} + 2\mu_m \right), \quad C_1 = r_m \left(\frac{2\mu_m \lambda_m}{\lambda_m + 2\mu_m} + 2\mu_m \right), \quad C_2 = \frac{r_m}{R} \frac{2\mu_m \lambda_m}{\lambda_m + 2\mu_m}. \quad (2.8)$$

The coefficients μ_m and λ_m are the Lamé coefficients for the membrane. Note that we can write the system (2.6)-(2.7) more compactly as

$$\rho_m r_m \frac{\partial^2 \hat{\boldsymbol{\eta}}}{\partial t^2} + \hat{\mathcal{L}} \hat{\boldsymbol{\eta}} = \hat{\mathbf{f}}, \quad \hat{\mathcal{L}} := \begin{pmatrix} -C_1 \partial_{\hat{x}\hat{x}} & -C_2 \partial_{\hat{x}} \\ C_2 \partial_{\hat{x}} & C_0 \end{pmatrix}. \quad (2.9)$$

The fluid domain is bounded by a deformable porous matrix consisting of a skeleton and connecting pores filled with fluid, whose dynamics is described by the Biot model, which in the primal, Eulerian formulation reads as follows:

$$\rho_p \frac{D^2 \mathbf{U}}{Dt^2} - \nabla \cdot \boldsymbol{\sigma}^p = \mathbf{h} \quad \text{in } \Omega^p(t) \times (0, T), \quad (2.10)$$

$$\frac{D}{Dt}(s_0 p_p + \alpha \nabla \cdot \mathbf{U}) - \nabla \cdot (\kappa \nabla p_p) = s \quad \text{in } \Omega^p(t) \times (0, T), \quad (2.11)$$

where $\frac{D}{Dt}$ denotes the classical concept of material derivative. The stress tensor of the poroelastic medium is given by $\boldsymbol{\sigma}^p = \boldsymbol{\sigma}^E - \alpha p_p \mathbf{I}$, where $\boldsymbol{\sigma}^E$ denotes the elasticity stress tensor. With the assumption that the displacement $\mathbf{U} = (U_x, U_y)$ of the skeleton is connected to stress tensor $\boldsymbol{\sigma}^E$ via the Saint-Venant Kirchhoff elastic model, we have $\boldsymbol{\sigma}^E(\mathbf{U}) = 2\mu_p \mathbf{D}(\mathbf{U}) + \lambda_p \text{tr}(\mathbf{D}(\mathbf{U})) \mathbf{I}$, where λ_p and μ_p denote the Lamé coefficients for the skeleton, and, with the hypothesis of “small” deformations, $\mathbf{D}(\mathbf{U}) = (\nabla \mathbf{U} + (\nabla \mathbf{U})^T)/2$.

System (2.10)-(2.11) consists of the momentum equation for the balance of total forces (2.10), and the storage equation (2.11) for the fluid mass conservation in the pores of the matrix, where p_p is the fluid pressure. The density of saturated porous medium is denoted by ρ_p , and κ denotes the uniformly positive definite hydraulic conductivity tensor. For simplicity of the presentation we assume that κ is a scalar function. The coefficient $c_0 > 0$ is the storage coefficient, and the Biot-Willis constant α is the pressure-storage coupling coefficient. The relative velocity of the fluid within the porous structure \mathbf{q} can be reconstructed via Darcy’s law

$$\mathbf{q} = -\kappa \nabla p_p \quad \text{in } \Omega^p(t) \times (0, T).$$

Denote the inlet and outlet poroelastic structure boundaries, respectively, by $\Gamma_{in}^p = \{(0, y) \mid R < y < R + r_p\}$ and $\Gamma_{out}^p = \{(L, y) \mid R < y < R + r_p\}$, and the reference exterior boundary by $\hat{\Gamma}_{ext}^p = \{(x, R + r_p) \mid 0 < x < L\}$. We assume that the poroelastic structure is fixed at the inlet and outlet boundaries:

$$\mathbf{U} = 0 \quad \text{on } \Gamma_{in}^p \cup \Gamma_{out}^p \times (0, T), \quad (2.12)$$

that the external structure boundary $\Gamma_{ext}^p(t)$ is exposed to external ambient pressure

$$\mathbf{n}_{ext} \cdot \boldsymbol{\sigma}^E \mathbf{n}_{ext} = -p_e \quad \text{on } \Gamma_{ext}^p(t) \times (0, T), \quad (2.13)$$

where \mathbf{n}_{ext} is the outward unit normal vector on $\Gamma_{ext}^p(t)$, and that the tangential displacement of the exterior boundary is zero:

$$U_x = 0 \quad \text{on } \Gamma_{ext}^p(t) \times (0, T). \quad (2.14)$$

On the fluid pressure in the porous medium, we impose drained boundary conditions [18]:

$$p_p = 0 \quad \text{on } \Gamma_{ext}^p(t) \cup \Gamma_{in}^p \cup \Gamma_{out}^p \times (0, T). \quad (2.15)$$

Initially, the fluid, elastic membrane and the poroelastic structure are assumed to be at rest, with zero displacement from the reference configuration

$$\mathbf{v} = 0, \quad \mathbf{U} = 0, \quad \frac{DU}{Dt} = 0, \quad \hat{\boldsymbol{\eta}} = 0, \quad \frac{\partial \hat{\boldsymbol{\eta}}}{\partial t} = 0, \quad \mathbf{q} = 0, \quad p_p = 0. \quad (2.16)$$

To deal with the motion of the fluid domain we adopt the Arbitrary Lagrangian-Eulerian (ALE) approach [29, 19, 40]. In the context of finite element method approximation of moving-boundary problems, ALE method deals efficiently with the deformation of the mesh, especially at the boundary and near the interface between the fluid and the structure, and with the issues related to the approximation of the time-derivatives $\partial \mathbf{v} / \partial t \approx (\mathbf{v}(t^{n+1}) - \mathbf{v}(t^n)) / \Delta t$ which, due to the fact that $\Omega^f(t)$ depends on time, is not well defined since the values $\mathbf{v}(t^{n+1})$ and $\mathbf{v}(t^n)$ correspond to the values of \mathbf{v} defined at two different domains. Following the ALE approach, we introduce two families of (arbitrary, invertible, smooth) mappings \mathcal{A}_t and \mathcal{S}_t , defined on reference domains $\hat{\Omega}^f$ and $\hat{\Omega}^p$, respectively, which track the domain in time:

$$\mathcal{A}_t : \hat{\Omega}^f \rightarrow \Omega^f(t) \subset \mathbb{R}^2, \quad \mathbf{x} = \mathcal{A}_t(\hat{\mathbf{x}}) \in \Omega^f(t), \quad \text{for } \hat{\mathbf{x}} \in \hat{\Omega}^f, \quad (2.17)$$

$$\mathcal{S}_t : \hat{\Omega}^p \rightarrow \Omega^p(t) \subset \mathbb{R}^2, \quad \mathbf{x} = \mathcal{S}_t(\hat{\mathbf{x}}) \in \Omega^p(t), \quad \text{for } \hat{\mathbf{x}} \in \hat{\Omega}^p. \quad (2.18)$$

Note that the fluid domain is determined by the displacement of the membrane $\hat{\boldsymbol{\eta}}$, while the porous medium domain is determined by its displacement $\hat{\mathbf{U}}$, where $\hat{\mathbf{U}}$ is the displacement of the porous medium evaluated at the reference configuration.. However, because of condition (2.22), we can define a homeomorphism over $\Omega^f(t) \cup \Omega^p(t)$ by setting mappings \mathcal{A}_t and \mathcal{S}_t equal on $\Gamma(t)$. For the structure, we adopt the material mapping

$$\mathcal{S}_t(\hat{\mathbf{x}}) = \hat{\mathbf{x}} + \hat{\mathbf{U}}(\hat{\mathbf{x}}, t), \quad \forall \hat{\mathbf{x}} \in \hat{\Omega}^p. \quad (2.19)$$

Since the mapping \mathcal{A}_t is arbitrary, with the only requirement that it matches \mathcal{S}_t on $\Gamma(t)$, we can define \mathcal{A}_t as

$$\mathcal{A}_t(\hat{\mathbf{x}}) = \hat{\mathbf{x}} + \text{Ext}(\hat{\boldsymbol{\eta}}(\hat{\mathbf{x}}, t)) = \hat{\mathbf{x}} + \text{Ext}(\hat{\mathbf{U}}(\hat{\mathbf{x}}, t)|_{\hat{\Gamma}}), \quad \forall \hat{\mathbf{x}} \in \hat{\Omega}^f. \quad (2.20)$$

2.1. The coupling conditions

In order to prescribe the coupling conditions on the physical fluid-structure interface $\Gamma(t)$, denote by $\boldsymbol{\eta} := \hat{\boldsymbol{\eta}} \circ (\mathcal{A}_t^{-1}|_{\Gamma(t)})$, where \mathcal{A}_t is defined in (2.17). While the lumen and the poroelastic medium contain fluid, we assume that the elastic membrane does not contain fluid, but allows the flow through it in the normal direction. This is a reasonable assumption because the elastic membrane represents tunica intima. It has been shown by experimental studies that the normal transport in tunica intima is significantly greater than tangential transport [33]. Denote by \mathbf{n} the outward normal to the fluid domain and by $\boldsymbol{\tau}$ the tangential unit vector. Thus, the fluid, elastic membrane and poroelastic structure are coupled via the following boundary conditions:

- Mass conservation: since the thin lamina allows the flow through it, the continuity of normal flux is

$$\mathbf{v} \cdot \mathbf{n} = \left(\alpha \frac{DU}{Dt} - \kappa \nabla p_p \right) \cdot \mathbf{n} \quad \text{on } \Gamma(t). \quad (2.21)$$

- Since we do not allow filtration in the tangential direction, we prescribe no-slip boundary conditions between the fluid in the lumen and the elastic membrane, and between the elastic membrane and poroelastic medium:

$$\mathbf{v} \cdot \boldsymbol{\tau} = \frac{\partial \boldsymbol{\eta}}{\partial t} \cdot \boldsymbol{\tau}, \quad \boldsymbol{\eta} = \mathbf{U} \quad \text{on } \Gamma(t). \quad (2.22)$$

- Balance of normal components of the stress in the fluid phase:

$$\mathbf{n} \cdot \boldsymbol{\sigma}^f \mathbf{n} = -p_p \quad \text{on } \Gamma(t). \quad (2.23)$$

- The conservation of momentum describes balance of contact forces. Precisely, it says that the sum of contact forces at the fluid-porous medium interface is equal to zero:

$$\alpha \mathbf{n} \cdot \boldsymbol{\sigma}^f \mathbf{n} - \mathbf{n} \cdot \boldsymbol{\sigma}^p \mathbf{n} + J^{-1} \mathbf{f} \cdot \mathbf{n} = 0 \quad \text{on } \Gamma(t), \quad (2.24)$$

$$\boldsymbol{\tau} \cdot \boldsymbol{\sigma}^f \mathbf{n} - \boldsymbol{\tau} \cdot \boldsymbol{\sigma}^p \mathbf{n} + J^{-1} \mathbf{f} \cdot \boldsymbol{\tau} = 0 \quad \text{on } \Gamma(t), \quad (2.25)$$

where $\mathbf{f} := \hat{\mathbf{f}} \circ (\mathcal{A}_t^{-1}|_{\Gamma(t)})$, and J denotes the Jacobian of the transformation from $\Gamma(t)$ to $\hat{\Gamma}$ given by

$$J = \sqrt{\left(1 + \frac{\partial \eta_x}{\partial x}\right)^2 + \left(\frac{\partial \eta_y}{\partial x}\right)^2}. \quad (2.26)$$

2.2. Weak formulation of the monolithic problem

For a domain Ω , we denote by $\|\cdot\|_{H^k(\Omega)}$ the norm in the Sobolev space $H^k(\Omega)$. The norm in $L^2(\Omega)$ is denoted by $\|\cdot\|_{L^2(\Omega)}$, and the $L^2(\Omega)$ -inner product by $(\cdot, \cdot)_\Omega$. To find a weak form of the Navier-Stokes equation, introduce the following test function spaces:

$$V^f(t) = \{\boldsymbol{\varphi} : \Omega^f(t) \rightarrow \mathbb{R}^2 \mid \boldsymbol{\varphi} = \hat{\boldsymbol{\varphi}} \circ (\mathcal{A}_t)^{-1}, \hat{\boldsymbol{\varphi}} \in (H^1(\hat{\Omega}^f))^2, \varphi_y = 0 \text{ on } \Gamma_0^f\}, \quad (2.27)$$

$$Q^f(t) = \{\psi : \Omega^f(t) \rightarrow \mathbb{R} \mid \psi = \hat{\psi} \circ (\mathcal{A}_t)^{-1}, \hat{\psi} \in L^2(\hat{\Omega}^f)\}, \quad (2.28)$$

for all $t \in [0, T]$. The variational formulation of the Navier-Stokes equations now reads: given $t \in (0, T)$ find $(\mathbf{v}, p_f) \in V^f(t) \times Q^f(t)$ such that for all $(\boldsymbol{\varphi}^f, \psi^f) \in V^f(t) \times Q^f(t)$

$$\begin{aligned} & \rho_f \int_{\Omega^f(t)} \frac{\partial \mathbf{v}}{\partial t} \cdot \boldsymbol{\varphi}^f d\mathbf{x} + \rho_f \int_{\Omega^f(t)} (\mathbf{v} \cdot \nabla) \mathbf{v} \cdot \boldsymbol{\varphi}^f d\mathbf{x} + 2\mu_f \int_{\Omega^f(t)} \mathbf{D}(\mathbf{v}) : \mathbf{D}(\boldsymbol{\varphi}^f) d\mathbf{x} \\ & - \int_{\Omega^f(t)} p_f \nabla \cdot \boldsymbol{\varphi}^f d\mathbf{x} + \int_{\Omega^f(t)} \psi^f \nabla \cdot \mathbf{v} d\mathbf{x} = \int_{\Gamma(t)} \boldsymbol{\sigma}^f \mathbf{n} \cdot \boldsymbol{\varphi}^f ds \\ & + \int_{\Omega^f(t)} \mathbf{g} \cdot \boldsymbol{\varphi}^f d\mathbf{x} + \int_{\Gamma_{in}} p_{in}(t) \varphi_x^f dy. \end{aligned} \quad (2.29)$$

In order to write the weak form of the linearly elastic Koiter membrane, let $\hat{V}^m = (H_0^1(0, L))^2$. Then the weak formulation reads as follows: given $t \in (0, T)$ find $\hat{\boldsymbol{\eta}} \in \hat{V}^m$ such that for all $\hat{\boldsymbol{\zeta}} \in \hat{V}^m$

$$\begin{aligned} & \rho_m r_m \int_0^L \frac{\partial^2 \hat{\eta}_x}{\partial t^2} \hat{\zeta}_x d\hat{x} + \rho_m r_m \int_0^L \frac{\partial^2 \hat{\eta}_y}{\partial t^2} \hat{\zeta}_y d\hat{x} - C_2 \int_0^L \frac{\partial \hat{\eta}_y}{\partial \hat{x}} \hat{\zeta}_x d\hat{x} + C_1 \int_0^L \frac{\partial \hat{\eta}_x}{\partial \hat{x}} \frac{\partial \hat{\zeta}_x}{\partial \hat{x}} d\hat{x} \\ & + C_0 \int_0^L \hat{\eta}_y \hat{\zeta}_y d\hat{x} + C_2 \int_0^L \frac{\partial \hat{\eta}_x}{\partial \hat{x}} \hat{\zeta}_y d\hat{x} = \int_0^L \hat{\mathbf{f}} \cdot \hat{\boldsymbol{\zeta}} d\hat{x}. \end{aligned} \quad (2.30)$$

Finally, let us introduce

$$\begin{aligned} V^p(t) &= \{\boldsymbol{\varphi} : \Omega^p(t) \rightarrow \mathbb{R}^2 \mid \boldsymbol{\varphi} = \hat{\boldsymbol{\varphi}} \circ (\mathcal{S}_t)^{-1}, \hat{\boldsymbol{\varphi}} \in (H^1(\hat{\Omega}^p))^2, \boldsymbol{\varphi} = 0 \text{ on } \Gamma_{in}^p \cup \Gamma_{out}^p, \varphi_x = 0 \text{ on } \Gamma_{ext}^p(t)\}, \\ Q^p(t) &= \{\psi : \Omega^p(t) \rightarrow \mathbb{R} \mid \psi = \hat{\psi} \circ (\mathcal{S}_t)^{-1}, \hat{\psi} \in H^1(\hat{\Omega}^p), \psi|_{\partial\Omega^p(t) \setminus \Gamma(t)} = 0\}. \end{aligned}$$

Now the weak form of the Biot system reads as follows: given $t \in (0, T)$ find $(\mathbf{U}, p_p) \in V^p(t) \times Q^p(t)$ such that for all $(\boldsymbol{\varphi}^p, \psi^p) \in V^p(t) \times Q^p(t)$

$$\begin{aligned} & \rho_p \int_{\Omega^p(t)} \frac{D^2 \mathbf{U}}{Dt^2} \boldsymbol{\varphi}^p d\mathbf{x} + \int_{\Omega^p(t)} \boldsymbol{\sigma}^E : \nabla \boldsymbol{\varphi}^p d\mathbf{x} - \alpha \int_{\Omega^p(t)} p_p \nabla \cdot \boldsymbol{\varphi}^p d\mathbf{x} + \int_{\Omega^p(t)} s_0 \frac{Dp_p}{Dt} \psi^p d\mathbf{x} \\ & + \alpha \int_{\Omega^p(t)} \nabla \cdot \frac{D\mathbf{U}}{Dt} \psi^p d\mathbf{x} + \int_{\Omega^p(t)} \kappa \nabla p_p \cdot \nabla \psi^p d\mathbf{x} = - \int_{\Gamma(t)} \boldsymbol{\sigma}^p \mathbf{n} \cdot \boldsymbol{\varphi}^p d\mathbf{x} - \int_{\Gamma(t)} \kappa \nabla p_p \cdot \mathbf{n} \psi^p d\mathbf{x} \\ & - \int_{\Gamma_{ext}^p} p_e \boldsymbol{\varphi}_y^p d\mathbf{x} + \int_{\Omega^p(t)} \mathbf{h} \cdot \boldsymbol{\varphi}^p d\mathbf{x} + \int_{\Omega^p(t)} s \boldsymbol{\varphi}^s d\mathbf{x}. \end{aligned} \quad (2.31)$$

To write a weak formulation of the coupled Navier-Stokes/Koiter/Biot system, define a space of admissible solutions

$$W(t) = \{(\boldsymbol{\varphi}^f, \hat{\boldsymbol{\zeta}}, \boldsymbol{\varphi}^p) \in V^f(t) \times \hat{V}^m \times V^p(t) \mid \boldsymbol{\zeta} = \boldsymbol{\varphi}^p|_{\Gamma(t)}, \boldsymbol{\varphi}^f|_{\Gamma(t)} \cdot \boldsymbol{\tau} = \boldsymbol{\zeta} \cdot \boldsymbol{\tau}\}, \quad (2.32)$$

where $\boldsymbol{\zeta} := \hat{\boldsymbol{\zeta}} \circ (\mathcal{A}_t^{-1}|_{\Gamma(t)})$, and add together equations (2.29), (2.30) and (2.31):

$$\begin{aligned} & \rho_f \int_{\Omega^f(t)} \frac{\partial \mathbf{v}}{\partial t} \cdot \boldsymbol{\varphi}^f d\mathbf{x} + \rho_f \int_{\Omega^f(t)} (\mathbf{v} \cdot \nabla) \mathbf{v} \cdot \boldsymbol{\varphi}^f d\mathbf{x} + 2\mu_f \int_{\Omega^f(t)} \mathbf{D}(\mathbf{v}) : \mathbf{D}(\boldsymbol{\varphi}^f) d\mathbf{x} \\ & - \int_{\Omega^f(t)} p_f \nabla \cdot \boldsymbol{\varphi}^f d\mathbf{x} + \int_{\Omega^f(t)} \psi^f \nabla \cdot \mathbf{v} d\mathbf{x} + \rho_m r_m \int_0^L \frac{\partial^2 \hat{\eta}_x}{\partial t^2} \hat{\zeta}_x dx + \rho_m r_m \int_0^L \frac{\partial^2 \hat{\eta}_y}{\partial t^2} \hat{\zeta}_y dx \\ & - C_2 \int_0^L \frac{\partial \hat{\eta}_y}{\partial \hat{x}} \hat{\zeta}_x dx + C_1 \int_0^L \frac{\partial \hat{\eta}_x}{\partial \hat{x}} \frac{\partial \hat{\zeta}_x}{\partial \hat{x}} dx + C_0 \int_0^L \hat{\eta}_y \hat{\zeta}_y dx + C_2 \int_0^L \frac{\partial \hat{\eta}_x}{\partial \hat{x}} \hat{\zeta}_y dx \\ & + \rho_p \int_{\Omega^p(t)} \frac{D^2 \mathbf{U}}{Dt^2} \boldsymbol{\varphi}^p d\mathbf{x} + \int_{\Omega^p(t)} \boldsymbol{\sigma}^E : \nabla \boldsymbol{\varphi}^p d\mathbf{x} - \alpha \int_{\Omega^p(t)} p_p \nabla \cdot \boldsymbol{\varphi}^p d\mathbf{x} + \int_{\Omega^p(t)} s_0 \frac{Dp_p}{Dt} \psi^p d\mathbf{x} \\ & + \alpha \int_{\Omega^p(t)} \nabla \cdot \frac{D\mathbf{U}}{Dt} \psi^p d\mathbf{x} + \int_{\Omega^p(t)} \kappa \nabla p_p \cdot \nabla \psi^p d\mathbf{x} = \int_{\Gamma(t)} \boldsymbol{\sigma}^f \mathbf{n} \cdot \boldsymbol{\varphi}^f ds - \int_{\Gamma(t)} \boldsymbol{\sigma}^p \mathbf{n} \cdot \boldsymbol{\varphi}^p d\mathbf{x} \\ & - \int_{\Gamma(t)} \kappa \nabla p_p \cdot \mathbf{n} \psi^p d\mathbf{x} + \int_0^L \hat{\mathbf{f}} \cdot \hat{\boldsymbol{\zeta}} dx + \int_{\Omega^f(t)} \mathbf{g} \cdot \boldsymbol{\varphi}^f d\mathbf{x} + \int_{\Gamma_{in}} p_{in}(t) \varphi_x^f dy \\ & - \int_{\Gamma_{ext}^p} p_e \boldsymbol{\varphi}_y^p d\mathbf{x} + \int_{\Omega^p(t)} \mathbf{h} \cdot \boldsymbol{\varphi}^p d\mathbf{x} + \int_{\Omega^p(t)} s \psi^p d\mathbf{x}. \end{aligned} \quad (2.33)$$

Denote by $I_{\Gamma(t)}$ the interface integral

$$I_{\Gamma(t)} = \int_{\Gamma(t)} (\boldsymbol{\sigma}^f \mathbf{n} \cdot \boldsymbol{\varphi}^f - \boldsymbol{\sigma}^p \mathbf{n} \cdot \boldsymbol{\varphi}^p - \kappa \nabla p_p \cdot \mathbf{n} \psi^p + J^{-1} \mathbf{f} \cdot \boldsymbol{\zeta}) d\mathbf{x}.$$

Decomposing the stress terms and thin shell forcing term into their normal and tangential components and employing conditions (2.21) and (2.23) we have

$$I_{\Gamma(t)} = \int_{\Gamma(t)} \left(-p_p \boldsymbol{\varphi}^f \cdot \mathbf{n} - (\mathbf{n} \cdot \boldsymbol{\sigma}^p \mathbf{n})(\boldsymbol{\varphi}^p \cdot \mathbf{n}) + J^{-1}(\mathbf{f} \cdot \mathbf{n})(\boldsymbol{\zeta} \cdot \mathbf{n}) + \mathbf{v} \cdot \mathbf{n} \psi^p - \alpha \frac{D\mathbf{U}}{Dt} \cdot \mathbf{n} \psi^p \right)$$

$$+(\boldsymbol{\tau} \cdot \boldsymbol{\sigma}^f \mathbf{n})(\boldsymbol{\varphi}^f \cdot \boldsymbol{\tau}) - (\boldsymbol{\tau} \cdot \boldsymbol{\sigma}^p \mathbf{n})(\boldsymbol{\varphi}^p \cdot \boldsymbol{\tau}) + J^{-1}(\mathbf{f} \cdot \boldsymbol{\tau})(\boldsymbol{\zeta} \cdot \boldsymbol{\tau}) \Big) dx.$$

For each triple of test functions $(\boldsymbol{\varphi}^f, \hat{\boldsymbol{\zeta}}, \boldsymbol{\varphi}^p) \in W(t)$, and due to the condition (2.25) we have

$$I_{\Gamma(t)} = \int_{\Gamma(t)} \left(-p_p \boldsymbol{\varphi}^f \cdot \mathbf{n} - (\mathbf{n} \cdot \boldsymbol{\sigma}^p \mathbf{n})(\boldsymbol{\varphi}^p \cdot \mathbf{n}) + J^{-1}(\mathbf{f} \cdot \mathbf{n})(\boldsymbol{\varphi}^p \cdot \mathbf{n}) + \mathbf{v} \cdot \mathbf{n} \psi^p - \alpha \frac{D\mathbf{U}}{Dt} \cdot \mathbf{n} \psi^p \right) dx.$$

Finally, decomposing $\boldsymbol{\sigma}^p \mathbf{n}$ into $\boldsymbol{\sigma}^E \mathbf{n} - \alpha p_p \mathbf{n}$, and employing conditions (2.23) and (2.24) we have

$$I_{\Gamma(t)} = \int_{\Gamma(t)} \left(-p_p \boldsymbol{\varphi}^f \cdot \mathbf{n} + \alpha p_p \boldsymbol{\varphi}^p \cdot \mathbf{n} + \mathbf{v} \cdot \mathbf{n} \psi^p - \alpha \frac{D\mathbf{U}}{Dt} \cdot \mathbf{n} \psi^p \right) dx.$$

Thus, the weak formulation of the coupled Navier-Stokes/Koiter/Biot system reads as follows: given $t \in (0, T)$ find $(\mathbf{v}, \hat{\boldsymbol{\eta}}, \mathbf{U}, p_f, p_p) \in V^f(t) \times \hat{V}^m \times V^p(t) \times Q^f(t) \times Q^p(t)$, with $(\mathbf{v}, \frac{\partial \hat{\boldsymbol{\eta}}}{\partial t}, \frac{D\mathbf{U}}{Dt}) \in W(t)$, such that for all $(\boldsymbol{\varphi}^f, \hat{\boldsymbol{\zeta}}, \boldsymbol{\varphi}^p, \psi^f, \psi^p) \in W(t) \times Q^f(t) \times Q^p(t)$

$$\begin{aligned} & \rho_f \int_{\Omega^f(t)} \frac{\partial \mathbf{v}}{\partial t} \cdot \boldsymbol{\varphi}^f d\mathbf{x} + \int_{\Omega^f(t)} (\mathbf{v} \cdot \nabla) \mathbf{v} \cdot \boldsymbol{\varphi}^f d\mathbf{x} + 2\mu_f \int_{\Omega^f(t)} \mathbf{D}(\mathbf{v}) : \mathbf{D}(\boldsymbol{\varphi}^f) d\mathbf{x} \\ & - \int_{\Omega^f(t)} p_f \nabla \cdot \boldsymbol{\varphi}^f d\mathbf{x} + \int_{\Omega^f(t)} \psi^f \nabla \cdot \mathbf{v} d\mathbf{x} + \rho_m r_m \int_0^L \frac{\partial^2 \hat{\eta}_x}{\partial t^2} \hat{\zeta}_x dx + \rho_m r_m \int_0^L \frac{\partial^2 \hat{\eta}_y}{\partial t^2} \hat{\zeta}_y dx \\ & - C_2 \int_0^L \frac{\partial \hat{\eta}_y}{\partial \hat{x}} \hat{\zeta}_x dx + C_1 \int_0^L \frac{\partial \hat{\eta}_x}{\partial \hat{x}} \frac{\partial \hat{\zeta}_x}{\partial \hat{x}} dx + C_0 \int_0^L \hat{\eta}_y \hat{\zeta}_y dx + C_2 \int_0^L \frac{\partial \hat{\eta}_x}{\partial \hat{x}} \hat{\zeta}_y dx \\ & + \rho_p \int_{\Omega^p(t)} \frac{D^2 \mathbf{U}}{Dt^2} \boldsymbol{\varphi}^p d\mathbf{x} + \int_{\Omega^p(t)} \boldsymbol{\sigma}^E : \nabla \boldsymbol{\varphi}^p d\mathbf{x} - \alpha \int_{\Omega^p(t)} p_p \nabla \cdot \boldsymbol{\varphi}^p d\mathbf{x} + \int_{\Omega^p(t)} s_0 \frac{Dp_p}{Dt} \psi^p d\mathbf{x} \\ & + \alpha \int_{\Omega^p(t)} \nabla \cdot \frac{D\mathbf{U}}{Dt} \psi^p d\mathbf{x} + \int_{\Omega^p(t)} \kappa \nabla p_p \cdot \nabla \psi^p d\mathbf{x} + \int_{\Gamma(t)} p_p \boldsymbol{\varphi}^f \cdot \mathbf{n} dx - \alpha \int_{\Gamma(t)} p_p \boldsymbol{\varphi}^p \cdot \mathbf{n} dx \\ & - \int_{\Gamma(t)} \mathbf{v} \cdot \mathbf{n} \psi^p dx + \alpha \int_{\Gamma(t)} \frac{D\mathbf{U}}{Dt} \cdot \mathbf{n} \psi^p dx = \int_{\Omega^f(t)} \mathbf{g} \cdot \boldsymbol{\varphi}^f d\mathbf{x} + \int_{\Gamma_{in}} p_{in}(t) \varphi_x^f dy - \int_{\Gamma_{ext}^p} p_e \varphi_y^p dx \\ & + \int_{\Omega^p(t)} \mathbf{h} \cdot \boldsymbol{\varphi}^p d\mathbf{x} + \int_{\Omega^p(t)} s \psi^p d\mathbf{x}. \end{aligned} \quad (2.34)$$

2.3. Energy equality

In this section we will use an equivalent variational formulation to (2.30) (see [12] for details), given by:

$$\begin{aligned} & \rho_m r_m \int_0^L \frac{\partial^2 \hat{\eta}_x}{\partial t^2} \hat{\zeta}_x d\hat{x} + \rho_m r_m \int_0^L \frac{\partial^2 \hat{\eta}_y}{\partial t^2} \hat{\zeta}_y d\hat{x} + \frac{r_m}{2} \int_0^L 4\mu_m \left(\frac{\partial \hat{\eta}_x}{\partial \hat{x}} \frac{\partial \hat{\zeta}_x}{\partial \hat{x}} + \frac{1}{R^2} \hat{\eta}_y \hat{\zeta}_y \right) d\hat{x} \\ & + \frac{r_m}{2} \int_0^L \frac{4\mu_m \lambda_m}{\lambda_m + 2\mu_m} \left(\frac{\partial \hat{\eta}_x}{\partial \hat{x}} + \frac{1}{R} \hat{\eta}_y \right) \left(\frac{\partial \hat{\zeta}_x}{\partial \hat{x}} + \frac{1}{R} \hat{\zeta}_y \right) d\hat{x} = \int_0^L \hat{\mathbf{f}} \cdot \hat{\boldsymbol{\zeta}} d\hat{x}. \end{aligned} \quad (2.35)$$

To formally derive the energy of the coupled problem, we add together variational formulations for Navier-Stokes equations (2.29), Koiter membrane model (2.35), and Biot system (2.31). The coupling

conditions are then used to couple the fluid, thin structure, and porous medium sub-problems, using manipulations as in the previous section, resulting in an equation similar to (2.34). Let

$$(\boldsymbol{\varphi}^f, \hat{\zeta}, \boldsymbol{\varphi}^p, \psi^f, \psi^p) = (\mathbf{v}, \frac{\partial \hat{\boldsymbol{\eta}}}{\partial t}, \frac{DU}{Dt}, p_f, p_p).$$

Then, the energy equality for coupled system is given as follows:

$$\begin{aligned} & \frac{1}{2} \frac{d}{dt} \left\{ \rho_f \|\mathbf{v}\|_{L^2(\Omega^f(t))}^2 + \rho_m r_m \left\| \frac{\partial \hat{\boldsymbol{\eta}}_x}{\partial t} \right\|_{L^2(0,L)}^2 + \rho_m r_m \left\| \frac{\partial \hat{\boldsymbol{\eta}}_y}{\partial t} \right\|_{L^2(0,L)}^2 \right\} \\ & + r_m \left[4\mu_m \left\| \frac{\hat{\boldsymbol{\eta}}_y}{R} \right\|_{L^2(0,L)}^2 + 4\mu_m \left\| \frac{\partial \hat{\boldsymbol{\eta}}_x}{\partial \hat{x}} \right\|_{L^2(0,L)}^2 + \frac{4\mu_m \lambda_m}{\lambda_m + 2\mu_m} \left\| \frac{\partial \hat{\boldsymbol{\eta}}_x}{\partial \hat{x}} + \frac{\hat{\boldsymbol{\eta}}_y}{R} \right\|_{L^2(0,L)}^2 \right] \\ & + \rho_p \left\| \frac{DU}{Dt} \right\|_{L^2(\Omega^p(t))}^2 + 2\mu_p \|\mathbf{D}(\mathbf{U})\|_{L^2(\Omega^p(t))}^2 + \lambda_p \|\nabla \cdot \mathbf{U}\|_{L^2(\Omega^p(t))}^2 + s_0 \|p_p\|_{L^2(\Omega^p(t))}^2 \Big\} \\ & + 2\mu_f \|\mathbf{D}(\mathbf{v})\|_{L^2(\Omega(t))}^2 + \|\kappa \nabla p_p\|_{L^2(\Omega^p(t))}^2 = \int_{\Omega^f(t)} \mathbf{g} \cdot \mathbf{v} d\mathbf{x} + \int_{\Gamma_{in}} p_{in}(t) v_x dy \\ & - \int_{\Gamma_{ext}^p} p_e \frac{DU_y}{Dt} dx + \int_{\Omega^p(t)} s p_p d\mathbf{x} + \int_{\Omega^p(t)} \mathbf{h} \cdot \frac{DU}{Dt} d\mathbf{x}. \end{aligned}$$

3. A loosely-coupled scheme based on the operator-splitting approach

To solve the fluid-multilayer structure interaction problem described in Section 1 numerically, we propose a loosely coupled scheme based on a time-splitting approach known as the Lie splitting [25]. Details of the Lie splitting are described below.

3.1. The Lie scheme

Let A be an operator from a Hilbert space H into itself, and suppose $\phi_0 \in H$. Consider the following initial value problem:

$$\frac{\partial \phi}{\partial t} + A(\phi) = 0, \quad \text{in } (0, T), \quad \text{where } A = \sum_{i=1}^P A_i, \quad \phi(0) = \phi_0. \quad (3.1)$$

The Lie scheme consists of splitting the full problem into P sub-problems, each defined by the operator $A_i, i = 1, \dots, P$. The original problem is discretized in time with the time step $\Delta t > 0$, so that $t^n = n\Delta t$. The Lie splitting scheme consist of solving a series of problems $\frac{\partial \phi_i}{\partial t} + A_i(\phi_i) = 0$, for $i = 1, \dots, P$, each defined over the entire time interval (t^n, t^{n+1}) , but with the initial data for the i^{th} problem given by the solution of the $(i-1)^{st}$ problem at t^{n+1} . More precisely, set $\phi^0 = \phi_0$. Then, for $n \geq 0$ compute ϕ^{n+1} by solving

$$\frac{\partial \phi_i}{\partial t} + A_i(\phi_i) = 0 \quad \text{in } (t^n, t^{n+1}), \quad \phi_i(t^n) = \phi^{n+(i-1)/P}, \quad (3.2)$$

and then set $\phi^{n+i/P} = \phi_i(t^{n+1})$, for $i = 1, \dots, P$. This method is first-order accurate in time. To increase the accuracy in time to second-order, a symmetrization of the scheme can be performed.

3.2. The first-order system in the ALE framework

To apply the Lie operator splitting scheme, we have to rewrite our system in a first-order form. Therefore, we express the second-order time derivatives of both elastic and poroelastic structure displacements in terms of the first-order derivative of structure velocities. Furthermore, we consider the Navier-Stokes equation in the ALE formulation. To write the Navier-Stokes equations in the ALE form, we notice that for a function $f = f(\mathbf{x}, t)$ defined on $\Omega^f(t) \times (0, T)$ the corresponding function $\hat{f} := f \circ \mathcal{A}_t$ defined on $\hat{\Omega} \times (0, T)$ is given by

$$\hat{f}(\hat{\mathbf{x}}, t) = f(\mathcal{A}_t(\hat{\mathbf{x}}), t).$$

Differentiation with respect to time, after using the chain rule, gives

$$\left. \frac{\partial f}{\partial t} \right|_{\hat{\mathbf{x}}} = \frac{\partial f}{\partial t} + \mathbf{w} \cdot \nabla f, \quad \mathbf{w}(\mathbf{x}, t) = \frac{\partial \mathcal{A}_t(\hat{\mathbf{x}})}{\partial t}. \quad (3.3)$$

where \mathbf{w} denotes the domain velocity. We will apply this rule to write the time-derivative of the velocity in Navier-Stokes equations on the reference domain. Note that we do not have to apply the same rule to the time-derivatives in the Biot system and in Koiter membrane equations since the material time-derivative is suitable for the time discretization, due to $\frac{Dq}{Dt} = \frac{\partial q}{\partial t}|_{\hat{\mathbf{x}}}$, and the membrane equations are given on the reference configuration. With these assumptions, our problem now reads: Given $t \in (0, T)$, find $\mathbf{v} = (v_x, v_y)$, p_f , $\hat{\boldsymbol{\eta}} = (\hat{\eta}_x, \hat{\eta}_y)$, $\hat{\boldsymbol{\xi}} = (\hat{\xi}_x, \hat{\xi}_y)$, $\mathbf{U} = (U_x, U_y)$, $\mathbf{V} = (V_x, V_y)$ and p_p , with $\boldsymbol{\eta}(\mathbf{x}, t) = \hat{\boldsymbol{\eta}}(\mathcal{A}_t^{-1}(\mathbf{x}), t)$, for $\mathbf{x} \in \Gamma(t)$, such that

$$\rho_f \left(\left. \frac{\partial \mathbf{v}}{\partial t} \right|_{\hat{\mathbf{x}}} + (\mathbf{v} - \mathbf{w}) \cdot \nabla \mathbf{v} \right) = \nabla \cdot \boldsymbol{\sigma}^f + \mathbf{g} \quad \text{in } \Omega^f(t) \times (0, T), \quad (3.4a)$$

$$\nabla \cdot \mathbf{v} = 0 \quad \text{in } \Omega^f(t) \times (0, T), \quad (3.4b)$$

$$\rho_m r_m \frac{\partial \hat{\boldsymbol{\xi}}}{\partial t} + \hat{\mathcal{L}} \hat{\boldsymbol{\eta}} = \hat{\mathbf{f}}^k \quad \text{on } \hat{\Gamma} \times (0, T), \quad (3.4c)$$

$$\rho_m r_m \left(\hat{\boldsymbol{\xi}} - \frac{\partial \hat{\boldsymbol{\eta}}}{\partial t} \right) = 0 \quad \text{on } \hat{\Gamma} \times (0, T), \quad (3.4d)$$

$$\rho_p \frac{D\mathbf{V}}{Dt} = \nabla \cdot \boldsymbol{\sigma}^p + \mathbf{h} \quad \text{in } \Omega^p(t) \times (0, T), \quad (3.4e)$$

$$s_0 \frac{D}{Dt} p_p + \alpha \nabla \cdot \mathbf{V} - \nabla \cdot (\kappa \nabla p_p) = s \quad \text{in } \Omega^p(t) \times (0, T), \quad (3.4f)$$

$$\rho_p \left(\mathbf{V} - \frac{D\mathbf{U}}{Dt} \right) = 0 \quad \text{in } \Omega^p(t) \times (0, T), \quad (3.4g)$$

with the kinematic coupling conditions on $\Gamma(t)$:

$$\boldsymbol{\xi} \cdot \boldsymbol{\tau} = \mathbf{v} \cdot \boldsymbol{\tau}, \quad \boldsymbol{\eta} = \mathbf{U}, \quad (3.5)$$

dynamic coupling conditions on $\Gamma(t)$:

$$\boldsymbol{\tau} \cdot \boldsymbol{\sigma}^f \mathbf{n} - \boldsymbol{\tau} \cdot \boldsymbol{\sigma}^p \mathbf{n} + J^{-1} \boldsymbol{\tau} \cdot \mathbf{f}^k = 0, \quad (3.6)$$

$$\alpha \mathbf{n} \cdot \boldsymbol{\sigma}^f \mathbf{n} - \mathbf{n} \cdot \boldsymbol{\sigma}^p \mathbf{n} + J^{-1} \mathbf{n} \cdot \mathbf{f}^k = 0, \quad (3.7)$$

$$\mathbf{n} \cdot \boldsymbol{\sigma}^f \mathbf{n} = -p_p, \quad (3.8)$$

and the continuity of normal flux on $\Gamma(t)$:

$$\mathbf{v} \cdot \mathbf{n} = \left(\alpha \frac{\partial \boldsymbol{\eta}}{\partial t} - \kappa \nabla p_p \right) \cdot \mathbf{n}, \quad (3.9)$$

with the boundary and initial conditions given in Section 1.

Remark 1. Denote by \mathcal{L} the inverse Piola transformation of $\hat{\mathcal{L}}$, namely $\mathcal{L} = J^{-1} \hat{\mathcal{L}} F^{-T}$, where $F = \nabla_{\mathbf{x}} \mathcal{A}_t$. Then, composing the Koiter shell equations (2.9) with \mathcal{A}_t^{-1} , and employing the first condition in (3.5), condition (3.8), and relation

$$\frac{\partial}{\partial t}(\boldsymbol{\xi} \cdot \boldsymbol{\tau}) = \frac{\partial \boldsymbol{\xi}}{\partial t} \cdot \boldsymbol{\tau} + \frac{\partial \boldsymbol{\tau}}{\partial t} \cdot \boldsymbol{\xi},$$

we can write conditions (3.6) and (3.7) as follows:

$$\rho_m r_m \frac{\partial(\mathbf{v} \cdot \boldsymbol{\tau})}{\partial t} + \boldsymbol{\tau} \cdot \mathcal{L} \boldsymbol{\eta} - \rho_m r_m \frac{\partial \boldsymbol{\tau}}{\partial t} \cdot \boldsymbol{\xi} + J \boldsymbol{\tau} \cdot \boldsymbol{\sigma}^f \mathbf{n} - J \boldsymbol{\tau} \cdot \boldsymbol{\sigma}^p \mathbf{n} = 0, \quad \text{on } \Gamma(t) \quad (3.10a)$$

$$\rho_m r_m \frac{\partial \boldsymbol{\xi}}{\partial t} \cdot \mathbf{n} + \mathbf{n} \cdot \mathcal{L} \boldsymbol{\eta} - J \alpha p_p - J \mathbf{n} \cdot \boldsymbol{\sigma}^p \mathbf{n} = 0, \quad \text{on } \Gamma(t). \quad (3.10b)$$

We will use conditions (3.6)-(3.7) written the form (3.10a)-(3.10b) when performing the operator splitting.

3.3. Details of the loosely-coupled scheme

In this section we will apply the Lie splitting scheme to problem (3.4), where the discretization in time will be done using the backward Euler scheme. We will denote the discrete time derivatives by

$$d_t \boldsymbol{\varphi}^{n+1} = \frac{\boldsymbol{\varphi}^{n+1} - \boldsymbol{\varphi}^n}{\Delta t}, \quad \text{and} \quad d_{tt} \boldsymbol{\varphi}^{n+1} = \frac{d_t \boldsymbol{\varphi}^{n+1} - d_t \boldsymbol{\varphi}^n}{\Delta t},$$

and the discrete time average by

$$\boldsymbol{\varphi}^{n+1/2} = \frac{\boldsymbol{\varphi}^{n+1} + \boldsymbol{\varphi}^n}{2},$$

where all quantities are evaluated on the reference domain. In our case, using the notation from Section 3.1, $\boldsymbol{\phi}$ that appears in equation (3.1) is a vector $\boldsymbol{\phi} = (\mathbf{v}, \mathbf{v}|_{\Gamma(t)} \cdot \boldsymbol{\tau}, \boldsymbol{\xi} \cdot \mathbf{n}, \boldsymbol{\eta}, \mathbf{V}, p_p, \mathbf{U})^T$. We will split the first-order system (3.4)-(3.9) into two main sub-problems, separating the problem defined on the fluid domain $\Omega^f(t)$ from the problem defined on the poroelastic medium domain $\Omega^p(t)$. In that case, we will split the sum of all operators that appear in the system (3.4) into two parts, as $A_1 + A_2$, where $A_i = (A_i^f, A_i^{k1}, A_i^{k2}, A_i^\eta, A_i^V, A_i^{p_p}, A_i^U)^T$, for $i = 1, 2$. For each of the equations, this will be done in the following way:

- Equation (3.4a) will be split so that $A_1^f = \rho_f(\mathbf{v} - \mathbf{w}) \cdot \nabla \mathbf{v} - \nabla \cdot \boldsymbol{\sigma}^f$ and $A_2^f = 0$,
- Equation (3.4c) will be used in form (3.10), where equation (3.10a) will be split so

$$A_1^{k1} = -\rho_m r_m \frac{\partial \boldsymbol{\tau}}{\partial t} \cdot \boldsymbol{\xi} + J \boldsymbol{\tau} \cdot \boldsymbol{\sigma}^f \mathbf{n} \quad \text{and} \quad A_2^{k1} = \boldsymbol{\tau} \cdot \mathcal{L} \boldsymbol{\eta} - J \boldsymbol{\tau} \cdot \boldsymbol{\sigma}^p \mathbf{n},$$

and equation (3.10b) will be split so

$$A_1^{k2} = 0 \quad \text{and} \quad A_2^{k2} = \mathbf{n} \cdot \mathcal{L} \boldsymbol{\eta} - J \alpha p_p - J \mathbf{n} \cdot \boldsymbol{\sigma}^p \mathbf{n}.$$

- Equation (3.4d) will be split so that $A_1^\eta = 0$, and $A_1^\eta = \boldsymbol{\xi}$,
- Equation (3.4e) will be split so that $A_1^V = 0$ and $A_2^V = -\nabla \cdot \boldsymbol{\sigma}^p$,
- Equation (3.4f) will be split so that $A_1^{p_p} = 0$ and $A_2^{p_p} = \alpha \nabla \cdot \mathbf{V} - \nabla \cdot (\kappa \nabla p_p)$, and finally,
- Equation (3.4g) will be split so that $A_1^U = 0$ and $A_2^U = \mathbf{V}$.

Using this approach, our system is decoupled into a fluid problem and the Biot problem. Furthermore, we not only split the coupled problem into two different domains, but we also treat different physical phenomena separately. Details of the loosely coupled scheme are given as follows.

- **Step 1.** Step 1 is a geometry problem which involves computation of a fluid domain and ALE velocity \mathbf{w} :

$$\mathcal{A}_{t^n}(\hat{\mathbf{x}}) = \hat{\mathbf{x}} + \text{Ext}(\hat{\boldsymbol{\eta}}^n), \quad \Omega^f(t^n) = \mathcal{A}_{t^n}(\hat{\Omega}^f), \quad \mathbf{w}^n = d_t \mathbf{x}^n, \quad (3.11)$$

where $\hat{\mathbf{x}} \in \hat{\Omega}$, $\mathbf{x}^n \in \Omega(t^n)$, and $\mathbf{x}^{n-1} \in \Omega(t^{n-1})$.

- **Step 2.** Step 2 involves solving the Navier-Stokes equations, and equation

$$\rho_m r_m \frac{\partial(\mathbf{v}|_{\Gamma(t^n)} \cdot \boldsymbol{\tau})}{\partial t} - \rho_m r_m \frac{\partial \boldsymbol{\tau}}{\partial t} \cdot \boldsymbol{\xi} + J \boldsymbol{\tau} \cdot \boldsymbol{\sigma}^f \mathbf{n} = 0 \quad \text{on } \Gamma(t^n) \times (t^n, t^{n+1}). \quad (3.12)$$

while time-derivatives of all the other functions are equal to zero. In particular, since the time derivative of the displacement of the elastic shell is equal to zero, the fluid domain is not changing in this step, which implies

$$\frac{\partial \boldsymbol{\tau}}{\partial t} = 0 \quad \text{and } J = 1 \quad \text{for } t \in (t^n, t^{n+1}).$$

Therefore, equation (3.12) can be seen as a Robin-type boundary condition for fluid velocity. Now, in the time-discrete framework, Step 2 reads as follows: Find \mathbf{v}^{n+1} and p_f^{n+1} , with \mathbf{v}^n, p_f^n and p_p^n obtained at the previous time step, such that

$$\rho_f d_t \mathbf{v}^{n+1} + (\mathbf{v}^{n+1} - \mathbf{w}^n) \cdot \nabla \mathbf{v}^{n+1} = \nabla \cdot \boldsymbol{\sigma}^f(\mathbf{v}^{n+1}, p_f^{n+1}) + \mathbf{g} \quad \text{in } \Omega^f(t^n), \quad (3.13a)$$

$$\nabla \cdot \mathbf{v}^{n+1} = 0 \quad \text{in } \Omega^f(t^n), \quad (3.13b)$$

$$\boldsymbol{\tau} \cdot \boldsymbol{\sigma}^f(\mathbf{v}^{n+1}, p_f^{n+1}) \mathbf{n} + \rho_m r_m d_t \mathbf{v}^{n+1} \cdot \boldsymbol{\tau} = 0 \quad \text{on } \Gamma(t^n), \quad (3.13c)$$

$$\mathbf{n} \cdot \boldsymbol{\sigma}^f \mathbf{n} = p_p^n \quad \text{on } \Gamma(t^n). \quad (3.13d)$$

with the following boundary conditions on $\Gamma_{\text{in}}^f \cup \Gamma_{\text{out}}^f \cup \Gamma_0^f$:

$$\frac{\partial v_x^{n+1}}{\partial y} = \quad v_y^{n+1} = 0 \quad \text{on } \Gamma_0^f, \quad \mathbf{v}^{n+1}(0, R, t) = \mathbf{v}^{n+1}(L, R, t) = 0,$$

$$\boldsymbol{\sigma}^f(\mathbf{v}^{n+1}, p_f^{n+1}) \mathbf{n} = -p_{\text{in}}(t) \mathbf{n} \quad \text{on } \Gamma_{\text{in}}^f, \quad \boldsymbol{\sigma}^f(\mathbf{v}^{n+1}, p_f^{n+1}) \mathbf{n} = 0 \quad \text{on } \Gamma_{\text{out}}^f.$$

- **Step 3:** Step 3 involves solving Biot problem together with equations

$$\rho_m r_m \frac{\partial(\mathbf{v} \cdot \boldsymbol{\tau})}{\partial t} + \boldsymbol{\tau} \cdot \mathcal{L} \boldsymbol{\eta} - J \boldsymbol{\tau} \cdot \boldsymbol{\sigma}^p \mathbf{n} = 0 \quad \text{on } \Gamma(t^n) \times (t^n, t^{n+1}), \quad (3.14a)$$

$$\rho_m r_m \frac{\partial \boldsymbol{\xi}}{\partial t} \cdot \mathbf{n} + \mathbf{n} \cdot \mathcal{L} \boldsymbol{\eta} - J \alpha p_p - J \mathbf{n} \cdot \boldsymbol{\sigma}^p \mathbf{n} = 0 \quad \text{on } \Gamma(t^n) \times (t^n, t^{n+1}), \quad (3.14b)$$

and conditions

$$\alpha \frac{\partial \boldsymbol{\eta}}{\partial t} \cdot \mathbf{n} = \mathbf{v} \cdot \mathbf{n} + \kappa \nabla p_p \cdot \mathbf{n} \quad \text{on } \Gamma(t^n) \times (t^n, t^{n+1}), \quad (3.15)$$

$$\boldsymbol{\eta} \cdot \mathbf{n} = \mathbf{U} \cdot \mathbf{n}, \quad \boldsymbol{\eta} \cdot \boldsymbol{\tau} = \mathbf{U} \cdot \boldsymbol{\tau}, \quad \boldsymbol{\xi} \cdot \boldsymbol{\tau} = \mathbf{v} \cdot \boldsymbol{\tau} \quad \text{on } \Gamma(t^n) \times (t^n, t^{n+1}), \quad (3.16)$$

while the fluid velocity in $\Omega^f(t^n)$ does not change in this step. Since $\boldsymbol{\eta} \cdot \mathbf{n} = \mathbf{U}|_{\Gamma(t^n)} \cdot \mathbf{n}$ and $\boldsymbol{\eta} \cdot \boldsymbol{\tau} = \mathbf{U}|_{\Gamma(t^n)} \cdot \boldsymbol{\tau}$, we have $\boldsymbol{\eta} = \mathbf{U}|_{\Gamma(t^n)}$ and $\boldsymbol{\xi} = \mathbf{V}|_{\Gamma(t^n)}$. Thus, we can rewrite conditions (3.14a), (3.14b), and (3.15) in the following way:

$$\rho_m r_m \frac{\partial (\mathbf{V} \cdot \boldsymbol{\tau})}{\partial t} + \boldsymbol{\tau} \cdot \mathcal{L} \mathbf{U} - J \boldsymbol{\tau} \cdot \boldsymbol{\sigma}^p \mathbf{n} = 0 \quad \text{on } \Gamma(t^n) \times (t^n, t^{n+1}), \quad (3.17)$$

$$\rho_m r_m \frac{\partial \mathbf{V}}{\partial t} \cdot \mathbf{n} + \mathbf{n} \cdot \mathcal{L} \mathbf{U} - J \alpha p_p - J \mathbf{n} \cdot \boldsymbol{\sigma}^p \mathbf{n} = 0 \quad \text{on } \Gamma(t^n) \times (t^n, t^{n+1}), \quad (3.18)$$

$$\alpha \frac{\partial \mathbf{U}}{\partial t} \cdot \mathbf{n} = \mathbf{v} \cdot \mathbf{n} + \kappa \nabla p_p \cdot \mathbf{n} \quad \text{on } \Gamma(t^n) \times (t^n, t^{n+1}), \quad (3.19)$$

in which case they become Robin-type boundary conditions for the Biot system.

Finally, using the Newmark scheme for the elasticity equations, Step 3 reads as follows: Find $\mathbf{U}^{n+1}, \mathbf{V}^{n+1}, \hat{\boldsymbol{\eta}}^{n+1}, \hat{\boldsymbol{\xi}}^{n+1}$ and p_p^{n+1} , with \mathbf{v}^{n+1} computed in Step 1 and $\mathbf{U}^n, \mathbf{V}^n$ and p_p^n computed in the previous time-step, such that $\boldsymbol{\eta}^{n+1} = \mathbf{U}|_{\Gamma(t^n)}^{n+1}, \boldsymbol{\xi}^{n+1} = \mathbf{V}|_{\Gamma(t^n)}^{n+1}$ and

$$\rho_p d_t \mathbf{V}^{n+1} = \nabla \cdot \boldsymbol{\sigma}^p(\mathbf{U}^{n+1/2}, p_p^{n+1}) + \mathbf{h} \quad \text{in } \Omega^p(t^n), \quad (3.20a)$$

$$s_0 d_t p_p^{n+1} + \alpha \nabla \cdot d_t \mathbf{U}^{n+1} - \nabla \cdot (\kappa \nabla p_p^{n+1}) = s \quad \text{in } \Omega^p(t^n), \quad (3.20b)$$

$$\rho_p (\mathbf{V}^{n+1/2} - d_t \mathbf{U}^{n+1}) = 0 \quad \text{in } \Omega^p(t^n), \quad (3.20c)$$

$$J \boldsymbol{\tau} \cdot \boldsymbol{\sigma}^p(\mathbf{U}^{n+1}, p_p^{n+1}) \mathbf{n} = \rho_m r_m d_t \mathbf{V}^{n+1} \cdot \boldsymbol{\tau} + \boldsymbol{\tau} \cdot \mathcal{L} \mathbf{U}^{n+1/2} \quad \text{on } \Gamma(t^n), \quad (3.20d)$$

$$J \mathbf{n} \cdot \boldsymbol{\sigma}^p(\mathbf{U}^{n+1}, p_p^{n+1}) \mathbf{n} = \rho_m r_m d_t \mathbf{V}^{n+1} \cdot \mathbf{n} + \mathbf{n} \cdot \mathcal{L} \mathbf{U}^{n+1/2} - J \alpha p_p^{n+1} \quad \text{on } \Gamma(t^n), \quad (3.20e)$$

$$\kappa \nabla p_p^{n+1} \cdot \mathbf{n} = \alpha d_t \mathbf{U}^{n+1} \cdot \mathbf{n} - \mathbf{v}^{n+1} \cdot \mathbf{n} \quad \text{on } \Gamma(t^n), \quad (3.20f)$$

with boundary conditions:

$$\hat{\boldsymbol{\eta}}^{n+1}|_{\hat{x}=0,L} = 0, \quad p_p^{n+1} = 0 \quad \text{on } \Omega^p(t^n) \setminus \Gamma(t^n), \quad \mathbf{U}^{n+1} = 0 \quad \text{on } \Gamma_{in}^p \cup \Gamma_{out}^p,$$

$$\mathbf{n}_{ext} \cdot \boldsymbol{\sigma}^E(\mathbf{U}^{n+1}) \mathbf{n}_{ext} = -p_e \quad \text{on } \Gamma_{ext}^p, \quad U_x^{n+1} = 0 \quad \text{on } \Gamma_{ext}^p.$$

Do $t^n = t^{n+1}$ and return to Step 1.

Remark 2. In practice, the structure is usually handled in Lagrangian framework. Together with the hypothesis of “small” deformations we can assume the structure is linearly elastic, in which case we can easily recast Step 3 in the reference domain, where the boundary conditions (3.20d)-(3.20e) simplify as follows:

$$\begin{aligned} \mathbf{e}_1 \cdot \hat{\boldsymbol{\sigma}}^p(\hat{\mathbf{U}}^{n+1}, \hat{p}_p^{n+1}) \hat{\mathbf{n}} &= \rho_m r_m d_t \hat{V}_x^{n+1} - C_2 \frac{\partial \hat{U}_y^{n+1/2}}{\partial \hat{x}} - C_1 \frac{\partial^2 \hat{U}_x^{n+1/2}}{\partial \hat{x}^2} \quad \text{on } \hat{\Gamma} \times (t^n, t^{n+1}), \\ \mathbf{e}_2 \cdot \hat{\boldsymbol{\sigma}}^p(\hat{\mathbf{U}}^{n+1}, \hat{p}_p^{n+1}) \hat{\mathbf{n}} &= \rho_m r_m d_t \hat{V}_y^{n+1} + C_0 \hat{U}_y^{n+1/2} + C_2 \frac{\partial \hat{U}_x^{n+1/2}}{\partial \hat{x}} - \alpha \hat{p}_p^{n+1} \quad \text{on } \hat{\Gamma} \times (t^n, t^{n+1}), \end{aligned}$$

where \mathbf{e}_1 and \mathbf{e}_2 are the Cartesian unit vectors.

The proposed scheme is an explicit loosely-coupled scheme where the first step consists of a fluid (Navier-Stokes) problem, and the second step consists of a poroelastic problem. Both sub-problems are solved with a Robin-type boundary conditions, which take into account thin-shell inertia and kinematic conditions implicitly. We note that the original monolithic problem becomes fully decoupled, and there are no sub-iterations needed between the two sub-problems.

Remark 3. One can apply additional splitting to Step 1 and Step 2 of the algorithm described above. Namely, the fluid problem described in Step 1 can be split into its viscous part (the Stokes equations for an incompressible fluid) and the pure advection part (incorporating the fluid and ALE advection simultaneously). The Biot system described in Step 2 can be split so the elastodynamics is treated separately from the pressure. For the details of possible Biot splitting strategies see [36] and the references therein.

4. Weak formulation and stability

In this section we write the variational formulation and prove the conditional stability of the loosely coupled scheme proposed in Section 2. For simplicity, we work out the analysis assuming that the displacement of the boundary is small enough and can be neglected. Under these assumptions, domains $\Omega^f(t)$ and $\Omega^p(t)$ are fixed:

$$\Omega^f(t) = \hat{\Omega}^f, \quad \Omega^p(t) = \hat{\Omega}^p, \quad \forall t \in (0, T).$$

Although simplified, this problem still retains the main difficulties associated with the “added-mass” effect and the difficulties that partitioned schemes encounter when modeling fluid-porous medium coupling. Since from now on all the variable are defined on the fixed domain, we will drop the “hat” notation to avoid cumbersome expressions.

Let $t^n := n\Delta t$ for $n = 1, \dots, N$, where $T = N\Delta t$ is the final time. Let the test function spaces V^f, Q^f, V^p and Q^p be defined as in (2.27), (2.28), (2.31), and (2.31) respectively.

We introduce the following bilinear forms

$$\begin{aligned} a_f(\mathbf{v}, \boldsymbol{\varphi}^f) &= 2\mu_f \int_{\Omega^f} \mathbf{D}(\mathbf{v}) : \mathbf{D}(\boldsymbol{\varphi}^f) d\mathbf{x}, \\ b_f(p_f, \boldsymbol{\varphi}^f) &= \int_{\Omega^f} p_f \nabla \cdot \boldsymbol{\varphi}^f d\mathbf{x}, \\ a_e(\mathbf{U}, \boldsymbol{\varphi}^p) &= 2\mu_p \int_{\Omega^p} \mathbf{D}(\mathbf{U}) : \mathbf{D}(\boldsymbol{\varphi}^p) d\mathbf{x} + \lambda_p \int_{\Omega^p} (\nabla \cdot \mathbf{U})(\nabla \cdot \boldsymbol{\varphi}^p) d\mathbf{x}, \\ a_p(p_p, \psi^p) &= \int_{\Omega^p} \kappa \nabla p_p \cdot \nabla \psi^p d\mathbf{x}, \\ b_{ep}(p_p, \boldsymbol{\varphi}^p) &= \alpha \int_{\Omega^p} p_p \nabla \cdot \boldsymbol{\varphi}^p d\mathbf{x}, \\ a_m(\boldsymbol{\eta}, \boldsymbol{\zeta}) &= -C_2 \int_0^L \frac{\partial \eta_y}{\partial x} \zeta_x dx + C_1 \int_0^L \frac{\partial \eta_x}{\partial x} \frac{\partial \zeta_x}{\partial x} dx + C_0 \int_0^L \eta_y \zeta_y dx + C_2 \int_0^L \frac{\partial \eta_x}{\partial x} \zeta_y dx, \\ c_{fp}(p_p, \boldsymbol{\varphi}^f) &= \int_{\Gamma} p_p \boldsymbol{\varphi}^f \cdot \mathbf{n} dx, \\ c_{ep}(p_p, \boldsymbol{\varphi}^p) &= \alpha \int_{\Gamma} p_p \boldsymbol{\varphi}^p \cdot \mathbf{n} dx, \end{aligned}$$

and the trilinear form

$$d_f(\mathbf{v}, \mathbf{u}, \boldsymbol{\varphi}) = \rho_f \int_{\Omega^f} (\mathbf{v} \cdot \nabla) \mathbf{u} \cdot \boldsymbol{\varphi} d\mathbf{x}.$$

To discretize the problem in space, we use the finite element method. Thus, we define the finite element spaces $V_h^f \subset V^f, Q_h^f \subset Q^f, V_h^p \subset V^p$ and $Q_h^p \subset Q^p$. The definition of these discrete spaces will be made precise at the beginning of Section 5. We assume that all the finite element initial conditions are equal to zero:

$$\mathbf{v}_h^0 = 0, \quad \mathbf{U}_h^0 = 0, \quad \mathbf{V}_h^0 = 0, \quad \boldsymbol{\eta}_h^0 = 0, \quad \boldsymbol{\xi}_h^0 = 0, \quad p_{p,h}^0 = 0.$$

Finally, the fully discrete numerical scheme is given as follows:

- **Step 1.** Given $t^{n+1} \in (0, T], n = 0, \dots, N-1$, find $\mathbf{v}_h^{n+1} \in V_h^f$ and $p_{f,h}^{n+1} \in Q_h^f$ such that for all $(\boldsymbol{\varphi}_h^f, \psi_h^f) \in V_h^f \times Q_h^f$, with $p_{p,h}^n$ obtained at the previous time step:

$$\begin{aligned} \rho_f \int_{\Omega^f} d_t \mathbf{v}_h^{n+1} \cdot \boldsymbol{\varphi}_h^f d\mathbf{x} + d_f(\mathbf{v}_h^{n+1}, \mathbf{v}_h^{n+1}, \boldsymbol{\varphi}_h^f) + a_f(\mathbf{v}_h^{n+1}, \boldsymbol{\varphi}_h^f) + \rho_m r_m \int_{\Gamma} (d_t \mathbf{v}_h|_{\Gamma}^{n+1} \cdot \boldsymbol{\tau})(\boldsymbol{\varphi}_h^f|_{\Gamma} \cdot \boldsymbol{\tau}) d\mathbf{x} \\ - b_f(p_{f,h}^{n+1}, \boldsymbol{\varphi}_h^f) + b_f(\psi_h^f, \mathbf{v}_h^{n+1}) + c_{fp}(p_{p,h}^n, \boldsymbol{\varphi}_h^f) = \int_{\Omega^f} \mathbf{f}^f(t^{n+1}) \cdot \boldsymbol{\varphi}_h^f d\mathbf{x} \\ + \int_{\Gamma_{in}} p_{in}(t^{n+1}) \boldsymbol{\varphi}_{x,h}^f dy. \end{aligned} \quad (4.1)$$

- **Step 2.** Given \mathbf{v}_h^{n+1} computed in Step 1, find $\mathbf{U}_h^{n+1} \in V_h^p, \mathbf{V}_h^{n+1} \in V_h^p, \boldsymbol{\eta}_h^{n+1} \in V_h^m, \boldsymbol{\xi}_h^{n+1} \in V_h^m$ and $p_{p,h}^{n+1} \in Q_h^p$, with $\boldsymbol{\eta}_h^{n+1} = \mathbf{U}_h|_{\Gamma}^{n+1}$ and $\boldsymbol{\xi}_h^{n+1} = \mathbf{V}_h|_{\Gamma}^{n+1}$, such that for all $(\boldsymbol{\varphi}_h^p, \phi_h^p, \psi_h^p) \in V_h^p \times V_h^p \times Q_h^p$:

$$\begin{aligned} \rho_p \int_{\Omega^p} (\mathbf{V}_h^{n+1/2} - d_t \mathbf{U}_h^{n+1}) \cdot \phi_h^p d\mathbf{x} + \rho_p \int_{\Omega^p} d_t \mathbf{V}_h^{n+1} \cdot \boldsymbol{\varphi}_h^p d\mathbf{x} + a_e(\mathbf{U}_h^{n+1/2}, \boldsymbol{\varphi}_h^p) + \int_{\Omega^p} s_0 d_t p_{p,h}^{n+1} \psi_h^p d\mathbf{x} \\ + a_p(p_{p,h}^{n+1}, \psi_h^p) - b_{ep}(p_{p,h}^{n+1}, \boldsymbol{\varphi}_h^p) + b_{ep}(\psi_h^p, d_t \mathbf{U}_h^{n+1}) + \rho_m r_m \int_0^L (\mathbf{V}_h|_{\Gamma}^{n+1/2} - d_t \mathbf{U}_h|_{\Gamma}^{n+1}) \cdot \phi_h^p|_{\Gamma} d\mathbf{x} \\ + \rho_m r_m \int_0^L d_t \mathbf{V}_h|_{\Gamma}^{n+1} \cdot \boldsymbol{\varphi}_h^p|_{\Gamma} d\mathbf{x} + a_m(\mathbf{U}_h|_{\Gamma}^{n+1/2}, \boldsymbol{\varphi}_h^p|_{\Gamma}) - c_{ep}(p_{p,h}^{n+1}, \boldsymbol{\varphi}_h^p) + c_{ep}(\psi_h^p, d_t \mathbf{U}_h^{n+1}) \\ - c_{fp}(\psi_h^p, \mathbf{v}_h^{n+1}) = - \int_{\Gamma_{ext}^p} p_e \boldsymbol{\varphi}_{y,h}^p d\mathbf{x} + \int_{\Omega^p} \mathbf{f}^s(t^{n+1}) \cdot \boldsymbol{\varphi}_h^p d\mathbf{x} + \int_{\Omega^p} s(t^{n+1}) \psi_h^p d\mathbf{x}. \end{aligned} \quad (4.2)$$

4.1. Stability analysis

To present our results in a more compact manner, in the analysis we study the Stokes equations instead of the Navier-Stokes equations. Handling the convective term in the Navier-Stokes equations can be done using classical approaches, see for example [48, 38]. Let us introduce the following time discrete norms:

$$\|\boldsymbol{\varphi}\|_{l^2(0,T;H^k(S))} = \left(\sum_{n=0}^{N-1} \|\boldsymbol{\varphi}^{n+1}\|_{H^k(S)}^2 \Delta t \right)^{1/2}, \quad \|\boldsymbol{\varphi}\|_{l^\infty(0,T;H^k(S))} = \max_{0 \leq n \leq N} \|\boldsymbol{\varphi}^n\|_{H^k(S)},$$

where $S \in \{\Omega^f, \Omega^p, (0, L)\}$. Let \mathcal{E}_f^n denote the discrete energy of the fluid problem, \mathcal{E}_p^n denote the discrete energy of the Biot problem, and \mathcal{E}_m^n denote the discrete energy of the Koiter membrane at time level n , defined respectively by

$$\begin{aligned}\mathcal{E}_f^n &= \frac{\rho_f}{2} \|\mathbf{v}_h^n\|_{L^2(\Omega^f)}^2 + \frac{\rho_m r_m}{2} \|\mathbf{v}_h^n \cdot \boldsymbol{\tau}\|_{L^2(\Gamma)}^2 \\ \mathcal{E}_p^n &= \frac{\rho_p}{2} \|\mathbf{V}_h^n\|_{L^2(\Omega^p)}^2 + \mu_p \|D(\mathbf{U}_h^n)\|_{L^2(\Omega^p)}^2 + \frac{\lambda_p}{2} \|\nabla \cdot \mathbf{U}_h^n\|_{L^2(\Omega^p)}^2 + \frac{s_0}{2} \|p_{p,h}^n\|_{L^2(\Omega^p)}^2, \\ \mathcal{E}_m^n &= \frac{\rho_m r_m}{2} \|\xi_x^n\|_{L^2(0,L)}^2 + \frac{\rho_m r_m}{2} \|\xi_y^n\|_{L^2(0,L)}^2 \\ &\quad + r_m \left[4\mu_m \left\| \frac{\hat{\eta}_y}{R} \right\|_{L^2(0,L)}^2 + 4\mu_m \left\| \frac{\partial \hat{\eta}_x}{\partial \hat{x}} \right\|_{L^2(0,L)}^2 + \frac{4\mu_m \lambda_m}{\lambda_m + 2\mu_m} \left\| \frac{\partial \hat{\eta}_x}{\partial \hat{x}} + \frac{\hat{\eta}_y}{R} \right\|_{L^2(0,L)}^2 \right].\end{aligned}\tag{4.3}$$

The stability of the loosely-coupled scheme (4.1)-(4.2) is stated in the following result. The constants that appear in (4.5) are defined in the Appendix.

Theorem 1. *Assume that the fluid-poroelastic system is isolated, i.e. $p_{in} = 0, p_e = 0, \mathbf{f}^f = 0, \mathbf{f}^s = 0$ and $s = 0$. Let $\{(\mathbf{v}_h^n, p_{p,h}^n, \mathbf{V}_h^n, \mathbf{U}_h^n, \xi_h^n, \eta_h^n, p_{p,h}^n)\}_{0 \leq n \leq N}$ be the solution of (4.1)-(4.2). Then, under the condition*

$$\left(2\mu_f - \frac{C_K^2 C_{TI} C_T^2 C_{PF} \Delta t}{s_0 h} \right) \geq \gamma > 0 \quad \text{i.e.} \quad \Delta t < \frac{2\mu_f s_0 h}{C_K^2 C_{TI} C_T^2 C_{PF}},\tag{4.4}$$

the following estimate holds:

$$\begin{aligned}\mathcal{E}_f^N + \mathcal{E}_p^N + \mathcal{E}_m^N + \frac{\Delta t}{2} \rho_f \|d_t \mathbf{v}_h\|_{l^2(0,T;L^2(\Omega^f))}^2 + \frac{\Delta t}{2} \rho_m r_m \|d_t \mathbf{v}_h \cdot \boldsymbol{\tau}\|_{l^2(0,T;L^2(\Gamma))}^2 \\ + \gamma \|\mathbf{v}_h\|_{l^2(0,T;H^1(\Omega^f))}^2 + \delta \Delta t \|p_{f,h}\|_{l^2(0,T;L^2(\Omega^f))}^2 + \frac{\Delta t}{4} s_0 \|d_t p_{p,h}\|_{l^2(0,T;L^2(\Omega^p))}^2 + \|\sqrt{\kappa} p_{p,h}\|_{l^2(0,T;H^1(\Omega^p))}^2 \\ \leq \mathcal{E}_f^0 + \mathcal{E}_p^0 + \mathcal{E}_m^0.\end{aligned}\tag{4.5}$$

Proof. To prove the energy estimate, we test the problem (4.1) with $(\boldsymbol{\varphi}_h^f, \psi_h^f) = (\mathbf{v}_h^{n+1}, p_{f,h}^{n+1})$, and problem (4.2) with $(\boldsymbol{\varphi}_h^p, \phi_h^p, \psi_h^p) = (d_t \mathbf{U}_h^{n+1}, d_t \mathbf{V}_h^{n+1}, p_{p,h}^{n+1})$. Then, after adding them together and multiplying by Δt we get

$$\begin{aligned}\mathcal{E}_f^{n+1} + \mathcal{E}_p^{n+1} + \mathcal{E}_m^{n+1} + \frac{\rho_f}{2} \|\mathbf{v}_h^{n+1} - \mathbf{v}_h^n\|_{L^2(\Omega^f)}^2 + 2\mu_f \Delta t \|D(\mathbf{v}_h^{n+1})\|_{L^2(\Omega^f)}^2 + \frac{\rho_m r_m}{2} \|(\mathbf{v}_h^{n+1} - \mathbf{v}_h^n) \cdot \boldsymbol{\tau}\|_{L^2(\Gamma)}^2 \\ + \frac{s_0}{2} \|p_{p,h}^{n+1} - p_{p,h}^n\|_{L^2(\Omega^p)}^2 + \Delta t \|\sqrt{\kappa} \nabla p_{p,h}^{n+1}\|_{L^2(\Omega^p)}^2 \leq \Delta t c_{fp}(p_{p,h}^{n+1}, \mathbf{v}_h^{n+1}) - \Delta t c_{fp}(p_{p,h}^n, \mathbf{v}_h^{n+1}) + \mathcal{E}_f^n + \mathcal{E}_p^n + \mathcal{E}_m^n.\end{aligned}$$

The term $\Delta t c_{fp}(p_{p,h}^{n+1} - p_{p,h}^n, \mathbf{v}_h^{n+1})$ arises in classical partitioned schemes for Navier Stokes/Stokes-Darcy coupling, and has been previously addressed in [32]. Following the similar approach as in [32], we can estimate the interface term using Cauchy-Schwarz inequality (A.5), Young's inequality (A.3) (for $\epsilon_1 > 0$), and the local trace-inverse inequality (A.4) in the following way:

$$\begin{aligned}\Delta t c_{fp}(p_{p,h}^{n+1} - p_{p,h}^n, \mathbf{v}_h^{n+1}) &= \Delta t \int_{\Gamma} (p_{p,h}^{n+1} - p_{p,h}^n) \mathbf{v}_h^{n+1} \cdot \mathbf{n} dx \\ &\leq \frac{\epsilon_1 \Delta t}{2} \|p_{p,h}^{n+1} - p_{p,h}^n\|_{L^2(\Gamma)}^2 + \frac{\Delta t}{2\epsilon_1} \|\mathbf{v}_h^{n+1}\|_{L^2(\Gamma)}^2\end{aligned}$$

$$\leq \frac{\epsilon_1 \Delta t C_{TI}}{2h} \|p_{p,h}^{n+1} - p_{p,h}^n\|_{L^2(\Omega)}^2 + \frac{\Delta t}{2\epsilon_1} \|\mathbf{v}_h^{n+1}\|_{L^2(\Gamma)}^2.$$

Finally, using trace inequality (A.7), Poincaré-Friedrichs inequality (A.6), and Korn's inequality (A.8), we have

$$\Delta t c_{fp}(p_{p,h}^{n+1} - p_{p,h}^n, \mathbf{v}_h^{n+1}) \leq \frac{\epsilon_1 \Delta t C_{TI}}{2h} \|p_{p,h}^{n+1} - p_{p,h}^n\|_{L^2(\Omega)}^2 + \frac{\Delta t C_T^2 C_K^2 C_{PF}}{2\epsilon_1} \|D(\mathbf{v}_h^{n+1})\|_{L^2(\Omega)}^2. \quad (4.6)$$

In order to recover control on the pressure in the fluid domain, we exploit the *inf-sup* stability of the approximation spaces V_h^f and Q_h^f . Namely, spaces V_h^f and Q_h^f are *inf-sup* stable provided

$$\inf_{p_{f,h}^{n+1} \in Q_h^f} \sup_{\boldsymbol{\varphi}_h^f \in V_h^f} \frac{b_f(p_{f,h}^{n+1}, \boldsymbol{\varphi}_h^f)}{\|\boldsymbol{\varphi}_h^f\|_{H^1(\Omega^f)} \|p_{f,h}^{n+1}\|_{L^2(\Omega^f)}} = \beta_f > 0. \quad (4.7)$$

Combining the *inf-sup* condition (4.7) with (4.1) tested with $\psi_h^f = 0$ we obtain,

$$\beta_f \|p_{f,h}^{n+1}\|_{L^2(\Omega^f)} \leq \sup_{\boldsymbol{\varphi}_h^f \in V_h^f} \frac{\sum_{k=1,2} \mathcal{T}_k(\boldsymbol{\varphi}_h^f)}{\|\boldsymbol{\varphi}_h^f\|_{H^1(\Omega^f)}} \quad (4.8)$$

where $\beta_f > 0$ is a constant independent of the mesh characteristic size and $\mathcal{T}_k(\boldsymbol{\varphi}_h^f)$ is a shorthand notation for the following terms,

$$\begin{aligned} \mathcal{T}_1(\boldsymbol{\varphi}_h^f) &:= \rho_f \int_{\Omega^f} d_t \mathbf{v}_h^{n+1} \cdot \boldsymbol{\varphi}_h^f d\mathbf{x} + \rho_m r_m \int_{\Gamma} (d_t \mathbf{v}_h^{n+1} \cdot \boldsymbol{\tau})(\boldsymbol{\varphi}_h^f \cdot \boldsymbol{\tau}) dx, \\ \mathcal{T}_2(\boldsymbol{\varphi}_h^f) &:= a_f(\mathbf{v}_h^{n+1}, \boldsymbol{\varphi}_h^f) + c_{fp}(p_{p,h}^n, \boldsymbol{\varphi}_h^f). \end{aligned}$$

Exploiting Cauchy-Schwarz (A.5) and trace (A.7) inequalities, we obtain the following upper bounds,

$$\begin{aligned} \sup_{\boldsymbol{\varphi}_h^f \in V_h^f} \frac{\mathcal{T}_1(\boldsymbol{\varphi}_h^f)}{\|\boldsymbol{\varphi}_h^f\|_{H^1(\Omega^f)}} &\leq C_T \left(\rho_f \|d_t \mathbf{v}_h^{n+1}\|_{L^2(\Omega^f)} + \rho_m r_m \|d_t \mathbf{v}_h^{n+1}\|_{L^2(\Gamma)} \right), \\ \sup_{\boldsymbol{\varphi}_h^f \in V_h^f} \frac{\mathcal{T}_2(\boldsymbol{\varphi}_h^f)}{\|\boldsymbol{\varphi}_h^f\|_{H^1(\Omega^f)}} &\leq 2\mu_f \|D(\mathbf{v}_h^{n+1})\|_{L^2(\Omega^f)}^2 + C_T C_{PF} \kappa^{-1} \|\sqrt{\kappa} \nabla p_{p,h}^n\|_{L^2(\Omega^p)}^2. \end{aligned}$$

Let us now multiply (4.8) as well as the bounds for $\mathcal{T}_k(\boldsymbol{\varphi}_h^f)$ by $\epsilon_2 \Delta t^2$ and combine the resulting inequality with (4.1) and (4.6) to get,

$$\begin{aligned} &\mathcal{E}_f^{n+1} + \mathcal{E}_p^{n+1} + \mathcal{E}_m^{n+1} + \frac{\Delta t^2}{2} (1 - \epsilon_2 C_T^2) \rho_f \|d_t \mathbf{v}_h^{n+1}\|_{L^2(\Omega^f)}^2 \\ &+ \frac{\Delta t^2}{2} \rho_m r_m (1 - \epsilon_2 C_T^2) \|d_t \mathbf{v}_h^{n+1} \cdot \boldsymbol{\tau}\|_{L^2(\Gamma)}^2 + 2\mu_f C_K (1 - (2\epsilon_1)^{-1} - \epsilon_2 \mu_f) \Delta t \|\mathbf{v}_h^{n+1}\|_{H^1(\Omega^f)}^2 \\ &+ \frac{\Delta t^2}{2} \left(s_0 - \frac{\epsilon_1 \Delta t C_{TI}}{2h} \right) \|d_t p_{p,h}^{n+1}\|_{L^2(\Omega^p)}^2 + \epsilon_2 \beta_f \Delta t^2 \|p_{f,h}^{n+1}\|_{L^2(\Omega^f)}^2 \\ &\Delta t \|\sqrt{\kappa} \nabla p_{p,h}^{n+1}\|_{L^2(\Omega^p)}^2 - \epsilon_2 \Delta t^2 \frac{C_T^2 C_{PF}^2}{\kappa^2} \|\sqrt{\kappa} \nabla p_{p,h}^n\|_{L^2(\Omega^p)}^2 \leq \mathcal{E}_f^n + \mathcal{E}_p^n + \mathcal{E}_m^n. \end{aligned}$$

After summing up with respect to the time index n we observe that

$$\begin{aligned} \Delta t \sum_{n=0}^{N-1} \left[\|\sqrt{\kappa} \nabla p_{p,h}^{n+1}\|_{L^2(\Omega^p)}^2 - \epsilon_2 \Delta t^2 \frac{C_T^2 C_{PF}^2}{\kappa^2} \|\sqrt{\kappa} \nabla p_{p,h}^n\|_{L^2(\Omega^p)}^2 \right] \\ = \Delta t \sum_{n=1}^{N-1} \left(1 - \epsilon_2 \Delta t \frac{C_T^2 C_{PF}^2}{\kappa^2} \right) \|\sqrt{\kappa} \nabla p_{p,h}^n\|_{L^2(\Omega^p)}^2 + \Delta t \|\sqrt{\kappa} \nabla p_{p,h}^N\|_{L^2(\Omega^p)}^2. \end{aligned}$$

By setting $\epsilon_1 = \frac{s_0 h}{2 \Delta t C_{TI}}$, and $\epsilon_2 = \frac{1}{2} \min \left(\frac{1}{\mu_f}, \Delta t \frac{\kappa^2}{C_T^2 C_{PF}^2} \right)$ we prove the desired estimate. \square

5. Error Analysis

In this section, we analyze the convergence rate of the proposed method. For the spatial approximation, we apply Lagrangian finite elements of polynomial degree k for all the variables, except for the fluid pressure, for which we use elements of degree $s < k$. We assume the regularity assumptions reported in Lemma 1 of the Appendix are satisfied and that our FEM spaces satisfy the usual approximation properties, as well as fluid velocity-pressure spaces satisfy the discrete *inf-sup* condition (4.7). We will consider the fluid problem over the discretely divergence free velocity space

$$X_h^f := \{\mathbf{v}_h \in V_h^f \mid (\psi_h^f, \nabla \cdot \mathbf{v}_h)_{\Omega^f} = 0, \quad \text{for all } \psi_h^f \in Q_h^f\}. \quad (5.1)$$

Let S_h be an orthogonal projection operator with respect to $a_f(\cdot, \cdot)$, onto X_h^f , given by

$$a_f(\mathbf{v} - S_h \mathbf{v}, \varphi_h^f) = 0 \quad \forall \varphi_h^f \in X_h^f, \quad (5.2)$$

P_h be the Lagrangian interpolation operator onto V_h^p , and let $\Pi_h^{f/p}$ be the L^2 -orthogonal projection onto $Q_h^{f/p}$, satisfying

$$(p_r - \Pi_h^r p_r, \psi_h) = 0, \quad \forall \psi_h \in Q_h^r, r \in \{f, p\}. \quad (5.3)$$

Then, using piecewise polynomials of degree k , the finite element theory for Lagrangian and L^2 projections [15] gives the classical approximation properties reported in Lemma 2. Since P_h is the Lagrangian interpolant, so is its trace on Γ . Therefore, we inherit optimal approximation properties also on this subset. We refer to Lemma 2 for a precise statement of these properties.

To analyze the error of our numerical scheme, we start by subtracting (4.1)-(4.2) from the continuous problem. We assume that the continuous fluid velocity lives in the space $\{\mathbf{v} \in V^f \mid \nabla \cdot \mathbf{v} = 0\}$. This gives rise to the following error equations:

$$\begin{aligned} \rho_f \int_{\Omega^f} (d_t \mathbf{v}^{n+1} - d_t \mathbf{v}_h^{n+1}) \cdot \varphi_h^f d\mathbf{x} + a_f(\mathbf{v}^{n+1} - \mathbf{v}_h^{n+1}, \varphi_h^f) - b_f(p_f^{n+1}, \varphi_h^f) + c_{fp}(p_p^n - p_{p,h}^n, \varphi_h^f) \\ + \rho_m r_m \int_{\Gamma} (d_t \mathbf{v}^{n+1} \cdot \boldsymbol{\tau} - d_t \mathbf{v}_h^{n+1} \cdot \boldsymbol{\tau})(\varphi_h^f \cdot \boldsymbol{\tau}) d\mathbf{x} = \mathcal{R}_f^{n+1}(\varphi_h^f), \quad \forall \varphi_h^f \in X_h^f, \quad (5.4) \\ \rho_p \int_{\Omega^p} (\mathbf{V}^{n+1/2} - \mathbf{V}_h^{n+1/2} - (d_t \mathbf{U}^{n+1} - d_t \mathbf{U}_h^{n+1})) \cdot \boldsymbol{\phi}_h^p d\mathbf{x} + \rho_p \int_{\Omega^p} (d_t \mathbf{V}^{n+1} - d_t \mathbf{V}_h^{n+1}) \cdot \boldsymbol{\varphi}_h^p d\mathbf{x} \\ + a_e(\mathbf{U}^{n+1/2} - \mathbf{U}_h^{n+1/2}, \boldsymbol{\varphi}_h^p) + \int_{\Omega^p} s_0 (d_t p_p^{n+1} - d_t p_{p,h}^{n+1}) \psi_h^p d\mathbf{x} + a_p(p_p^{n+1} - p_{p,h}^{n+1}, \psi_h^p) \end{aligned}$$

$$\begin{aligned}
& -b_{ep}(p_p^{n+1} - p_{p,h}^{n+1}, \varphi_h^p) + b_{ep}(\psi_h^p, d_t \mathbf{U}^{n+1} - d_t \mathbf{U}_h^{n+1}) + \rho_m r_m \int_{\Gamma} (\mathbf{V}^{n+1/2} - \mathbf{V}_h^{n+1/2}) \cdot \phi_h^p dx \\
& - \rho_m r_m \int_{\Gamma} (d_t \mathbf{U}^{n+1} - d_t \mathbf{U}_h^{n+1}) \cdot \phi_h^p dx + \rho_m r_m \int_{\Gamma} (d_t \mathbf{V}^{n+1} - d_t \mathbf{V}_h) \cdot \varphi_h^p dx \\
& + a_m(\mathbf{U}|_{\Gamma}^{n+1/2} - \mathbf{U}_h|_{\Gamma}^{n+1/2}, \varphi_h^p|_{\Gamma}) - c_{ep}(p_p^{n+1} - p_{p,h}^{n+1}, \varphi_h^p) + c_{ep}(\psi_h^p, d_t \mathbf{U}^{n+1} - d_t \mathbf{U}_h^{n+1}) \\
& - c_{fp}(\psi_h^p, \mathbf{v}^{n+1} - \mathbf{v}_h^{n+1}) = \mathcal{R}_s^{n+1}(\varphi_h^p) + \mathcal{R}_v^{n+1}(\phi_h^p) + \mathcal{R}_p^{n+1}(\psi_h^p), \quad \forall (\varphi_h^p, \phi_h^p, \psi_h^p) \in V_h^p \times V_h^p \times Q_h^p, \quad (5.5)
\end{aligned}$$

where the consistency errors are given by

$$\begin{aligned}
\mathcal{R}_f^{n+1}(\varphi_h^f) &= \rho_f \int_{\Omega^f} (d_t \mathbf{v}^{n+1} - \partial_t \mathbf{v}^{n+1}) \cdot \varphi_h^f dx + c_{fp}(p_p^n - p_p^{n+1}, \varphi_h^f) \\
&+ \rho_m r_m \int_{\Gamma} (d_t \mathbf{v}^{n+1} \cdot \boldsymbol{\tau} - \partial_t \mathbf{v}^{n+1} \cdot \boldsymbol{\tau})(\varphi_h^f \cdot \boldsymbol{\tau}) dx, \\
\mathcal{R}_s^{n+1}(\varphi_h^p) &= \rho_p \int_{\Omega^p} (d_t \mathbf{V}^{n+1} - \partial_t \mathbf{V}^{n+1}) \cdot \varphi_h^p dx + a_e\left(\frac{\mathbf{U}^n - \mathbf{U}^{n+1}}{2}, \varphi_h^p\right) \\
&+ \rho_m r_m \int_{\Gamma} (d_t \mathbf{V}^{n+1} - \partial_t \mathbf{V}^{n+1}) \cdot \varphi_h^p dx + a_m\left(\frac{\mathbf{U}|_{\Gamma}^n - \mathbf{U}|_{\Gamma}^{n+1}}{2}, \varphi_h^p|_{\Gamma}\right), \\
\mathcal{R}_v^{n+1}(\phi_h^p) &= \rho_p \int_{\Omega^p} \frac{\mathbf{V}^n - \mathbf{V}^{n+1}}{2} \cdot \phi_h^p dx - \rho_p \int_{\Omega^p} (d_t \mathbf{U}^{n+1} - \partial_t \mathbf{U}^{n+1}) \cdot \phi_h^p dx \\
&+ \rho_m r_m \int_{\Gamma} \frac{\mathbf{V}^n - \mathbf{V}^{n+1}}{2} \cdot \phi_h^p dx - \rho_m r_m \int_{\Gamma} (d_t \mathbf{U}^{n+1} - \partial_t \mathbf{U}^{n+1}) \cdot \phi_h^p dx, \\
\mathcal{R}_p^{n+1}(\psi_h^p) &= \int_{\Omega^p} s_0(d_t p_p^{n+1} - \partial_t p_p^{n+1}) \psi_h^p dx + b_{ep}(\psi_h^p, d_t \mathbf{U}^{n+1} - \partial_t \mathbf{U}^{n+1}) \\
&+ c_{ep}(\psi_h^p, d_t \mathbf{U}^{n+1} - \partial_t \mathbf{U}^{n+1}). \quad (5.6)
\end{aligned}$$

Let us split the error of the method into the approximation error θ_r and the truncation error δ_r , with $r = f, fp, u, v, p$, as follows:

$$\begin{aligned}
e_f^{n+1} &= \mathbf{v}^{n+1} - \mathbf{v}_h^{n+1} = (\mathbf{v}^{n+1} - S_h \mathbf{v}^{n+1}) + (S_h \mathbf{v}^{n+1} - \mathbf{v}_h^{n+1}) =: \theta_f^{n+1} + \delta_f^{n+1}, \\
e_{fp}^{n+1} &= p_f^{n+1} - p_{f,h}^{n+1} = (p_f^{n+1} - \Pi_h^f p_f^{n+1}) + (\Pi_h^f p_f^{n+1} - p_{f,h}^{n+1}) =: \theta_{fp}^{n+1} + \delta_{fp}^{n+1}, \\
e_u^{n+1} &= \mathbf{U}^{n+1} - \mathbf{U}_h^{n+1} = (\mathbf{U}^{n+1} - P_h \mathbf{U}^{n+1}) + (P_h \mathbf{U}^{n+1} - \mathbf{U}_h^{n+1}) =: \theta_u^{n+1} + \delta_u^{n+1}, \\
e_v^{n+1} &= \mathbf{V}^{n+1} - \mathbf{V}_h^{n+1} = (\mathbf{V}^{n+1} - P_h \mathbf{V}^{n+1}) + (P_h \mathbf{V}^{n+1} - \mathbf{V}_h^{n+1}) =: \theta_v^{n+1} + \delta_v^{n+1}, \\
e_p^{n+1} &= p_p^{n+1} - p_{p,h}^{n+1} = (p_p^{n+1} - \Pi_h^p p_p^{n+1}) + (\Pi_h^p p_p^{n+1} - p_{p,h}^{n+1}) =: \theta_p^{n+1} + \delta_p^{n+1}.
\end{aligned}$$

Note that $\boldsymbol{\eta}^{n+1} - \boldsymbol{\eta}_h^{n+1} = \theta_u|_{\Gamma}^{n+1} + \delta_u|_{\Gamma}^{n+1}$ and $\boldsymbol{\xi}^{n+1} - \boldsymbol{\xi}_h^{n+1} = \theta_v|_{\Gamma}^{n+1} + \delta_v|_{\Gamma}^{n+1}$.

Our plan is to rearrange the terms in the error equations so that we have the truncation errors on the left hand side, and the consistency and interpolation errors on the right hand side. After that, we will choose $\varphi_h^f = \delta_f^{n+1}$, $\varphi_h^p = d_t \delta_u^{n+1}$, $\phi_h^p = d_t \delta_v^{n+1}$, and $\psi_h^p = \delta_p^{n+1}$, and use the stability estimate for the truncation errors. Finally, we will bound the remaining terms, and use the triangle inequality to get the error estimates for e_f, e_u, e_v , and e_p .

Rearranging the terms in the error equations, and using properties (5.2) and (5.3) of the projection operators S_h and Π_h , respectively, we have

$$\rho_f \int_{\Omega^f} d_t \delta_f^{n+1} \cdot \varphi_h^f dx + a_f(\delta_f^{n+1}, \varphi_h^f) + c_{fp}(\delta_p^n, \varphi_h^f) + \rho_m r_m \int_{\Gamma} (d_t \delta_f^{n+1} \cdot \boldsymbol{\tau})(\varphi_h^f \cdot \boldsymbol{\tau}) dx$$

$$\begin{aligned}
&= \mathcal{R}_f^{n+1}(\varphi_h^f) + b_f(p_f^{n+1}, \varphi_h^f) - \rho_f \int_{\Omega^f} d_t \theta_f^{n+1} \cdot \varphi_h^f d\mathbf{x} - \rho_m r_m \int_{\Gamma} (d_t \theta_f^{n+1} \cdot \boldsymbol{\tau}(\varphi_h^f \cdot \boldsymbol{\tau})) d\mathbf{x} \quad \forall \varphi_h^f \in X_h^f, \quad (5.7) \\
&\quad \rho_p \int_{\Omega^p} (\delta_v^{n+1/2} - d_t \delta_u^{n+1}) \cdot \phi_h^p d\mathbf{x} + \rho_p \int_{\Omega^p} d_t \delta_v^{n+1} \cdot \varphi_h^p d\mathbf{x} + a_e(\delta_u^{n+1/2}, \varphi_h^p) + \int_{\Omega^p} s_0 d_t \delta_p^{n+1} \psi_h^p d\mathbf{x} \\
&\quad + a_p(\delta_p^{n+1}, \psi_h^p) - b_{ep}(\delta_p^{n+1}, \varphi_h^p) + b_{ep}(\psi_h^p, d_t \delta_u^{n+1}) + \rho_m r_m \int_{\Gamma} (\delta_v^{n+1/2} - d_t \delta_u^{n+1}) \cdot \phi_h^p d\mathbf{x} \\
&\quad + \rho_m r_m \int_{\Gamma} d_t \delta_v^{n+1} \cdot \varphi_h^p d\mathbf{x} + a_m(\delta_u|_{\Gamma}^{n+1/2}, \varphi_h^p|_{\Gamma}) - c_{ep}(\delta_p^{n+1}, \varphi_h^p) + c_{ep}(\psi_h^p, d_t \delta_u^{n+1}) - c_{fp}(\psi_h^p, \delta_v^{n+1}) \\
&\quad = \mathcal{R}_s^{n+1}(\varphi_h^p) + \mathcal{R}_v^{n+1}(\phi_h^p) + \mathcal{R}_p^{n+1}(\psi_h^p) + \rho_p \int_{\Omega^p} d_t \theta_u^{n+1} \cdot \phi_h^p d\mathbf{x} - \rho_p \int_{\Omega^p} \theta_v^{n+1/2} \cdot \phi_h^p d\mathbf{x} \\
&\quad + \rho_p \int_{\Omega^p} d_t \theta_v^{n+1} \cdot \varphi_h^p d\mathbf{x} - a_e(\theta_u^{n+1/2}, \varphi_h^p) - a_p(\theta_p^{n+1}, \psi_h^p) + b_{ep}(\theta_p^{n+1}, \varphi_h^p) - b_{ep}(\psi_h^p, d_t \theta_u^{n+1}) \\
&\quad - \rho_m r_m \int_{\Gamma} (\theta_v^{n+1/2} - d_t \theta_u^{n+1}) \cdot \phi_h^p d\mathbf{x} - \rho_m r_m \int_{\Gamma} d_t \theta_v^{n+1} \cdot \varphi_h^p d\mathbf{x} - a_m(\theta_u|_{\Gamma}^{n+1/2}, \varphi_h^p|_{\Gamma}) \\
&\quad + c_{ep}(\theta_p^{n+1}, \varphi_h^p) - c_{ep}(\psi_h^p, d_t \theta_u^{n+1}) + c_{fp}(\psi_h^p, \theta_f^{n+1}), \quad \forall (\varphi_h^p, \phi_h^p, \psi_h^p) \in V_h^p \times V_h^p \times Q_h^p. \quad (5.8)
\end{aligned}$$

Let \mathcal{E}_{δ}^n be defined as

$$\begin{aligned}
\mathcal{E}_{\delta}^n &= \frac{\rho_f}{2} \|\delta_f^n\|_{L^2(\Omega^f)}^2 + \frac{\rho_m r_m}{2} \|\delta_f^n \cdot \boldsymbol{\tau}\|_{L^2(\Gamma)}^2 + \frac{\rho_p}{2} \|\delta_v^n\|_{L^2(\Omega^p)}^2 + \mu_p \|E(\delta_u^n)\|_{L^2(\Omega^p)}^2 \\
&\quad + \frac{\lambda_p}{2} \|\nabla \cdot \delta_u^n\|_{L^2(\Omega^p)}^2 + \frac{s_0}{2} \|\delta_p^n\|_{L^2(\Omega^p)}^2 + \frac{\rho_m r_m}{2} \|\delta_v^n\|_{L^2(\Gamma)}^2 + \mathcal{M}(\delta_u|_{\Gamma}^n),
\end{aligned}$$

where

$$\mathcal{M}(\boldsymbol{\xi}^n) = \frac{r_m}{2} \left[4\mu_m \left\| \frac{\hat{\xi}_y}{R} \right\|_{L^2(0,L)}^2 + 4\mu_m \left\| \frac{\partial \hat{\xi}_x}{\partial \hat{x}} \right\|_{L^2(0,L)}^2 + \frac{4\mu_m \lambda_m}{\lambda_m + 2\mu_m} \left\| \frac{\partial \hat{\xi}_x}{\partial \hat{x}} + \frac{\hat{\xi}_y}{R} \right\|_{L^2(0,L)}^2 \right].$$

Note that \mathcal{E}_{δ}^n corresponds to the total discrete energy of the scheme that appears in Theorem 1 in terms of the truncation error.

Theorem 2. Consider the solution $(\mathbf{v}_h, p_{p,h}, \mathbf{V}_h, \mathbf{U}_h, \boldsymbol{\xi}_h, \boldsymbol{\eta}_h, p_{p,h})$ of (4.1)-(4.2). Assume that the time step condition (4.4) holds, and that the true solution $(\mathbf{v}, p_p, \mathbf{V}, \mathbf{U}, \boldsymbol{\xi}, \boldsymbol{\eta}, p_p)$ satisfies (A.9). Then, the following estimate holds:

$$\begin{aligned}
&\|\mathbf{v} - \mathbf{v}_h\|_{l^\infty(0,T;L^2(\Omega^f))}^2 + \Delta t \|d_t(\mathbf{v} - \mathbf{v}_h)\|_{l^2(0,T;L^2(\Omega^f))}^2 + \Delta t \|d_t(\mathbf{v} - \mathbf{v}_h)\|_{l^2(0,T;L^2(\Gamma))}^2 + \frac{\gamma}{2} \|\mathbf{v} - \mathbf{v}_h\|_{l^2(0,T;H^1(\Omega^f))}^2 \\
&+ \|\mathbf{V} - \mathbf{V}_h\|_{l^\infty(0,T;L^2(\Omega^p))}^2 + \|p_p - p_{p,h}\|_{l^\infty(0,T;L^2(\Omega^p))}^2 + \|p_p - p_{p,h}\|_{l^2(0,T;H^1(\Omega^p))}^2 + \|\boldsymbol{\xi} - \boldsymbol{\xi}_h\|_{l^\infty(0,T;L^2(0,L))}^2 \\
&+ \|\mathbf{U} - \mathbf{U}_h\|_{l^\infty(0,T;H^1(\Omega^p))}^2 + \|\boldsymbol{\eta} - \boldsymbol{\eta}_h\|_{l^\infty(0,T;H^1(0,L))}^2 + \Delta t \|p_f - p_{f,h}\|_{l^2(0,T;L^2(\Omega^f))}^2 \leq Ch^{2k} \mathcal{B}_1(\mathbf{v}, \mathbf{U}, \boldsymbol{\eta}, p_p) \\
&\quad + Ch^{2k+2} \mathcal{B}_2(\mathbf{U}, \mathbf{V}, \boldsymbol{\eta}, \boldsymbol{\xi}, p_p) + C\Delta t^2 \mathcal{B}_3(\mathbf{v}, \mathbf{U}, \mathbf{V}, \boldsymbol{\eta}, \boldsymbol{\xi}, p_p) + Ch^{2s+2} \|p_f\|_{l^2(0,T;H^{s+1}(\Omega^f))}^2,
\end{aligned}$$

where

$$\begin{aligned}
\mathcal{B}_1(\mathbf{v}, \mathbf{U}, \boldsymbol{\eta}, p_p) &= \|\mathbf{v}\|_{l^2(0,T;H^{k+1}(\Omega^f))}^2 + \|p_p\|_{l^2(0,T;H^{k+1}(\Omega^p))}^2 + \|\partial_t \mathbf{v}\|_{l^2(0,T;H^{k+1}(\Omega^f))}^2 + \|\partial_t \mathbf{U}\|_{l^2(0,T;H^{k+1}(\Omega^p))}^2 \\
&\quad + \|\partial_t p_p\|_{l^2(0,T;H^{k+1}(\Omega^p))}^2 + \|\partial_{tt} \boldsymbol{\eta}\|_{l^2(0,T;H^{k+1}(0,L))}^2 + \|p_p\|_{l^\infty(0,T;H^{k+1}(\Omega^p))}^2 + \|\mathbf{U}\|_{l^\infty(0,T;H^{k+1}(\Omega^p))}^2
\end{aligned}$$

$$\begin{aligned}
& + \|\boldsymbol{\eta}\|_{l^\infty(0,T;H^{k+1}(0,L))}^2, \\
\mathcal{B}_2(\boldsymbol{U}, \boldsymbol{V}, \boldsymbol{\eta}, \boldsymbol{\xi}, p_p) &= \|\partial_t p_p\|_{l^2(0,T;H^{k+1}(\Omega^p))}^2 + \|\partial_{tt} \boldsymbol{U}\|_{l^2(0,T;H^{k+1}(\Omega^p))}^2 + \|\partial_{tt} \boldsymbol{\eta}\|_{l^2(0,T;H^{k+1}(0,L))}^2 \\
& + \|\partial_{tt} \boldsymbol{\xi}\|_{l^2(0,T;H^{k+1}(0,L))}^2 + \|p_p\|_{l^\infty(0,T;H^{k+1}(\Omega^p))}^2 + \|\boldsymbol{V}\|_{l^\infty(0,T;H^{k+1}(\Omega^p))}^2 + \|\boldsymbol{\xi}\|_{l^\infty(0,T;H^{k+1}(0,L))}^2 \\
& + \|\partial_t \boldsymbol{U}\|_{l^\infty(0,T;H^{k+1}(\Omega^p))}^2 + \|\partial_t \boldsymbol{\eta}\|_{l^\infty(0,T;H^{k+1}(0,L))}^2 + \|\partial_t \boldsymbol{V}\|_{l^\infty(0,T;H^{k+1}(\Omega^p))}^2 + \|\partial_t \boldsymbol{\xi}\|_{l^\infty(0,T;H^{k+1}(0,L))}^2, \\
\mathcal{B}_3(\boldsymbol{v}, \boldsymbol{U}, \boldsymbol{V}, \boldsymbol{\eta}, \boldsymbol{\xi}, p_p) &= \|\partial_{tt} \boldsymbol{v}\|_{L^2(0,T;L^2(\Omega^f))}^2 + \|\partial_{tt} \boldsymbol{\xi}\|_{L^2(0,T;L^2(0,L))}^2 + \|\partial_t p_p\|_{L^2(0,T;H^1(\Omega^p))}^2 \\
& + \|\partial_{tt} p_p\|_{L^2(0,T;L^2(\Omega^p))}^2 + \|\partial_{tt} \boldsymbol{U}\|_{L^2(0,T;H^1(\Omega^p))}^2 + \|\partial_{ttt} \boldsymbol{U}\|_{L^2(0,T;L^2(\Omega^p))}^2 + \|\partial_{tt} \boldsymbol{V}\|_{L^2(0,T;L^2(\Omega^p))}^2 \\
& + \|\partial_{ttt} \boldsymbol{\eta}\|_{L^2(0,T;L^2(0,L))}^2 + \|\partial_{ttt} \boldsymbol{V}\|_{L^2(0,T;L^2(\Omega^p))}^2 + \|\partial_{ttt} \boldsymbol{\xi}\|_{L^2(0,T;L^2(0,L))}^2 + \|\partial_{tt} \boldsymbol{\eta}\|_{L^2(0,T;H^1(0,L))}^2 \\
& + \|\partial_{tt} \boldsymbol{U}\|_{l^\infty(0,T;L^2(\Omega^p))}^2 + \|\partial_{tt} \boldsymbol{\eta}\|_{l^\infty(0,T;L^2(0,L))}^2 + \|\partial_{tt} \boldsymbol{V}\|_{l^\infty(0,T;L^2(\Omega^p))}^2 + \|\partial_{tt} \boldsymbol{\xi}\|_{l^\infty(0,T;L^2(0,L))}^2 \\
& + \|\partial_t \boldsymbol{V}\|_{l^\infty(0,T;L^2(\Omega^p))}^2 + \|\partial_t \boldsymbol{\xi}\|_{l^\infty(0,T;L^2(0,L))}^2 + \|\partial_t \boldsymbol{U}\|_{l^\infty(0,T;H^1(\Omega^p))}^2 + \|\partial_t \boldsymbol{\eta}\|_{l^\infty(0,T;H^1(0,L))}^2.
\end{aligned}$$

Proof. With the purpose of presenting the proof in a clear manner, we will separate the proof into four main steps.

Step 1: Application of the stability result (4.5) to the truncation error equation. Choose $\boldsymbol{\varphi}_h^f = \delta_f^{n+1}$, $\boldsymbol{\varphi}_h^p = d_t \delta_u^{n+1}$, $\boldsymbol{\phi}_h^p = d_t \delta_v^{n+1}$, and $\psi_h^p = \delta_p^{n+1}$ in equations (5.7) and (5.8). Then, multiplying the equations by Δt , adding them together, summing over $0 \leq n \leq N-1$, and using the stability estimate (4.5) for the truncation error, we get

$$\begin{aligned}
& \mathcal{E}_\delta^N + \frac{\rho_f \Delta t^2}{2} \sum_{n=0}^{N-1} \|d_t \delta_f^{n+1}\|_{L^2(\Omega^f)}^2 + \frac{\rho_m r_m \Delta t^2}{2} \sum_{n=0}^{N-1} \|d_t \delta_f^{n+1} \cdot \boldsymbol{\tau}\|_{L^2(\Gamma)}^2 + \gamma \Delta t \sum_{n=0}^{N-1} \|D(\delta_f^{n+1})\|_{L^2(\Omega^f)}^2 \\
& + \Delta t \sum_{n=0}^{N-1} \|\sqrt{\kappa} \nabla \delta_p^{n+1}\|_{L^2(\Omega^p)}^2 \leq \mathcal{E}_\delta^0 + \Delta t \sum_{n=0}^{N-1} \left(\mathcal{R}_f^{n+1}(\delta_f^{n+1}) + \mathcal{R}_s^{n+1}(d_t \delta_u^{n+1}) + \mathcal{R}_v^{n+1}(d_t \delta_v^{n+1}) + \mathcal{R}_p^{n+1}(\delta_p^{n+1}) \right) \\
& + \Delta t \sum_{n=0}^{N-1} b_f(p_f^{n+1}, \delta_f^{n+1}) - \rho_f \Delta t \sum_{n=0}^{N-1} \int_{\Omega^f} d_t \theta_f^{n+1} \cdot \delta_f^{n+1} d\boldsymbol{x} - \Delta t \sum_{n=0}^{N-1} c_{fp}(\theta_p^n, \delta_f^{n+1}) \\
& - \rho_m r_m \Delta t \sum_{n=0}^{N-1} \int_{\Gamma} (d_t \theta_f^{n+1} \cdot \boldsymbol{\tau})(\delta_f^{n+1} \cdot \boldsymbol{\tau}) d\boldsymbol{x} + \rho_p \Delta t \sum_{n=0}^{N-1} \int_{\Omega^p} d_t \theta_u^{n+1} \cdot d_t \delta_v^{n+1} d\boldsymbol{x} - \rho_p \Delta t \sum_{n=0}^{N-1} \int_{\Omega^p} \theta_v^{n+1/2} \cdot d_t \delta_v^{n+1} d\boldsymbol{x} \\
& + \rho_p \Delta t \sum_{n=0}^{N-1} \int_{\Omega^p} d_t \theta_v^{n+1} \cdot d_t \delta_u^{n+1} d\boldsymbol{x} - \Delta t \sum_{n=0}^{N-1} a_e(\theta_u^{n+1/2}, d_t \delta_u^{n+1}) + \Delta t \sum_{n=0}^{N-1} b_{ep}(\theta_p^{n+1}, d_t \delta_u^{n+1}) \\
& - \Delta t \sum_{n=0}^{N-1} b_{ep}(\delta_p^{n+1}, d_t \theta_u^{n+1}) - \rho_m r_m \sum_{n=0}^{N-1} \Delta t \int_{\Gamma} (\theta_v^{n+1/2} - d_t \theta_u^{n+1}) \cdot d_t \delta_v^{n+1} d\boldsymbol{x} \\
& - \rho_m r_m \Delta t \sum_{n=0}^{N-1} \int_{\Gamma} d_t \theta_v^{n+1} \cdot d_t \delta_u^{n+1} d\boldsymbol{x} - \Delta t \sum_{n=0}^{N-1} a_p(\theta_p^{n+1}, \delta_p^{n+1}) - \Delta t \sum_{n=0}^{N-1} a_m(\theta_u|_{\Gamma}^{n+1/2}, d_t \delta_u|_{\Gamma}^{n+1})
\end{aligned}$$

$$+ \Delta t \sum_{n=0}^{N-1} c_{ep}(\theta_p^{n+1}, d_t \delta_u^{n+1}) - \Delta t \sum_{n=0}^{N-1} c_{ep}(\delta_p^{n+1}, d_t \theta_u^{n+1}) + \Delta t \sum_{n=0}^{N-1} c_{fp}(\delta_p^{n+1}, \theta_f^{n+1}). \quad (5.9)$$

The right hand side of (5.9) consists of consistency error terms $\mathcal{R}_f^{n+1}, \mathcal{R}_s^{n+1}, \mathcal{R}_v^{n+1}$ and \mathcal{R}_p^{n+1} , and mixed truncation and interpolation error terms. We will proceed by bounding the consistency error terms.

Step 2: The consistency error estimate. In this step we will use Lemma 4 of the Appendix to bound the consistency error terms. Referring to the formulation of Lemma 4 and in particular to the terms collected into the expression $\mathcal{A}(\delta_f, \delta_p, \delta_v, \delta_u)$, we observe that the Gronwall Lemma is required to obtain an upper bound.

Step 3: The mixed truncation and interpolation error terms estimate. In this step we estimate the remaining terms of (5.9), which are terms that contain both truncation and interpolation error.

Using Cauchy-Schwartz (A.5), Young's (A.3), Poincaré - Friedrichs (A.6), and Korn's (A.8) inequalities, we have the following:

$$-\rho_f \Delta t \sum_{n=0}^{N-1} \int_{\Omega^f} d_t \theta_f^{n+1} \cdot \delta_f^{n+1} d\mathbf{x} \leq C \Delta t \sum_{n=0}^{N-1} \|\nabla d_t \theta_f^{n+1}\|_{L^2(\Omega^f)}^2 + \frac{\gamma \Delta t}{8} \sum_{n=0}^{N-1} \|D(\delta_f^{n+1})\|_{L^2(\Omega^f)}^2.$$

Furthermore, using Young's (A.3), Korn's (A.8), and trace (A.7) inequalities we can estimate

$$\begin{aligned} -\Delta t \sum_{n=0}^{N-1} \left(a_p(\theta_p^{n+1}, \delta_p^{n+1}) - c_{fp}(\delta_p^{n+1}, \theta_f^{n+1}) + c_{fp}(\theta_p^n, \delta_f^{n+1}) \right) &\leq C \Delta t \sum_{n=0}^{N-1} \|D(\theta_f^{n+1})\|_{L^2(\Omega^f)}^2 \\ &+ \frac{\gamma \Delta t}{8} \sum_{n=0}^{N-1} \|D(\delta_f^{n+1})\|_{L^2(\Omega^f)}^2 + C \Delta t \sum_{n=0}^{N-1} \|\nabla \theta_p^{n+1}\|_{L^2(\Omega^p)}^2 + \frac{\Delta t}{8} \sum_{n=0}^{N-1} \|\sqrt{\kappa} \nabla \delta_p^{n+1}\|_{L^2(\Omega^p)}^2. \end{aligned}$$

In a similar way, we bound

$$-\rho_m r_m \Delta t \sum_{n=0}^{N-1} \int_{\Gamma} (d_t \theta_f^{n+1} \cdot \boldsymbol{\tau})(\delta_f^{n+1} \cdot \boldsymbol{\tau}) dx \leq C \Delta t \sum_{n=0}^{N-1} \|\nabla d_t \theta_f^{n+1}\|_{L^2(\Omega^f)}^2 + \frac{\gamma \Delta t}{8} \sum_{n=0}^{N-1} \|D(\delta_f^{n+1})\|_{L^2(\Omega^f)}^2.$$

The next two terms can be controlled as follows

$$-\Delta t \sum_{n=0}^{N-1} \left(b_{ep}(\delta_p^{n+1}, d_t \theta_u^{n+1}) + c_{ep}(\delta_p^{n+1}, d_t \theta_u^{n+1}) \right) \leq \frac{\Delta t}{8} \sum_{n=0}^{N-1} \|\sqrt{\kappa} \nabla \delta_p^{n+1}\|_{L^2(\Omega^p)}^2 + C \Delta t \sum_{n=0}^{N-1} \|\nabla d_t \theta_u^{n+1}\|_{L^2(\Omega^p)}^2.$$

To bound the pressure term, note that $b_f(p_f^{n+1}, \delta_f^{n+1}) = b_f(p_f^{n+1} - \Pi_h^f p_f^{n+1}, \delta_f^{n+1})$ since $\Pi_h^f p_f^{n+1} \in Q_h^f$ and $\delta_f^{n+1} \in X_h^f$. Hence, using notation $\theta_{fp}^{n+1} = p_f^{n+1} - \Pi_h^f p_f^{n+1}$, we have

$$\Delta t \sum_{n=0}^{N-1} b_f(\theta_{fp}^{n+1}, \delta_f^{n+1}) \leq C \Delta t \sum_{n=0}^{N-1} \|\theta_{fp}^{n+1}\|_{L^2(\Omega^f)}^2 + \frac{\gamma \Delta t}{8} \sum_{n=0}^{N-1} \|D(\delta_f^{n+1})\|_{L^2(\Omega^f)}^2.$$

To estimate the remaining terms, we use discrete integration by parts in time. Using equation (A.2), we have

$$\Delta t \sum_{n=0}^{N-1} b_{ep}(\theta_p^{n+1}, d_t \delta_u^{n+1}) = \alpha \int_{\Omega_p} \theta_p^N \nabla \cdot \delta_u^N d\mathbf{x} - \alpha \Delta t \sum_{n=0}^{N-1} \int_{\Omega^p} d_t \theta_p^{n+1} \nabla \cdot \delta_u^n d\mathbf{x} \leq C_\epsilon \|\theta_p^N\|_{L^2(\Omega^p)}^2$$

$$+ \epsilon \|D(\delta_u^N)\|_{L^2(\Omega^p)}^2 + C\Delta t \sum_{n=0}^{N-1} \|d_t \theta_p^{n+1}\|_{L^2(\Omega^p)}^2 + C\Delta t \sum_{n=0}^{N-1} \|D(\delta_u^n)\|_{L^2(\Omega^p)}^2,$$

and

$$\begin{aligned} \Delta t \sum_{n=0}^{N-1} c_{ep}(\theta_p^{n+1}, d_t \delta_u^{n+1}) &= \alpha \int_{\Gamma} \theta_p^N \delta_u^N \cdot \mathbf{n} dx - \alpha \Delta t \sum_{n=0}^{N-1} \int_{\Gamma} d_t \theta_p^{n+1} \delta_u^n \cdot \mathbf{n} dx \leq C_{\epsilon} \|\nabla \theta_p^N\|_{L^2(\Omega^p)}^2 \\ &+ \epsilon \|D(\delta_u^N)\|_{L^2(\Omega^p)}^2 + C\Delta t \sum_{n=0}^{N-1} \|\nabla d_t \theta_p^{n+1}\|_{L^2(\Omega^p)}^2 + C\Delta t \sum_{n=0}^{N-1} \|D(\delta_u^n)\|_{L^2(\Omega^p)}^2. \end{aligned}$$

Also,

$$\begin{aligned} \rho_p \Delta t \sum_{n=0}^{N-1} \int_{\Omega^p} d_t \theta_u^{n+1} \cdot d_t \delta_v^{n+1} d\mathbf{x} &= \rho_p \int_{\Omega^p} d_t \theta_u^N \cdot \delta_v^N d\mathbf{x} - \rho_p \Delta t \sum_{n=1}^{N-1} \int_{\Omega^p} d_{tt} \theta_u^{n+1} \cdot \delta_v^n d\mathbf{x} \\ &\leq C_{\epsilon} \|d_t \theta_u^N\|_{L^2(\Omega^p)}^2 + \epsilon \|\delta_v^N\|_{L^2(\Omega^p)}^2 + C\Delta t \sum_{n=1}^{N-1} \|d_{tt} \theta_u^{n+1}\|_{L^2(\Omega^p)}^2 + C\Delta t \sum_{n=1}^{N-1} \|\delta_v^n\|_{L^2(\Omega^p)}^2, \\ -\rho_p \Delta t \sum_{n=0}^{N-1} \int_{\Omega^p} \theta_v^{n+1/2} \cdot d_t \delta_v^{n+1} d\mathbf{x} &= -\rho_p \int_{\Omega^p} \theta_v^{N-1/2} \cdot \delta_u^N d\mathbf{x} + \rho_p \Delta t \sum_{n=1}^{N-1} \int_{\Omega^p} \frac{\theta_v^{n+1} - \theta_v^{n-1}}{2\Delta t} \cdot \delta_v^n d\mathbf{x} \\ &\leq C_{\epsilon} (\|\theta_v^N\|_{L^2(\Omega^p)}^2 + \|\theta_v^{N-1}\|_{L^2(\Omega^p)}^2) + \epsilon \|D(\delta_u^N)\|_{L^2(\Omega^p)}^2 + C\Delta t \sum_{n=1}^{N-1} \left\| \frac{\theta_v^{n+1} - \theta_v^{n-1}}{2\Delta t} \right\|_{L^2(\Omega^p)}^2 \\ &\quad + C\Delta t \sum_{n=1}^{N-1} \|D(\delta_u^n)\|_{L^2(\Omega^p)}^2, \end{aligned}$$

and

$$\begin{aligned} \rho_p \Delta t \sum_{n=0}^{N-1} \int_{\Omega^p} d_t \theta_v^{n+1} \cdot d_t \delta_u^{n+1} d\mathbf{x} &= \rho_p \int_{\Omega^p} d_t \theta_v^N \cdot \delta_u^N d\mathbf{x} - \rho_p \Delta t \sum_{n=1}^{N-1} \int_{\Omega^p} d_{tt} \theta_v^{n+1} \cdot \delta_u^n d\mathbf{x} \\ &\leq C_{\epsilon} \|d_t \theta_v^N\|_{L^2(\Omega^p)}^2 + \epsilon \|D(\delta_u^N)\|_{L^2(\Omega^p)}^2 + C\Delta t \sum_{n=1}^{N-1} \|d_{tt} \theta_v^{n+1}\|_{L^2(\Omega^p)}^2 + C\Delta t \sum_{n=1}^{N-1} \|D(\delta_u^n)\|_{L^2(\Omega^p)}^2. \end{aligned}$$

In a similar way,

$$\begin{aligned} \rho_m r_m \Delta t \sum_{n=0}^{N-1} \int_{\Gamma} d_t \theta_u^{n+1} \cdot d_t \delta_v^{n+1} dx &= \rho_m r_m \int_{\Gamma} d_t \theta_u^N \cdot \delta_v^N dx - \rho_m r_m \Delta t \sum_{n=1}^{N-1} \int_{\Gamma} d_{tt} \theta_u^{n+1} \cdot \delta_v^n dx \\ &\leq C_{\epsilon} \|d_t \theta_u^N\|_{L^2(\Gamma)}^2 + \epsilon \|\delta_v^N\|_{L^2(\Gamma)}^2 + C\Delta t \sum_{n=1}^{N-1} \|d_{tt} \theta_u^{n+1}\|_{L^2(\Gamma)}^2 + C\Delta t \sum_{n=1}^{N-1} \|\delta_v^n\|_{L^2(\Gamma)}^2, \end{aligned}$$

and

$$-\rho_m r_m \Delta t \sum_{n=0}^{N-1} \int_{\Gamma} d_t \theta_v^{n+1} \cdot d_t \delta_u^{n+1} dx = -\rho_m r_m \int_{\Gamma} d_t \theta_v^N \cdot \delta_u^N dx + \rho_m r_m \Delta t \sum_{n=1}^{N-1} \int_{\Gamma} d_{tt} \theta_v^{n+1} \cdot \delta_u^n dx$$

$$\leq C_\epsilon \|d_t \theta_v^N\|_{L^2(\Gamma)}^2 + \epsilon \|D(\delta_u^N)\|_{L^2(\Omega^p)}^2 + C\Delta t \sum_{n=1}^{N-1} \|d_{tt} \theta_v^{n+1}\|_{L^2(\Gamma)}^2 + C\Delta t \sum_{n=1}^{N-1} \|D(\delta_u^n)\|_{L^2(\Omega^p)}^2.$$

Furthermore,

$$\begin{aligned} -\rho_m r_m \Delta t \sum_{n=0}^{N-1} \int_{\Gamma} \theta_v^{n+1/2} \cdot d_t \delta_v^{n+1} dx &= -\rho_m r_m \int_{\Gamma} \theta_v^{N-1/2} \cdot \delta_u^N dx + \rho_m r_m \Delta t \sum_{n=1}^{N-1} \int_{\Gamma} \frac{\theta_v^{n+1} - \theta_v^{n-1}}{2\Delta t} \cdot \delta_u^n dx \\ &\leq C_\epsilon (\|\theta_v^N\|_{L^2(\Gamma)}^2 + \|\theta_v^{N-1}\|_{L^2(\Gamma)}^2) + \epsilon \|D(\delta_u^N)\|_{L^2(\Omega^p)}^2 + C\Delta t \sum_{n=1}^{N-1} \left\| \frac{\theta_v^{n+1} - \theta_v^{n-1}}{2\Delta t} \right\|_{L^2(\Gamma)}^2 + C\Delta t \sum_{n=1}^{N-1} \|D(\delta_u^n)\|_{L^2(\Omega^p)}^2, \end{aligned}$$

and

$$\begin{aligned} -\Delta t \sum_{n=0}^{N-1} a_e(\theta_u^{n+1/2}, d_t \delta_u^{n+1}) &= -a_e(\theta_u^{N-1/2}, \delta_u^N) + \Delta t \sum_{n=1}^{N-1} a_e\left(\frac{\theta_u^{n+1} - \theta_u^{n-1}}{2\Delta t}, \delta_u^n\right) \leq C_\epsilon (\|D(\theta_u^N)\|_{L^2(\Omega^p)}^2 \\ &+ \|D(\theta_u^{N-1})\|_{L^2(\Omega^p)}^2) + \epsilon \|D(\delta_u^N)\|_{L^2(\Omega^p)}^2 + C\Delta t \sum_{n=1}^{N-1} \left\| D\left(\frac{\theta_u^{n+1} - \theta_u^{n-1}}{2\Delta t}\right) \right\|_{L^2(\Gamma)}^2 + C\Delta t \sum_{n=1}^{N-1} \|D(\delta_u^n)\|_{L^2(\Omega^p)}^2. \end{aligned}$$

Lastly,

$$\begin{aligned} -\Delta t \sum_{n=0}^{N-1} a_m(\theta_u|_{\Gamma}^{n+1/2}, d_t \delta_u|_{\Gamma}^{n+1}) &= -a_m(\theta_u|_{\Gamma}^{N-1/2}, \delta_u|_{\Gamma}^N) + \Delta t \sum_{n=1}^{N-1} a_m\left(\frac{\theta_u|_{\Gamma}^{n+1} - \theta_u|_{\Gamma}^{n-1}}{2\Delta t}, \delta_u|_{\Gamma}^n\right) \\ &\leq C_\epsilon (\mathcal{M}(\theta_u|_{\Gamma}^N) + \mathcal{M}(\theta_u|_{\Gamma}^{N-1})) + \epsilon \mathcal{M}(\delta_u|_{\Gamma}^N) + C\Delta t \sum_{n=1}^{N-1} \mathcal{M}\left(\frac{\theta_u|_{\Gamma}^{n+1} - \theta_u|_{\Gamma}^{n-1}}{2\Delta t}\right) + C\Delta t \sum_{n=1}^{N-1} \mathcal{M}(\delta_u|_{\Gamma}^n). \end{aligned}$$

Using the estimates from Steps 1-3, we have

$$\begin{aligned} \mathcal{E}_\delta^N + \frac{\rho_f \Delta t^2}{2} \sum_{n=0}^{N-1} \|d_t \delta_f^{n+1}\|_{L^2(\Omega^f)}^2 + \frac{\rho_m r_m \Delta t^2}{2} \sum_{n=0}^{N-1} \|d_t \delta_f^{n+1} \cdot \tau\|_{L^2(\Gamma)}^2 + \frac{\gamma}{2} \Delta t \sum_{n=0}^{N-1} \|D(\delta_f^{n+1})\|_{L^2(\Omega^f)}^2 \\ + \frac{\Delta t}{2} \sum_{n=0}^{N-1} \|\sqrt{\kappa} \nabla \delta_p^{n+1}\|_{L^2(\Omega^p)}^2 \leq \epsilon \left(\|D(\delta_u^N)\|_{L^2(\Omega^p)}^2 + \|\nabla \cdot \delta_u^N\|_{L^2(\Omega^p)}^2 + \|\delta_v^N\|_{L^2(\Omega^p)}^2 + \|\delta_v^N\|_{L^2(\Gamma)}^2 + \mathcal{M}(\delta_u|_{\Gamma}^N) \right) \\ + C\Delta t \sum_{n=0}^{N-1} \left(\|D(\delta_u^n)\|_{L^2(\Omega^p)}^2 + \|\nabla \cdot \delta_u^n\|_{L^2(\Omega^p)}^2 + \|\delta_v^n\|_{L^2(\Omega^p)}^2 + \|\delta_v^n\|_{L^2(\Gamma)}^2 + \mathcal{M}(\delta_u|_{\Gamma}^n) \right) \\ + C\Delta t \sum_{n=0}^{N-1} \left(\|D(\theta_f^{n+1})\|_{L^2(\Omega^f)}^2 + \|\theta_{fp}^{n+1}\|_{L^2(\Omega^f)}^2 + \|\nabla \theta_p^{n+1}\|_{L^2(\Omega^p)}^2 + \|\nabla d_t \theta_f^{n+1}\|_{L^2(\Omega^f)}^2 + \|\nabla d_t \theta_u^{n+1}\|_{L^2(\Omega^p)}^2 \right. \\ \left. + \|d_t \theta_p^{n+1}\|_{L^2(\Omega^p)}^2 + \|\nabla d_t \theta_p^{n+1}\|_{L^2(\Omega^p)}^2 + \|d_{tt} \theta_u^{n+1}\|_{L^2(\Omega^p)}^2 + \|d_{tt} \theta_v^{n+1}\|_{L^2(\Omega^p)}^2 + \|d_{tt} \theta_u^{n+1}\|_{L^2(\Gamma)}^2 + \|d_{tt} \theta_v^{n+1}\|_{L^2(\Gamma)}^2 \right. \\ \left. + \left\| \frac{\theta_v^{n+1} - \theta_v^{n-1}}{2\Delta t} \right\|_{L^2(\Omega^p)}^2 + \left\| \frac{\theta_v^{n+1} - \theta_v^{n-1}}{2\Delta t} \right\|_{L^2(\Gamma)}^2 + \left\| D\left(\frac{\theta_u^{n+1} - \theta_u^{n-1}}{2\Delta t}\right) \right\|_{L^2(\Omega^p)}^2 + \mathcal{M}\left(\frac{\theta_u|_{\Gamma}^{n+1} - \theta_u|_{\Gamma}^{n-1}}{2\Delta t}\right) \right) \\ + C \max_{0 \leq n \leq N} \left(\|\theta_p^n\|_{L^2(\Omega^p)}^2 + \|\nabla \theta_p^n\|_{L^2(\Omega^p)}^2 + \|\theta_v^n\|_{L^2(\Omega^p)}^2 + \|\theta_v^n\|_{L^2(\Gamma)}^2 + \|D(\theta_u^n)\|_{L^2(\Omega^p)}^2 \right) \end{aligned}$$

$$\begin{aligned}
& + \mathcal{M}(\theta_u|_\Gamma^n) + \|d_t \theta_u^n\|_{L^2(\Omega^p)}^2 + \|d_t \theta_u^n\|_{L^2(\Gamma)}^2 + \|d_t \theta_v^n\|_{L^2(\Omega^p)}^2 + \|d_t \theta_v^n\|_{L^2(\Gamma)}^2 \Big) \\
& + C \Delta t^2 \Big(\|\partial_{tt} \mathbf{v}\|_{L^2(0,T;L^2(\Omega^f))}^2 + \|\partial_{tt} \boldsymbol{\xi}\|_{L^2(0,T;L^2(0,L))}^2 + \|\partial_{tt} p_p\|_{L^2(0,T;H^1(\Omega^p))}^2 + \|\partial_{tt} p_p\|_{L^2(0,T;L^2(\Omega^p))}^2 \\
& + \|\partial_{tt} \mathbf{U}\|_{L^2(0,T;H^1(\Omega^p))}^2 + \|\partial_{ttt} \mathbf{U}\|_{L^2(0,T;L^2(\Omega^p))}^2 + \|\partial_{tt} \mathbf{V}\|_{L^2(0,T;L^2(\Omega^p))}^2 + \|\partial_{ttt} \boldsymbol{\eta}\|_{L^2(0,T;L^2(0,L))}^2 \\
& + \|\partial_{ttt} \mathbf{V}\|_{L^2(0,T;L^2(\Omega^p))}^2 + \|\partial_{ttt} \boldsymbol{\xi}\|_{L^2(0,T;L^2(0,L))}^2 + \|\partial_{tt} \boldsymbol{\eta}\|_{L^2(0,T;H^1(0,L))}^2 + \|\partial_{tt} \mathbf{U}\|_{l^\infty(0,T;L^2(\Omega^p))}^2 \\
& + \|\partial_{tt} \boldsymbol{\eta}\|_{l^\infty(0,T;L^2(0,L))}^2 + \|\partial_{tt} \mathbf{V}\|_{l^\infty(0,T;L^2(\Omega^p))}^2 + \|\partial_{tt} \boldsymbol{\xi}\|_{l^\infty(0,T;L^2(0,L))}^2 + \|\partial_t \mathbf{V}\|_{l^\infty(0,T;L^2(\Omega^p))}^2 \\
& + \|\partial_t \boldsymbol{\xi}\|_{l^\infty(0,T;L^2(0,L))}^2 + \|\partial_t \mathbf{U}\|_{l^\infty(0,T;H^1(\Omega^p))}^2 + \|\partial_t \boldsymbol{\eta}\|_{l^\infty(0,T;H^1(0,L))}^2 \Big),
\end{aligned}$$

where $\epsilon > 0$ can be taken small enough. Finally, using Lemma 5, approximation properties (A.10)-(A.15), triangle inequality, and the discrete Gronwall inequality, we prove the desired estimate, except for the pressure error in the fluid domain.

Step 4: analysis of the fluid pressure error. To control this part of the error we proceed as for the stability estimate. More precisely, we start from (5.7) and we rearrange it as follows

$$\begin{aligned}
b_f(\delta_{fp}^{n+1}, \boldsymbol{\varphi}_h^f) &= \rho_f \int_{\Omega^f} d_t \delta_f^{n+1} \cdot \boldsymbol{\varphi}_h^f d\mathbf{x} + \rho_m r_m \int_{\Gamma} (d_t \delta_f^{n+1} \cdot \boldsymbol{\tau})(\boldsymbol{\varphi}_h^f \cdot \boldsymbol{\tau}) d\mathbf{x} + \rho_f \int_{\Omega^f} d_t \theta_f^{n+1} \cdot \boldsymbol{\varphi}_h^f d\mathbf{x} \\
&+ \rho_m r_m \int_{\Gamma} (d_t \theta_f^{n+1} \cdot \boldsymbol{\tau})(\boldsymbol{\varphi}_h^f \cdot \boldsymbol{\tau}) d\mathbf{x} + a_f(e_f^{n+1}, \boldsymbol{\varphi}_h^f) + c_{fp}(e_p^n, \boldsymbol{\varphi}_h^f) + b_f(\theta_{fp}^{n+1}, \boldsymbol{\varphi}_h^f) - \mathcal{R}_f^{n+1}(\boldsymbol{\varphi}_h^f). \quad (5.10)
\end{aligned}$$

For simplicity of notation, let us group the terms on the right hand side of the previous equation,

$$\begin{aligned}
\mathcal{T}(\boldsymbol{\varphi}_h^f) &:= \rho_f \int_{\Omega^f} d_t e_f^{n+1} \cdot \boldsymbol{\varphi}_h^f d\mathbf{x} + \rho_m r_m \int_{\Gamma} (d_t e_f^{n+1} \cdot \boldsymbol{\tau})(\boldsymbol{\varphi}_h^f \cdot \boldsymbol{\tau}) d\mathbf{x} \\
&+ a_f(e_f^{n+1}, \boldsymbol{\varphi}_h^f) + c_{fp}(e_p^n, \boldsymbol{\varphi}_h^f) + b_f(\theta_{fp}^{n+1}, \boldsymbol{\varphi}_h^f)
\end{aligned}$$

Owing to the *inf-sup* condition (4.7) between spaces V_h^f and Q_h^f there exists a positive constant β_f independent of the mesh characteristic size such that,

$$\beta_f \|\delta_{fp}^{n+1}\|_{L^2(\Omega^f)} \leq \sup_{\boldsymbol{\varphi}_h^f \in V_h^f} \frac{\mathcal{T}(\boldsymbol{\varphi}_h^f) - \mathcal{R}_f^{n+1}(\boldsymbol{\varphi}_h^f)}{\|\boldsymbol{\varphi}_h^f\|_{H^1(\Omega^f)}}. \quad (5.11)$$

Moving along the lines of the stability estimate, the following upper bounds for the right hand side of (5.11) hold true, with a generic constant C which depends on the trace (A.7), Korn (A.8) and Poincaré-Friedrichs (A.6) inequalities, as well as on the parameters of the problem,

$$\sup_{\boldsymbol{\varphi}_h^f \in V_h^f} \frac{\mathcal{T}(\boldsymbol{\varphi}_h^f)}{\|\boldsymbol{\varphi}_h^f\|_{H^1(\Omega^f)}} \leq C \Big(\|e_f^{n+1}\|_{H^1(\Omega^f)} + \|e_p^n\|_{H^1(\Omega^p)} + \|\theta_{fp}^{n+1}\|_{L^2(\Omega^f)} + \|d_t e_f^{n+1}\|_{L^2(\Omega^f)} + \|d_t e_f^{n+1}\|_{L^2(\Gamma)} \Big).$$

Using the bounds that will be detailed in Lemma 4 of the Appendix, we get

$$\sup_{\boldsymbol{\varphi}_h^f \in V_h^f} \frac{\mathcal{R}_f^{n+1}(\boldsymbol{\varphi}_h^f)}{\|\boldsymbol{\varphi}_h^f\|_{H^1(\Omega^f)}} \leq C \Big(\|(d_t - \partial_t) \mathbf{v}^{n+1}\|_{L^2(\Omega^f)} + \|(d_t - \partial_t) \mathbf{v}^{n+1} \cdot \boldsymbol{\tau}\|_{L^2(\Gamma)} + \|\nabla(p_p^{n+1} - p_p^n)\|_{L^2(\Omega^p)} \Big).$$

Finally, we replace the previous estimates into (5.11), square all terms, sum up with respect to n and multiply by Δt^2 . There exists a positive constant c small enough such that

$$c\Delta t^2 \sum_{n=0}^{N-1} \|\delta_{fp}^{n+1}\|_{L^2(\Omega^f)}^2 \leq \Delta t^2 \sum_{n=0}^{N-1} \left(\|d_t e_f^{n+1}\|_{L^2(\Omega^f)}^2 + \|d_t e_f^{n+1}\|_{L^2(\Gamma)}^2 + \|e_f^{n+1}\|_{H^1(\Omega^f)}^2 + \|e_p^n\|_{H^1(\Omega^p)}^2 \right. \\ \left. + \|\theta_{fp}^{n+1}\|_{L^2(\Omega^f)}^2 + \|d_t \mathbf{v}^{n+1} - \partial_t \mathbf{v}^{n+1}\|_{L^2(\Omega^f)}^2 + \|d_t \mathbf{v}^{n+1} \cdot \boldsymbol{\tau} - \partial_t \mathbf{v}^{n+1} \cdot \boldsymbol{\tau}\|_{L^2(\Gamma)}^2 + \|\nabla(p_p^{n+1} - p_p^n)\|_{L^2(\Omega^p)}^2 \right).$$

To conclude, combining the triangle inequality with the approximation properties of the discrete pressure space and bounding the right hand side with the available error estimates, we obtain

$$\Delta t \|p_f - p_{f,h}\|_{l^2(0,T;L^2(\Omega^f))}^2 \leq C \left(Ch^{2k} \mathcal{B}_1(\mathbf{v}, \mathbf{U}, \boldsymbol{\eta}, p_p) \right. \\ \left. + Ch^{2k+2} \mathcal{B}_2(\mathbf{v}, \mathbf{U}, \mathbf{V}, \boldsymbol{\eta}, \boldsymbol{\xi}, p_p) + C\Delta t^2 \mathcal{B}_3(\mathbf{v}, \mathbf{U}, \mathbf{V}, \boldsymbol{\eta}, \boldsymbol{\xi}, p_p) + Ch^{2s+2} \|p_f\|_{l^2(0,T;H^{s+1}(\Omega^f))}^2 \right).$$

□

6. Numerical results

The focus of this section is on verification of the results presented in this work and exploration of poroelastic effects in the model. We test the scheme on a classical benchmark problem used for convergence studies of fluid-structure iteration problems [22, 9, 2, 10, 6]. In Example 1, we present the convergence of our scheme in space and time. Furthermore, we validate the necessity of the stability condition (4.4).

In Example 2 we analyze the role of poroelastic effects in blood flow. In particular, we compare our results to the ones obtained using a purely elastic model in Example 2. We distinguish a high permeability and a high storativity case, and present a comparison between the two cases and the purely elastic model.

6.1. Example 1.

We consider the classical test problem used in several works [22, 9, 2, 10] as a benchmark problem for testing the results of fluid-structure interaction algorithms for blood flow. In our case, the flow is driven by the time-dependent pressure data:

$$p_{in}(t) = \begin{cases} \frac{p_{max}}{2} (1 - \cos(\frac{2\pi t}{T_{max}})) & \text{if } t \leq T_{max} \\ 0 & \text{if } t > T_{max}, \end{cases} \quad (6.1)$$

where $p_{max} = 1.3334 \text{ dyne/cm}^2$ and $T_{max} = 0.003 \text{ s}$. For the elastic skeleton, we consider the following equation of linear elasticity:

$$\rho_p \frac{D^2 \mathbf{U}}{Dt^2} + \beta \mathbf{U} - \nabla \cdot \boldsymbol{\sigma}^p = 0.$$

The additional term $\beta \mathbf{U}$ comes from the axially symmetric formulation, accounting for the recoil due to the circumferential strain. Namely, it acts like a spring term, keeping the top and bottom structure displacements connected in 2D, see, e.g., [4, 6, 35]. The values of the parameters used in this example are given in Table 1.

Parameters	Values	Parameters	Values
Radius R (cm)	0.5	Length L (cm)	6
Membrane thickness r_m (cm)	0.02	Poroelastic wall thickness r_p (cm)	0.1
Membrane density ρ_m (g/cm ³)	1.1	Poroelastic wall density ρ_p (g/cm ³)	1.1
Fluid density ρ_f (g/cm ³)	1	Dyn. viscosity μ (g/cm s)	0.035
Lamé coeff. μ_m (dyne/cm ²)	1.07×10^6	Lamé coeff. λ_m (dyne/cm ²)	4.28×10^6
Lamé coeff. μ_p (dyne/cm ²)	1.07×10^6	Lamé coeff. λ_p (dyne/cm ²)	4.28×10^6
Hydraulic conductivity κ (cm ³ s/g)	5×10^{-9}	Mass storativity coeff. s_0 (cm ² /dyne)	5×10^{-6}
Biot-Willis constant α	1	Spring coeff. β (dyne/cm ⁴)	5×10^7

Table 1: Geometry, fluid and structure parameters that are used in Example 1.

Parameters given in Table 1 are within the range of physiological values for blood flow. The problem was solved over the time interval $[0, 0.006]$ s.

In order to verify the convergence estimates from Theorem 2, let the errors between the computed and the reference solution be defined as $e_f = \mathbf{v} - \mathbf{v}_{ref}$, $e_{fp} = p_f - p_{f,ref}$, $e_v = \mathbf{V} - \mathbf{V}_{ref}$, $e_p = p_p - p_{p,ref}$, and $e_u = \mathbf{U} - \mathbf{U}_{ref}$. We start by computing the rates of convergence in time. In order to do so, fix $\Delta x = 0.016$ and define the reference solution to be the one obtained with $\Delta t = 5 \times 10^{-7}$. Table 2 shows the error between the reference solution and solutions obtained with $\Delta t = 10^{-6}, 5 \times 10^{-6}, 10^{-5}$, and 3×10^{-5} for the fluid velocity \mathbf{v} , fluid pressure p_f , pressure in the pores p_p , displacement \mathbf{U} and its velocity \mathbf{V} , respectively.

Δt	$\ e_f\ _{l^\infty(L^2)}$	rate	$\ e_f\ _{l^2(H^1)}$	rate	$\ e_{fp}\ _{l^2(L^2)}$	rate	$\ e_v\ _{l^\infty(L^2)}$	rate
3×10^{-5}	7.6e-1	-	8.8e-2	-	8.9e-1	-	3.0e-2	-
10^{-5}	2.7e-1	0.93	3.1e-2	0.95	3.4e-1	0.88	1.0e-2	0.84
5×10^{-6}	1.3e-1	1.04	1.5e-2	1.03	1.6e-1	1.05	6.0e-3	0.97
10^{-6}	1.5e-2	1.36	1.8e-3	1.32	1.8e-2	1.36	6.9e-4	1.36

Δt	$\ e_p\ _{l^\infty(L^2)}$	rate	$\ e_p\ _{l^2(H^1)}$	rate	$\ e_u\ _{l^\infty(H^1)}$	rate
3×10^{-5}	6.3e-1	-	4.1e-1	-	7.7e-5	-
10^{-5}	2.2e-1	0.95	1.5e-1	0.92	3.0e-5	0.85
5×10^{-6}	1.1e-1	1.04	7.4e-2	1.02	1.5e-5	0.97
10^{-6}	1.2e-2	1.35	8.5e-3	1.34	1.8e-6	1.32

Table 2: Convergence in time.

To study the convergence in space, we take $\Delta t = 5 \times 10^{-6}$ and define the reference solution to be the one obtained with $\Delta x = r_p/14 = 0.007$. Table 3 shows errors between the reference solution and the solutions obtain using $\Delta x = 0.01, 0.0125, 0.0167$ and 0.025 .

To verify the necessity of the time-step condition (4.4), we compute the total energy E^N of the system using different time steps. The time at which E^N is computed is either the time when E^N becomes greater than 10^{250} , or the final time $t^N = 6$ ms. Figure 2 shows the relation of the energy of the system and the time step (left), and the relation between Δx and the critical Δt (right). Indeed, we observe a linear relation between Δx and the critical value of Δt , with the proportionality constant $2.4e-3$. This is less restrictive than the prediction (4.4) from the theory, where the proportionality

Δx	$\ e_f\ _{l^\infty(L^2)}$	rate	$\ e_f\ _{l^2(H^1)}$	rate	$\ e_{fp}\ _{l^2(L^2)}$	rate	$\ e_v\ _{l^\infty(L^2)}$	rate
$r_p/4$	$2.4e-1$	-	$6.8e-1$	-	$3.1e-1$	-	$2.5e-2$	-
$r_p/5$	$1.9e-1$	1.01	$6.2e-1$	0.43	$2.6e-1$	0.83	$1.8e-2$	1.46
$r_p/6$	$1.5e-1$	1.55	$5.3e-1$	0.87	$2.1e-1$	1.12	$1.4e-2$	1.37
$r_p/7$	$1.2e-1$	1.37	$4.5e-1$	1.06	$1.7e-1$	1.32	$1.0e-2$	1.6

Δx	$\ e_p\ _{l^\infty(L^2)}$	rate	$\ e_p\ _{l^2(H^1)}$	rate	$\ e_u\ _{l^\infty(H^1)}$	rate
$r_p/4$	$1.2e+0$	-	$4.0e-1$	-	$3.1e-1$	-
$r_p/5$	$0.9e-1$	0.92	$3.6e-1$	0.47	$2.6e-1$	0.84
$r_p/6$	$0.8e-1$	1.10	$3.2e-1$	0.73	$2.1e-1$	1.08
$r_p/7$	$0.6e-1$	1.34	$2.7e-1$	1.01	$1.8e-1$	1.08

Table 3: Convergence in space.

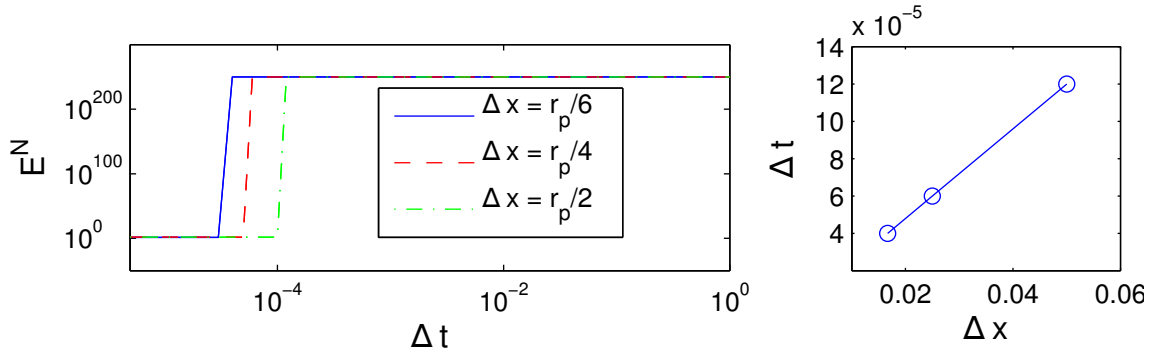


Figure 2: Verification of the time-step condition (4.4). Left: Relation between the total energy of the system and the time step. Right: Relation between Δx and the critical Δt .

constant for the parameters in Table 1 can be estimated as $3.5e-7$, indicating that the scheme enjoys better stability properties than prescribed by (4.4).

6.2. Example 2.

In this example we compare our numerical results to the ones obtained using a purely elastic model for the outer layer of the arterial wall. More precisely, while the fluid and the membrane are modeled as before, we assume there is no fluid contained within the wall, and we model the thick wall using 2D linear elasticity

$$\rho_p \frac{D^2 \mathbf{U}}{Dt^2} + \beta \mathbf{U} - \nabla \cdot \boldsymbol{\sigma}^E = 0 \quad \text{in } \Omega^p(t) \text{ for } t \in (0, T).$$

The problem is solved using an operator-splitting approach performed in the same spirit as in this manuscript.

For the purpose of understanding the poroelastic effects to the structure displacement, we distinguish two cases: the high storativity case $s_0 \gg \kappa$, and the high permeability case $\kappa \gg s_0$. We give a comparison of the results obtained using the elastic model for the outer wall, and poroelastic model using two different values for s_0 , and two different values for κ . The first test case for the poroelastic wall will correspond to the parameters s_0 and κ from Example 1 ($s_0 = 5 \times 10^{-6}$, $\kappa = 5 \times 10^{-9}$), the

second test case will correspond to the increased value of s_0 ($s_0 = 2 \times 10^{-5}, \kappa = 5 \times 10^{-9}$), and the third example to the increased value of κ ($s_0 = 5 \times 10^{-6}, \kappa = 10^{-4}$). Figure 3 shows the pressure pulse (colormap) and velocity streamlines obtained with the two models. The velocity magnitude is shown in Figure 4.

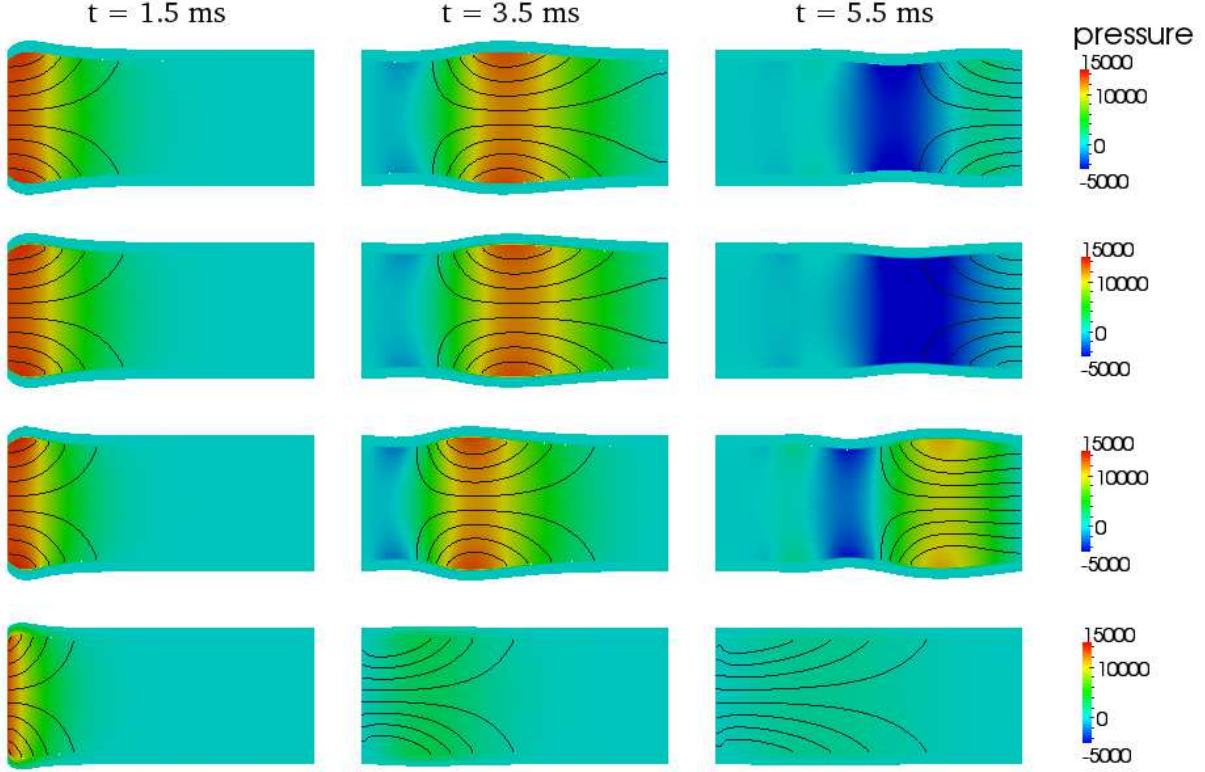


Figure 3: Pressure in the lumen, velocity streamlines, and pressure in the wall at times $t = 1.5$ ms, $t = 3.5$ ms and $t = 5.5$ ms. The outer layer of the arterial wall is model using a elastic model (top), poroelastic model with $s_0 = 5 \times 10^{-6}, \kappa = 5 \times 10^{-9}$ (middle top), poroelastic model with $s_0 = 2 \times 10^{-5}, \kappa = 5 \times 10^{-9}$ (middle bottom), and poroelastic model with $s_0 = 5 \times 10^{-6}, \kappa = 10^{-4}$ (bottom).

To quantify the differences, we compute average quantities on each vertical line S_i^r of the computational mesh Ω^r , corresponding to the position $x_i = i \cdot \Delta x$, where $\Delta x = 0.016$ and $r \in \{f, m\}$. The quantities of interest are membrane displacement, the mean pressure, and the flowrate in the lumen:

$$\bar{p}_f(x_i) = \frac{1}{S_i^f} \int_{S_i^f} p_{f,h} ds, \quad \bar{p}_p(x_i) = \frac{1}{S_i^p} \int_{S_i^p} p_{p,h} ds, \quad Q(x_i) = \int_{S_i^f} \mathbf{v}_h \cdot \mathbf{e}_x ds.$$

Figure 5 shows a comparison between the flowrate in the lumen, membrane displacement, and the mean pressure in the lumen and in the wall, obtained using a poroelastic model and an elastic model. In the high permeability regime the structure displacement is the smallest, while in this case we observe the largest mean pressure in the wall. In the high storativity regime, we observe a delay in the pressure wave propagation speed, and qualitatively different displacement.

Finally, Figure 6 shows the axial and radial velocity profiles at the center of the tube $x = 3$ cm for the three poroelastic test cases, computed at 6 different times. Again, we observe a different in the amplitude, and in the wave propagation speed between the three cases. In particular, there

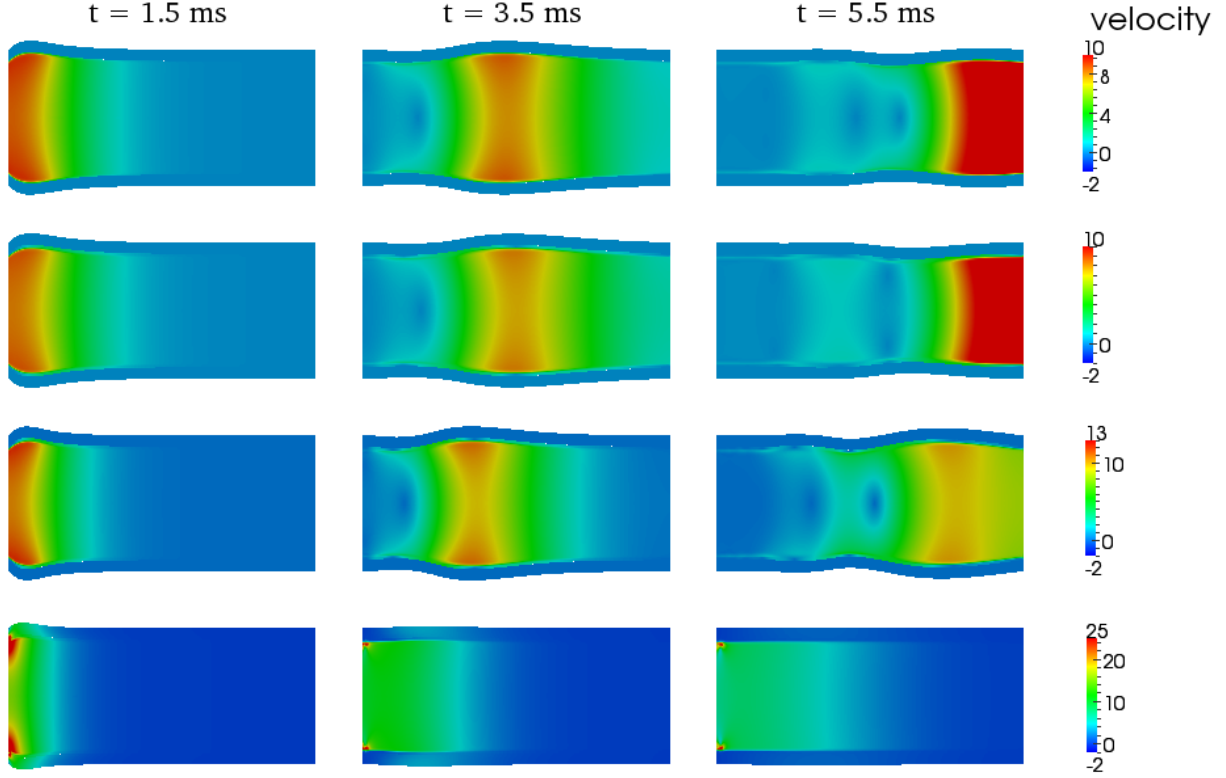


Figure 4: Velocity magnitude at times $t = 1.5$ ms, $t = 3.5$ ms and $t = 5.5$ ms. The outer layer of the arterial wall is model using a elastic model (top), poroelastic model with $s_0 = 5 \times 10^{-6}$, $\kappa = 5 \times 10^{-9}$ (middle top), poroelastic model with $s_0 = 2 \times 10^{-5}$, $\kappa = 5 \times 10^{-9}$ (middle bottom), and poroelastic model with $s_0 = 5 \times 10^{-6}$, $\kappa = 10^{-4}$ (bottom).

is a significant difference in the high permeability regime, where the amplitude of axial velocity is much smaller than in the other two cases, and the vertical velocity is always positive due to the high dissipation in the structure.

7. Conclusion

The focus of this paper is on modeling and implementation of a fluid-poroelastic structure interaction problem. In particular, we study the interaction between the fluid a multilayered wall, where the wall consists of a thin membrane, and a thick poroelastic medium. We proposed an explicit numerical algorithm based on the Lie operator splitting scheme. An alternative discrete problem formulation based on Nitsche's method for the enforcement of the interface conditions is under study. This new method can accommodate a mixed formulation for the Darcy's equations.

We prove the conditional stability of the algorithm, and derive error estimates. Stability and convergence results are validated by the numerical simulations. The drawback of the scheme is that it requires pressure formulation for the Darcy equation. Concerning the application of the scheme to blood flow in arteries, we test numerically the porous effects in the wall, comparing results obtained with different coefficients to the ones obtained using a purely elastic model. We observe different behavior depending on the storativity or permeability dominant regime.

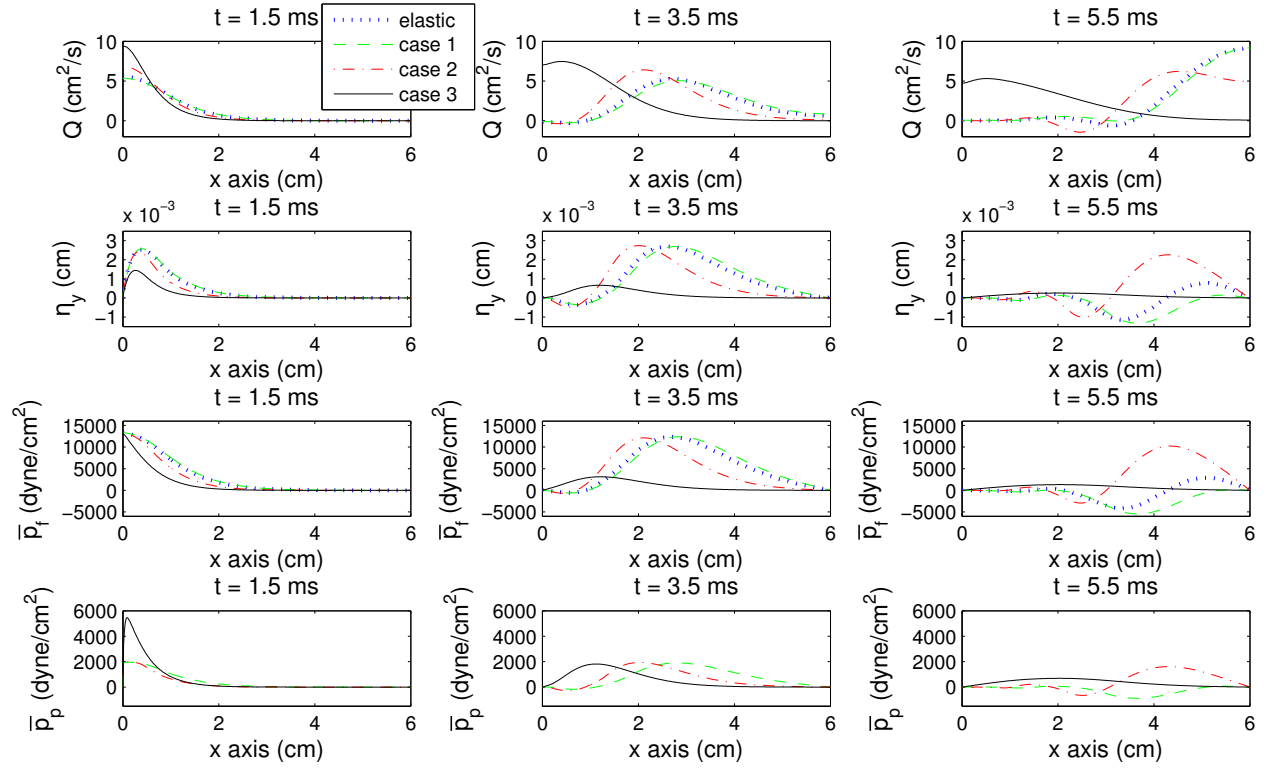


Figure 5: From top to bottom: Flowrate, radial displacement of the membrane, mean pressure in the lumen, and mean pressure in the pores. Results were obtained using the elastic model (dotted line), and poroelastic model with the following parameters: case 1 ($s_0 = 5 \times 10^{-6}$, $\kappa = 5 \times 10^{-9}$; dashed line), case 2 ($s_0 = 2 \times 10^{-5}$, $\kappa = 5 \times 10^{-9}$; dash dot line), and case 3 ($s_0 = 5 \times 10^{-6}$, $\kappa = 1 \times 10^{-4}$; solid line).

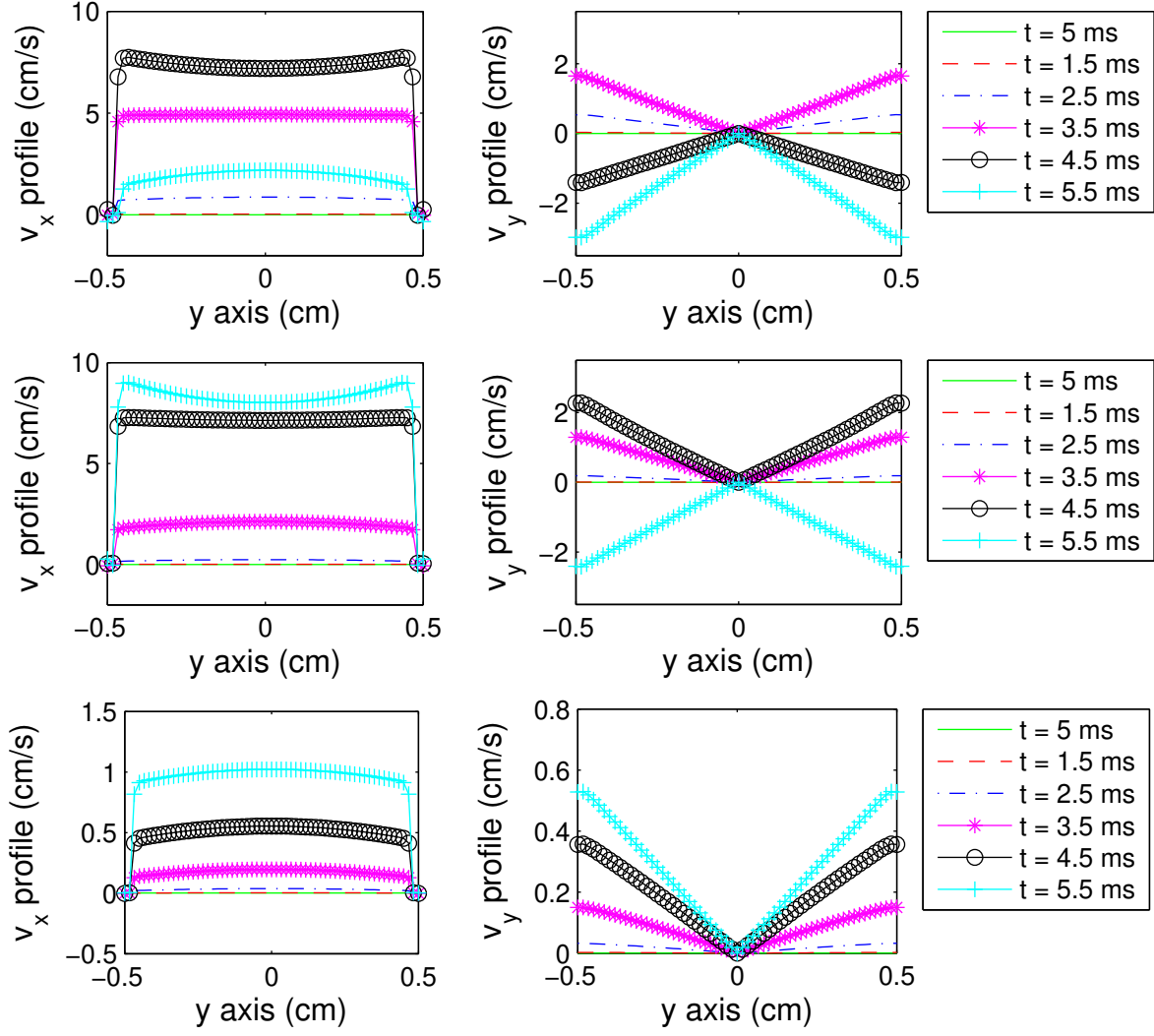


Figure 6: Fluid velocity profiles at six different times obtained using a poroelastic model with coefficients $s_0 = 5 \times 10^{-6}$, $\kappa = 5 \times 10^{-9}$ (top), $s_0 = 2 \times 10^{-6}$, $\kappa = 5 \times 10^{-9}$ (middle), and $s_0 = 5 \times 10^{-6}$, $\kappa = 10^{-4}$ (bottom).

Appendix A. Auxiliary results

We collect in this section some auxiliary results and proofs that complement the stability and convergence analysis of the proposed scheme. They are either a consequence of the standard theory of the finite element method or they follow from basic results of approximation theory. For the reader's convenience we report them separately from the main body of the manuscript.

For any real numbers a, b the following algebraic identities are satisfied:

$$(a - b)a = \frac{1}{2}a^2 - \frac{1}{2}b^2 + \frac{1}{2}(a - b)^2, \quad (\text{A.1})$$

$$\Delta t \sum_{n=0}^{N-1} a^{n+1} d_t b^{n+1} = a^N b^N - \Delta t \sum_{n=0}^{N-1} d_t a^{n+1} b^n - a^0 b^0, \quad (\text{A.2})$$

and for non-negative real numbers a, b , and $\epsilon > 0$

$$ab \leq \frac{a^2}{2\epsilon} + \frac{\epsilon b^2}{2}. \quad (\text{A.3})$$

Lemma 1. *Given the functional spaces $V_h^f \subset V^f, Q_h^f \subset Q^f, V_h^p \subset V^p$ and $Q_h^p \subset Q^p$, the following inequalities hold true:*

- *local trace-inverse inequality:*

$$\|\psi_h\|_{L^2(\Gamma)}^2 \leq \frac{C_{TI}}{h} \|\psi_h\|_{L^2(\Omega^p)}^2, \quad \forall \psi_h \in Q_h^p; \quad (\text{A.4})$$

- *Cauchy-Schwarz inequality:*

$$\left| \int_{\Omega^{f/p}} \mathbf{v} \cdot \mathbf{u} d\mathbf{x} \right| \leq \|\mathbf{v}\|_{L^2(\Omega^{f/p})} \|\mathbf{u}\|_{L^2(\Omega^{f/p})} \quad \forall \mathbf{v}, \mathbf{u} \in V^{f/p}; \quad (\text{A.5})$$

- *Poincaré - Friedrichs inequality:*

$$\|\mathbf{v}\|_{L^2(\Omega^{f/p})} \leq C_{PF} \|\nabla \mathbf{v}\|_{L^2(\Omega^{f/p})} \quad \forall \mathbf{v} \in V^{f/p}; \quad (\text{A.6})$$

- *trace inequality:*

$$\|\mathbf{v}\|_{L^2(\Gamma)} \leq C_T \|\mathbf{v}\|_{L^2(\Omega^{f/p})}^{1/2} \|\nabla \mathbf{v}\|_{L^2(\Omega^{f/p})}^{1/2} \quad \forall \mathbf{v} \in V^{f/p}; \quad (\text{A.7})$$

- *Korn inequality:*

$$\|\nabla \mathbf{v}\|_{L^2(\Omega^{f/p})} \leq C_K \|D(\mathbf{v})\|_{L^2(\Omega^{f/p})} \quad \forall \mathbf{v} \in V^{f/p}. \quad (\text{A.8})$$

Here constants C_{PF}, C_T and C_K depend on the domain Ω , and constant C_{TI} depends on the angles in the finite element mesh.

Our analysis holds provided that the following regularity assumptions are satisfied by the exact solution of the problem.

Assumption 1. Let X be a Banach space, and $(0, T) \subset \mathbb{R}$ a time interval. We define the L^2 -space of functions $u : (0, T) \rightarrow X$ by

$$L^2(0, T; X) = \{u \mid u \text{ is measurable and } \int_0^T \|u\|_X^2 dt < \infty\},$$

and L^∞ -space by

$$L^\infty(0, T; X) = \{u \mid u \text{ is measurable and } \|u\|_X \text{ is essentially bounded}\}.$$

Then, the Sobolev space $W^{k,2}(0, T; X) = H^k(0, T; X)$ is defined to be the set of all functions $u \in L^2(0, T; X)$ whose distributional time derivative $D_t^\alpha u$ belongs to $L^2(0, T; X)$, for every α with $|\alpha| \leq k$. We assume that the weak solution of (3.4), complemented by the prescribed, interface, boundary and initial conditions, is such that

$$\begin{aligned} \mathbf{v} &\in H^1(0, T; H^{k+1}(\Omega^f)) \cap H^2(0, T; L^2(\Omega^f)), \\ p_f &\in L^2(0, T; H^{s+1}(\Omega^f)), \\ \boldsymbol{\eta} &\in L^\infty(0, T; H^{k+1}(0, L)) \cap H^2(0, T; H^{k+1}(0, L)) \cap H^3(0, T; L^2(0, L)), \\ \boldsymbol{\xi} &\in L^\infty(0, T; H^{k+1}(0, L)) \cap H^2(0, T; H^{k+1}(0, L)) \cap H^3(0, T; L^2(0, L)), \\ \partial_t \boldsymbol{\xi} &\in L^\infty(0, T; H^{k+1}(0, L)), \\ \partial_{tt} \boldsymbol{\xi} &\in L^\infty(0, T; L^2(0, L)), \\ \mathbf{U} &\in L^\infty(0, T; H^{k+1}(\Omega^p)) \cap H^2(0, T; H^{k+1}(\Omega^p)) \cap H^3(0, T; L^2(\Omega^p)), \\ \mathbf{V} &\in L^\infty(0, T; H^{k+1}(\Omega^p)) \cap H^3(0, T; L^2(\Omega^p)), \\ \partial_t \mathbf{V} &\in L^\infty(0, T; H^{k+1}(\Omega^p)), \\ \partial_{tt} \mathbf{V} &\in L^\infty(0, T; L^2(\Omega^p)), \\ p_p &\in L^\infty(0, T; H^{k+1}(\Omega^p)) \cap H^1(0, T; H^{k+1}(\Omega^p)) \cap H^2(0, T; L^2(\Omega^p)). \end{aligned} \tag{A.9}$$

Then, our finite element spaces satisfy the approximation properties reported below.

Lemma 2. Let S_h be an orthogonal projection operator with respect to $a_f(\cdot, \cdot)$, onto X_h^f , defined in (5.2), P_h be the Lagrangian interpolation operator onto V_h^p , and let $\Pi_h^{f/p}$ be the L^2 -orthogonal projections onto $Q_h^{f/p}$. Using piecewise polynomials of degree k and s , we have:

$$\|\mathbf{v} - S_h \mathbf{v}\|_{H^1(\Omega^f)} \leq Ch^k \|\mathbf{v}\|_{H^{k+1}(\Omega^f)}, \tag{A.10}$$

$$\|p_f - \Pi_h^f p_f\|_{L^2(\Omega^f)} \leq Ch^{s+1} \|p_f\|_{H^{s+1}(\Omega^f)}, \tag{A.11}$$

$$\|\mathbf{U} - P_h \mathbf{U}\|_{L^2(\Omega^p)} \leq Ch^{k+1} \|\mathbf{U}\|_{H^{k+1}(\Omega^p)}, \tag{A.12}$$

$$\|\mathbf{U} - P_h \mathbf{U}\|_{H^1(\Omega^p)} \leq Ch^k \|\mathbf{U}\|_{H^{k+1}(\Omega^p)}, \tag{A.13}$$

$$\|p_p - \Pi_h^p p_p\|_{L^2(\Omega^p)} \leq Ch^{k+1} \|p_p\|_{H^{k+1}(\Omega^p)}, \tag{A.14}$$

$$\|p_p - \Pi_h^p p_p\|_{H^1(\Omega^p)} \leq Ch^k \|p_p\|_{H^{k+1}(\Omega^p)}. \tag{A.15}$$

Finally, since $P_h|_\Gamma$ is a Lagrangian interpolant, we obtain:

$$\|\mathbf{U} - P_h \mathbf{U}\|_{L^2(\Gamma)} = \|\boldsymbol{\eta} - (P_h|_\Gamma) \boldsymbol{\eta}\|_{L^2(\Gamma)} \leq Ch^{k+1} \|\boldsymbol{\eta}\|_{H^{k+1}(\Gamma)}, \tag{A.16}$$

$$\|\mathbf{U} - P_h \mathbf{U}\|_{H^1(\Gamma)} = \|\boldsymbol{\eta} - (P_h|_\Gamma) \boldsymbol{\eta}\|_{H^1(\Gamma)} \leq Ch^k \|\boldsymbol{\eta}\|_{H^{k+1}(\Gamma)}, \tag{A.17}$$

$$\|\mathbf{V} - P_h \mathbf{V}\|_{L^2(\Gamma)} = \|\boldsymbol{\xi} - (P_h|_\Gamma) \boldsymbol{\xi}\|_{L^2(\Gamma)} \leq Ch^{k+1} \|\boldsymbol{\xi}\|_{H^{k+1}(\Gamma)}. \tag{A.18}$$

Proof. The proof of (A.10) follows from [24]. Precisely, since we assumed that V_h^f and Q_h^f satisfy the discrete *inf-sup* condition (4.7), there exists a constant C such that for $\mathbf{v} \in V_h^f$, with $\nabla \cdot \mathbf{v} = 0$, we have

$$\inf_{\mathbf{x}_h \in X_h^f} \|\mathbf{v} - \mathbf{x}_h\|_{H^1(\Omega^f)} \leq C \inf_{\mathbf{v}_h \in V_h^f} \|\mathbf{v} - \mathbf{v}_h\|_{H^1(\Omega^f)}.$$

For the proof of the other inequalities, see [15]. □

Lemma 3. (*Consistency errors:*) *The following inequalities hold:*

$$\begin{aligned} \Delta t \sum_{n=0}^{N-1} \|d_t \boldsymbol{\varphi}^{n+1} - \partial_t \boldsymbol{\varphi}^{n+1}\|_{L^2(\Omega)}^2 &\leq C \Delta t^2 \|\partial_{tt} \boldsymbol{\varphi}\|_{L^2(0,T;L^2(\Omega))}^2, \\ \Delta t \sum_{n=1}^{N-1} \|d_{tt} \boldsymbol{\varphi}^{n+1} - \partial_t(d_t \boldsymbol{\varphi}^{n+1})\|_{L^2(\Omega)}^2 &\leq C \Delta t^2 \|\partial_{ttt} \boldsymbol{\varphi}\|_{L^2(0,T;L^2(\Omega))}^2, \\ \Delta t^3 \sum_{n=1}^{N-1} \|d_{tt} \boldsymbol{\varphi}^{n+1}\|_{L^2(\Omega)}^2 &\leq C \Delta t^2 \|\partial_{tt} \boldsymbol{\varphi}\|_{L^2(0,T;L^2(\Omega))}^2, \\ \Delta t \sum_{n=0}^{N-1} \|\nabla(\boldsymbol{\varphi}^{n+1} - \boldsymbol{\varphi}^n)\|_{L^2(\Omega)}^2 &\leq C \Delta t^2 \|\partial_t \boldsymbol{\varphi}\|_{L^2(0,T;H^1(\Omega))}^2, \\ \Delta t \sum_{n=0}^{N-1} \|\nabla(d_t \boldsymbol{\varphi}^{n+1} - \partial_t \boldsymbol{\varphi}^{n+1})\|_{L^2(\Omega)}^2 &\leq C \Delta t^2 \|\partial_{tt} \boldsymbol{\varphi}\|_{L^2(0,T;H^1(\Omega))}^2, \\ \Delta t^3 \sum_{n=1}^{N-1} \|D(d_{tt} \boldsymbol{\varphi}^{n+1})\|_{L^2(\Omega)}^2 &\leq C \Delta t^2 \|\partial_{tt} \boldsymbol{\varphi}\|_{L^2(0,T;H^1(\Omega))}^2, \\ \Delta t^3 \sum_{n=1}^{N-1} \mathcal{M}(d_{tt} \boldsymbol{\eta}^{n+1}) &\leq C \Delta t^2 \|\partial_{tt} \boldsymbol{\eta}\|_{L^2(0,T;H^1(0,L))}^2, \\ \|d_t \boldsymbol{\varphi}^N - \partial_t \boldsymbol{\varphi}^N\|_{L^2(\Omega)}^2 &\leq \Delta t^2 \max_{0 \leq n \leq N} \|\partial_{tt} \boldsymbol{\varphi}^n\|_{L^2(\Omega)}^2 = \Delta t^2 \|\partial_{tt} \boldsymbol{\varphi}\|_{l^\infty(0,T;L^2(\Omega))}^2, \\ \Delta t^2 \|d_t \boldsymbol{\varphi}^N\|_{L^2(\Omega)}^2 &\leq \Delta t^2 \max_{0 \leq n \leq N} \|\partial_t \boldsymbol{\varphi}^n\|_{L^2(\Omega)}^2 = \Delta t^2 \|\partial_t \boldsymbol{\varphi}\|_{l^\infty(0,T;L^2(\Omega))}^2, \\ \Delta t^2 \|D(d_t \boldsymbol{\varphi}^N)\|_{L^2(\Omega)}^2 &\leq \Delta t^2 \max_{0 \leq n \leq N} \|\partial_t D(\boldsymbol{\varphi}^n)\|_{L^2(\Omega)}^2 = \Delta t^2 \|\partial_t \boldsymbol{\varphi}\|_{l^\infty(0,T;H^1(\Omega))}^2, \\ \Delta t^2 \mathcal{M}(d_t \boldsymbol{\eta}^N) &\leq \Delta t^2 \max_{0 \leq n \leq N} \mathcal{M}(\partial_t \boldsymbol{\eta}^n) = \Delta t^2 \|\partial_t \boldsymbol{\eta}\|_{l^\infty(0,T;H^1(0,L))}^2. \end{aligned}$$

Proof. We will prove the first three inequalities. The proofs for other inequalities are similar. Using Cauchy-Schwartz inequality, we have

$$\begin{aligned} \Delta t \sum_{n=0}^{N-1} \|d_t \boldsymbol{\varphi}^{n+1} - \partial_t \boldsymbol{\varphi}^{n+1}\|_{L^2(\Omega)}^2 &= \Delta t \sum_{n=0}^{N-1} \int_{\Omega} \left| \frac{1}{\Delta t} \int_{t^n}^{t^{n+1}} (t - t^n) \partial_{tt} \boldsymbol{\varphi}(t) dt \right|^2 dx \\ &\leq \frac{1}{\Delta t} \int_{\Omega} \sum_{n=0}^{N-1} \left(\int_{t^n}^{t^{n+1}} |t - t^n|^2 dt \int_{t^n}^{t^{n+1}} |\partial_{tt} \boldsymbol{\varphi}|^2 dt \right) dx \leq C \Delta t^2 \int_{\Omega} \int_0^T |\partial_{tt} \boldsymbol{\varphi}|^2 dt dx \leq C \Delta t^2 \|\boldsymbol{\varphi}\|_{L^2(0,T;L^2(\Omega))}^2. \end{aligned}$$

To prove the next two inequalities, we integrate by parts twice, and use Cauchy-Schwartz inequality:

$$\begin{aligned}
\Delta t \sum_{n=1}^{N-1} \|d_{tt}\varphi^{n+1} - \partial_t(d_t\varphi^{n+1})\|_{L^2(\Omega)}^2 &= \Delta t \sum_{n=0}^{N-1} \left\| \frac{1}{\Delta t^2} \left(\int_{t^n}^{t^{n+1}} (t-t^n) \partial_{tt}\varphi dt + \int_{t^n}^{t^{n-1}} (t-t^{n-1}) \partial_{tt}\varphi dt \right) \right\|_{L^2(\Omega)}^2 \\
&= \frac{1}{\Delta t^3} \sum_{n=0}^{N-1} \left\| \left(\frac{\Delta t^2}{2} \int_{t^n}^{t^{n+1}} \partial_{ttt}\varphi dt - \int_{t^n}^{t^{n+1}} \frac{(t-t^n)^2}{2} \partial_{ttt}\varphi dt - \int_{t^n}^{t^{n-1}} \frac{(t-t^{n-1})^2}{2} \partial_{ttt}\varphi dt \right) \right\|_{L^2(\Omega)}^2 \\
&\leq \frac{1}{\Delta t^3} \int_{\Omega} \sum_{n=0}^{N-1} \left(\frac{\Delta t^4}{4} \left| \int_{t^n}^{t^{n+1}} \partial_{ttt}\varphi dt \right|^2 + \left| \int_{t^n}^{t^{n+1}} \frac{(t-t^n)^2}{2} \partial_{ttt}\varphi dt \right|^2 + \left| \int_{t^n}^{t^{n-1}} \frac{(t-t^{n-1})^2}{2} \partial_{ttt}\varphi dt \right|^2 \right) dx \\
&\leq \frac{1}{\Delta t^3} \int_{\Omega} \sum_{n=0}^{N-1} \left(\frac{\Delta t^5}{4} \int_{t^n}^{t^{n+1}} |\partial_{ttt}\varphi|^2 dt + \frac{\Delta t^5}{10} \int_{t^n}^{t^{n+1}} |\partial_{ttt}\varphi|^2 dt + \frac{\Delta t^5}{10} \int_{t^n}^{t^{n-1}} |\partial_{ttt}\varphi|^2 dt \right) dx \\
&\leq C \Delta t^2 \|\partial_{ttt}\varphi\|_{L^2(0,T;L^2(\Omega))}^2
\end{aligned}$$

Finally,

$$\begin{aligned}
\Delta t^3 \sum_{n=1}^{N-1} \|d_{tt}\varphi^{n+1}\|_{L^2(\Omega)}^2 &= \frac{1}{\Delta t} \sum_{n=0}^{N-1} \left\| \left(\int_{t^n}^{t^{n+1}} \partial_t\varphi dt + \int_{t^n}^{t^{n-1}} \partial_t\varphi dt \right) \right\|_{L^2(\Omega)}^2 \\
&= \frac{1}{\Delta t} \sum_{n=0}^{N-1} \left\| \left(\int_{t^n}^{t^{n+1}} (t-t^{n+1}) \partial_{tt}\varphi dt + \int_{t^n}^{t^{n-1}} (t-t^{n-1}) \partial_{tt}\varphi dt \right) \right\|_{L^2(\Omega)}^2 \\
&\leq \frac{1}{\Delta t} \int_{\Omega} \sum_{n=0}^{N-1} \left(\int_{t^n}^{t^{n+1}} |t-t^{n+1}|^2 dt \int_{t^n}^{t^{n+1}} |\partial_{tt}\varphi|^2 dt + \int_{t^n}^{t^{n-1}} |t-t^{n-1}|^2 dt \int_{t^n}^{t^{n-1}} |\partial_{tt}\varphi|^2 dt \right) dx \\
&\leq C \Delta t^2 \int_{\Omega} \int_0^T |\partial_{tt}\varphi|^2 dt dx \leq C \Delta t^2 \|\partial_{tt}\varphi\|_{L^2(0,T;L^2(\Omega))}^2.
\end{aligned}$$

□

Lemma 4. *The following estimate holds:*

$$\begin{aligned}
\Delta t \sum_{n=0}^{N-1} (\mathcal{R}_f^{n+1}(\delta_f^{n+1}) + \mathcal{R}_s^{n+1}(\delta_s^{n+1}) + \mathcal{R}_v^{n+1}(\delta_v^{n+1}) + \mathcal{R}_p^{n+1}(\delta_p^{n+1})) &\leq C \Delta t^2 \left(\|\partial_{tt}\mathbf{v}\|_{L^2(0,T;L^2(\Omega^f))}^2 \right. \\
&+ \|\partial_{tt}\boldsymbol{\xi}\|_{L^2(0,T;L^2(0,L))}^2 + \|\partial_t p_p\|_{L^2(0,T;H^1(\Omega^p))}^2 + \|\partial_{tt} p_p\|_{L^2(0,T;L^2(\Omega^p))}^2 + \|\partial_{tt}\mathbf{U}\|_{L^2(0,T;H^1(\Omega^p))}^2 \\
&+ \|\partial_{ttt}\mathbf{U}\|_{L^2(0,T;L^2(\Omega^p))}^2 + \|\partial_{tt}\mathbf{V}\|_{L^2(0,T;L^2(\Omega^p))}^2 + \|\partial_{ttt}\boldsymbol{\eta}\|_{L^2(0,T;L^2(0,L))}^2 + \|\partial_{ttt}\mathbf{V}\|_{L^2(0,T;L^2(\Omega^p))}^2 \\
&+ \|\partial_{ttt}\boldsymbol{\xi}\|_{L^2(0,T;L^2(0,L))}^2 + \|\partial_{tt}\boldsymbol{\eta}\|_{L^2(0,T;H^1(0,L))}^2 + \|\partial_{tt}\mathbf{U}\|_{l^\infty(0,T;L^2(\Omega^p))} + \|\partial_{tt}\boldsymbol{\eta}\|_{l^\infty(0,T;L^2(0,L))} \\
&+ \|\partial_{tt}\mathbf{V}\|_{l^\infty(0,T;L^2(\Omega^p))} + \|\partial_{tt}\boldsymbol{\xi}\|_{l^\infty(0,T;L^2(0,L))} + \|\partial_t\mathbf{V}\|_{l^\infty(0,T;L^2(\Omega^p))} + \|\partial_t\boldsymbol{\xi}\|_{l^\infty(0,T;L^2(0,L))} \\
&\left. + \|\partial_t\mathbf{U}\|_{l^\infty(0,T;H^1(\Omega^p))} + \|\partial_t\boldsymbol{\eta}\|_{l^\infty(0,T;H^1(0,L))} \right) + \mathcal{A}(\delta_f, \delta_p, \delta_v, \delta_s),
\end{aligned}$$

where

$$\mathcal{A}(\delta_f, \delta_p, \delta_v, \delta_s) = \frac{\gamma \Delta t}{4} \sum_{n=0}^{N-1} \|D(\delta_f^{n+1})\|_{L^2(\Omega^f)}^2 + \frac{\Delta t}{4} \sum_{n=0}^{N-1} \|\sqrt{\kappa} \nabla \delta_p^{n+1}\|_{L^2(\Omega^p)}^2 + \epsilon \left(\|\delta_v^N\|_{L^2(\Omega^p)}^2 + \|\delta_v|_{\Gamma}^N\|_{L^2(0,L)}^2 \right)$$

$$\begin{aligned}
& + \|D(\delta_s^N)\|_{L^2(\Omega^p)}^2 + \|\nabla \cdot \delta_s^N\|_{L^2(\Omega^p)}^2 + \mathcal{M}(\delta_s|_\Gamma^N) \Big) + C\Delta t \sum_{n=1}^{N-1} \left(\|\delta_v^n\|_{L^2(\Omega^p)}^2 + \|\delta_v|_\Gamma^n\|_{L^2(0,L)}^2 \right. \\
& \left. + \|\delta_s^n\|_{L^2(\Omega^p)}^2 + \|D(\delta_s^n)\|_{L^2(\Omega^p)}^2 + \|\nabla \cdot \delta_s^n\|_{L^2(\Omega^p)}^2 + \|\delta_s|_\Gamma^n\|_{L^2(\Gamma)}^2 + \mathcal{M}(\delta_s|_\Gamma^n) \right).
\end{aligned}$$

Proof. Using the formula for integration by parts in time (A.2), the consistency errors are bounded as follows:

$$\begin{aligned}
& \bullet \Delta t \sum_{n=0}^{N-1} \mathcal{R}_f^{n+1}(\delta_f^{n+1}) \leq C\Delta t \sum_{n=0}^{N-1} \|d_t \mathbf{v}^{n+1} - \partial_t \mathbf{v}^{n+1}\|_{L^2(\Omega^f)}^2 + C\Delta t \sum_{n=0}^{N-1} \|\nabla(p_p^{n+1} - p_p^n)\|_{L^2(\Omega^p)}^2 \\
& \quad + C\Delta t \sum_{n=0}^{N-1} \|d_t \mathbf{v}^{n+1} \cdot \boldsymbol{\tau} - \partial_t \mathbf{v}^{n+1} \cdot \boldsymbol{\tau}\|_{L^2(\Gamma)}^2 + \frac{\gamma\Delta t}{4} \sum_{n=0}^{N-1} \|D(\delta_f^{n+1})\|_{L^2(\Omega^f)}^2, \\
& \bullet \Delta t \sum_{n=0}^{N-1} \mathcal{R}_p^{n+1}(\delta_p^{n+1}) \leq C\Delta t \sum_{n=0}^{N-1} \|d_t p_p^{n+1} - \partial_t p_p^{n+1}\|_{L^2(\Omega^p)}^2 + \frac{\Delta t}{4} \sum_{n=0}^{N-1} \|\sqrt{\kappa} \nabla \delta_p^{n+1}\|_{L^2(\Omega^p)}^2 \\
& \quad + C\Delta t \sum_{n=0}^{N-1} \|\nabla(d_t \mathbf{U}^{n+1} - \partial_t \mathbf{U}^{n+1})\|_{L^2(\Omega^p)}^2, \\
& \bullet \Delta t \sum_{n=0}^{N-1} \mathcal{R}_v^{n+1}(d_t \delta_v^{n+1}) = -\rho_p \int_{\Omega^p} (d_t \mathbf{U}^N - \partial_t \mathbf{U}^N) \cdot \delta_v^N d\mathbf{x} - \frac{\rho_p}{2} \Delta t \int_{\Omega^p} d_t \mathbf{V}^N \cdot \delta_v^N d\mathbf{x} \\
& \quad + \rho_p \Delta t \sum_{n=1}^{N-1} \int_{\Omega^p} (d_{tt} \mathbf{U}^{n+1} - \partial_t(d_t \mathbf{U}^{n+1})) \cdot \delta_v^n d\mathbf{x} + \frac{\rho_p}{2} \Delta t^2 \sum_{n=1}^{N-1} \int_{\Omega^p} d_{tt} \mathbf{V}^{n+1} \cdot \delta_v^n d\mathbf{x} \\
& \quad - \rho_m r_m \int_{\Gamma} (d_t \mathbf{U}^N - \partial_t \mathbf{U}^N) \cdot \delta_v^N d\mathbf{x} + \rho_m r_m \Delta t \sum_{n=1}^{N-1} \int_{\Gamma} (d_{tt} \mathbf{U}^{n+1} - \partial_t(d_t \mathbf{U}^{n+1})) \cdot \delta_v^n d\mathbf{x} \\
& \quad - \frac{\rho_m r_m}{2} \Delta t \int_{\Gamma} d_t \mathbf{V}^N \cdot \delta_v^N d\mathbf{x} + \frac{\rho_m r_m}{2} \Delta t^2 \sum_{n=1}^{N-1} \int_{\Gamma} d_{tt} \mathbf{V}^{n+1} \cdot \delta_v^n d\mathbf{x} \leq C_\epsilon \|d_t \mathbf{U}^N - \partial_t \mathbf{U}^N\|_{L^2(\Omega^p)}^2 \\
& \quad + C\Delta t \sum_{n=1}^{N-1} \|d_{tt} \mathbf{U}^{n+1} - \partial_t(d_t \mathbf{U}^{n+1})\|_{L^2(\Omega^p)}^2 + C_\epsilon \Delta t^2 \|d_t \mathbf{V}^N\|_{L^2(\Omega^p)}^2 + C\Delta t^3 \sum_{n=1}^{N-1} \|d_{tt} \mathbf{V}^{n+1}\|_{L^2(\Omega^p)}^2 \\
& \quad + C_\epsilon \|d_t \mathbf{U}^N - \partial_t \mathbf{U}^N\|_{L^2(\Gamma)}^2 + C\Delta t \sum_{n=1}^{N-1} \|d_{tt} \mathbf{U}^{n+1} - \partial_t(d_t \mathbf{U}^{n+1})\|_{L^2(\Gamma)}^2 + C_\epsilon \Delta t^2 \|d_t \mathbf{V}^N\|_{L^2(\Gamma)}^2 \\
& \quad + C\Delta t^3 \sum_{n=1}^{N-1} \|d_{tt} \mathbf{V}^{n+1}\|_{L^2(\Gamma)}^2 + \epsilon \|\delta_v^N\|_{L^2(\Omega^p)}^2 + \epsilon \|\delta_v^N\|_{L^2(\Gamma)}^2 + C\Delta t \sum_{n=1}^{N-1} \|\delta_v^n\|_{L^2(\Omega^p)}^2 + C\Delta t \sum_{n=1}^{N-1} \|\delta_v^n\|_{L^2(\Gamma)}^2
\end{aligned}$$

$$\begin{aligned}
\bullet \quad & \Delta t \sum_{n=0}^{N-1} \mathcal{R}_s^{n+1}(d_t \delta_s^{n+1}) = \rho_p \int_{\Omega^p} (d_t \mathbf{V}^N - \partial_t \mathbf{V}^N) \cdot \delta_s^N d\mathbf{x} - \frac{1}{2} \Delta t a_e(d_t \mathbf{U}^N, \delta_s^N) \\
& - \rho_p \Delta t \sum_{n=1}^{N-1} \int_{\Omega^p} (d_{tt} \mathbf{V}^{n+1} - \partial_t(d_t \mathbf{V}^{n+1})) \cdot \delta_s^n d\mathbf{x} + \frac{\Delta t^2}{2} \sum_{n=1}^{N-1} a_e(d_{tt} \mathbf{U}^{n+1}, \delta_s^n) \\
& + \rho_m r_m \int_{\Gamma} (d_t \mathbf{V}^N - \partial_t \mathbf{V}^N) \cdot \delta_s^N d\mathbf{x} - \rho_m r_m \Delta t \sum_{n=1}^{N-1} \int_{\Gamma} (d_{tt} \mathbf{V}^{n+1} - \partial_t(d_t \mathbf{V}^{n+1})) \cdot \delta_s^n d\mathbf{x} \\
& - \frac{\Delta t}{2} a_m(d_t \mathbf{U}|_{\Gamma}^N, \delta_s|_{\Gamma}^N) + \frac{\Delta t^2}{2} \sum_{n=1}^{N-1} a_m(d_{tt} \mathbf{U}|_{\Gamma}^{n+1}, \delta_s|_{\Gamma}^n) \leq C_{\epsilon} \|d_t \mathbf{V}^N - \partial_t \mathbf{V}^N\|_{L^2(\Omega^p)}^2 \\
& + C \Delta t \sum_{n=1}^{N-1} \|d_{tt} \mathbf{V}^{n+1} - \partial_t(d_t \mathbf{V}^{n+1})\|_{L^2(\Omega^p)}^2 + C_{\epsilon} \Delta t^2 \|D(d_t \mathbf{U}^N)\|_{L^2(\Omega^p)}^2 + C_{\epsilon} \Delta t^2 \|\nabla \cdot d_t \mathbf{U}^N\|_{L^2(\Omega^p)}^2 \\
& + C \Delta t^3 \sum_{n=1}^{N-1} \|D(d_{tt} \mathbf{U}^{n+1})\|_{L^2(\Omega^p)}^2 + C \Delta t^3 \sum_{n=1}^{N-1} \|\nabla \cdot d_{tt} \mathbf{U}^{n+1}\|_{L^2(\Omega^p)}^2 + C_{\epsilon} \|d_t \mathbf{V}^N - \partial_t \mathbf{V}^N\|_{L^2(\Gamma)}^2 \\
& + C \Delta t \sum_{n=1}^{N-1} \|d_{tt} \mathbf{V}^{n+1} - \partial_t(d_t \mathbf{V}^{n+1})\|_{L^2(\Gamma)}^2 + C_{\epsilon} \Delta t^2 \mathcal{M}(d_t \mathbf{U}|_{\Gamma}^N) + C \Delta t^3 \sum_{n=1}^{N-1} \mathcal{M}(d_{tt} \mathbf{U}|_{\Gamma}^{n+1}) \\
& + C \Delta t \sum_{n=1}^{N-1} \|\delta_s^n\|_{L^2(\Omega^p)}^2 + \epsilon \|D(\delta_s^N)\|_{L^2(\Omega^p)}^2 + \epsilon \|\nabla \cdot \delta_s^N\|_{L^2(\Omega^p)}^2 + C \Delta t \sum_{n=1}^{N-1} \|D(\delta_s^n)\|_{L^2(\Omega^p)}^2 \\
& + C \Delta t \sum_{n=1}^{N-1} \|\nabla \cdot \delta_s^n\|_{L^2(\Omega^p)}^2 + C \Delta t \sum_{n=1}^{N-1} \|\delta_s^n\|_{L^2(\Gamma)}^2 + \epsilon \mathcal{M}(\delta_s|_{\Gamma}^N) + C \Delta t \sum_{n=1}^{N-1} \mathcal{M}(\delta_s|_{\Gamma}^n).
\end{aligned}$$

The final consistency error estimate follows by applying Lemma 3. \square

Lemma 5. (Interpolation errors) *The following inequalities hold:*

$$\begin{aligned}
\Delta t \sum_{n=0}^{N-1} \|d_t \theta_p^{n+1}\|_{L^2(\Omega^p)}^2 & \leq \Delta t \sum_{n=0}^{N-1} \|\partial_t \theta_p^n\|_{L^2(0,T;L^2(\Omega^p))}^2 \leq h^{2k+2} \|\partial_t p_p\|_{l^2(0,T;H^{k+1}(\Omega^p))}^2, \\
\Delta t \sum_{n=0}^{N-1} \|\nabla d_t \theta_f^{n+1}\|_{L^2(\Omega^f)}^2 & \leq \Delta t \sum_{n=0}^{N-1} \|\partial_t \theta_f^n\|_{L^2(0,T;H^1(\Omega^f))}^2 \leq h^{2k} \|\partial_t \mathbf{v}\|_{l^2(0,T;H^{k+1}(\Omega^f))}^2, \\
\Delta t \sum_{n=0}^{N-1} \|d_{tt} \theta_s^{n+1}\|_{L^2(\Omega^p)}^2 & \leq \Delta t \sum_{n=0}^{N-1} \|\partial_{tt} \theta_s^n\|_{L^2(0,T;L^2(\Omega^p))}^2 \leq h^{2k+2} \|\partial_{tt} \mathbf{U}\|_{l^2(0,T;H^{k+1}(\Omega^p))}^2, \\
\Delta t \sum_{n=0}^{N-1} \left\| \frac{\theta_v^{n+1} - \theta_v^{n-1}}{2\Delta t} \right\|_{L^2(\Gamma)}^2 & \leq \Delta t \sum_{n=0}^{N-1} \|\partial_t \theta_v^n\|_{L^2(0,T;L^2(\Gamma))}^2 \leq h^{2k+2} \|\partial_{tt} \boldsymbol{\xi}\|_{l^2(0,T;H^{k+1}(0,L))}^2, \\
\Delta t \sum_{n=0}^{N-1} \mathcal{M}\left(\frac{\theta_s|_{\Gamma}^{n+1} - \theta_s|_{\Gamma}^{n-1}}{2\Delta t}\right) & \leq \Delta t \sum_{n=0}^{N-1} \|\partial_t \theta_s|_{\Gamma}\|_{L^2(0,T;H^1(0,L))}^2 \leq h^{2k} \|\partial_{tt} \boldsymbol{\eta}\|_{l^2(0,T;H^{k+1}(0,L))}^2,
\end{aligned}$$

$$\begin{aligned} \Delta t \sum_{n=0}^{N-1} \left(\|D(\theta_f^{n+1})\|_{L^2(\Omega^f)}^2 + \|\nabla \theta_p^{n+1}\|_{L^2(\Omega^p)}^2 + \|\nabla \theta_p^n\|_{L^2(\Omega^p)}^2 \right) &\leq \Delta t \sum_{n=0}^N h^{2k} (\|\mathbf{v}^n\|_{H^{k+1}(\Omega^f)}^2 + \|p_p^n\|_{H^{k+1}(\Omega^p)}^2) \\ &\leq h^{2k} (\|\mathbf{v}\|_{l^2(0,T;H^{k+1}(\Omega^f))}^2 + \|p_p\|_{l^2(0,T;H^{k+1}(\Omega^p))}^2). \end{aligned}$$

Proof. Inequalities in Lemma 5 can be easily shown using manipulations similar to the ones in Lemma 4, and approximation properties (A.10)-(A.15). \square

References

- [1] R.L. Armentano, J.G. Barra, J. Levenson, A. Simon, and R.H. Pichel. Arterial wall mechanics in conscious dogs: assessment of viscous, inertial, and elastic moduli to characterize aortic wall behavior. *Circ. Res.*, 76(3):468–478, 1995.
- [2] S. Badia, F. Nobile, and C. Vergara. Fluid-structure partitioned procedures based on Robin transmission conditions. *J. Comput. Phys.*, 227:7027–7051, 2008.
- [3] S. Badia, F. Nobile, and C. Vergara. Robin-Robin preconditioned Krylov methods for fluid-structure interaction problems. *Comput. Methods Appl. Mech. Eng.*, 198(33-36):2768–2784, 2009.
- [4] S. Badia, A. Quaini, and A. Quarteroni. Splitting methods based on algebraic factorization for fluid-structure interaction. *SIAM J. Sci. Comput.*, 30(4):1778–1805, 2008.
- [5] S. Badia, A. Quaini, and A. Quarteroni. Coupling Biot and Navier–Stokes equations for modelling fluid–poroelastic media interaction. *Journal of Computational Physics*, 228(21):7986–8014, 2009.
- [6] A.T. Barker and X.C. Cai. Scalable parallel methods for monolithic coupling in fluid-structure interaction with application to blood flow modeling. *Journal of Computational Physics*, 229(3):642–659, 2010.
- [7] R.D. Bauer, R. Busse, A. Schabert, Y. Summa, and E. Wetterer. Separate determination of the pulsatile elastic and viscous forces developed in the arterial wall *in vivo*. *Pflügers Archiv*, 380(3):221–226, 1979.
- [8] N.D. Botkin, K.-H. Hoffmann, O.A. Pykhiteev, and V.L. Turova. Dispersion relations for acoustic waves in heterogeneous multi-layered structures contacting with fluids. *Journal of the Franklin Institute*, 344(5):520–534, 2007.
- [9] M. Bukač, S. Čanić, R. Glowinski, J. Tambaca, and A. Quaini. Fluid-structure interaction in blood flow capturing non-zero longitudinal structure displacement. *Journal of Computational Physics*, 2012.
- [10] E. Burman and M. A. Fernández. Stabilization of explicit coupling in fluid-structure interaction involving fluid incompressibility. *Comput. Methods Appl. Mech. Eng.*, 198:766–784, 2009.
- [11] S. Canic, B. Muha, and M. Bukac. Stability of the kinematically coupled β -scheme for fluid-structure interaction problems in hemodynamics. *Submitted.*, 2012, arXiv:1205.6887.
- [12] S. Canic, J. Tambaca, G. Guidoboni, A. Mikelic, C.J. Hartley, and D. Rosenstrauch. Modeling viscoelastic behavior of arterial walls and their interaction with pulsatile blood flow. *SIAM Journal on Applied Mathematics*, 67(1):164–193, 2006.

- [13] P. Causin, J.F. Gerbeau, and F. Nobile. Added-mass effect in the design of partitioned algorithms for fluid-structure problems. *Comput. Methods Appl. Mech. Eng.*, 194(42-44):4506–4527, 2005.
- [14] S. Chung and K. Vafai. Effect of the fluid-structure interactions on low-density lipoprotein transport within a multi-layered arterial wall. *Journal of biomechanics*, 45(2):371–381, 2012.
- [15] P. Ciarlet. *The finite element method for elliptic problems*, volume 4. North Holland, 1978.
- [16] M. Cinthio, Å.R. Ahlgren, J. Bergkvist, T. Jansson, H.W. Persson, and K. Lindstrom. Longitudinal movements and resulting shear strain of the arterial wall. *Am. J. Physiol. Heart Circ. Physiol.*, 291(1):H394–H402, 2006.
- [17] M. Cinthio, A.R. Ahlgren, T. Jansson, A. Eriksson, H.W. Persson, and K. Lindstrom. Evaluation of an ultrasonic echo-tracking method for measurements of arterial wall movements in two dimensions. *IEEE Trans. Ultrason. Ferroelectr. Freq. Control*, 52(8):1300–1311, 2005.
- [18] E. Detournay and A.H.D. Cheng. Fundamentals of poroelasticity, Chapter 5 in Comprehensive Rock Engineering: Principles, Practice and Projects, Vol. II, Analysis and Design Method: 113–171, ed. C. Fairhurst, 1993.
- [19] J. Donea. *Arbitrary Lagrangian-Eulerian finite element methods*, in: *Computational methods for transient analysis*. North-Holland, Amsterdam, 1983.
- [20] M. A. Fernández and M. Landajuela. A fully decoupled scheme for the interaction of a thin-walled structure with an incompressible fluid. *Comptes Rendus Mathématique*, 2013.
- [21] M.A. Fernández. Incremental displacement-correction schemes for the explicit coupling of a thin structure with an incompressible fluid. *Comptes Rendus Mathématique*, 349(7):473–477, 2011.
- [22] L. Formaggia, J.F. Gerbeau, F. Nobile, and A. Quarteroni. On the coupling of 3D and 1D Navier–Stokes equations for flow problems in compliant vessels. *Comput. Methods Appl. Mech. Eng.*, 191(6-7):561–582, 2001.
- [23] Y. C. Fung. *Biomechanics: Its Foundation and Objectives*, Y.C.Fung, N.Perrone, M.Anliker (Eds). Prentice-Hall, Englewood Cliff, NJ, 1972.
- [24] V. Girault and P.-A. Raviart. Finite element approximation of the Navier–Stokes equations. *Lecture Notes in Mathematics*, 794, 1979.
- [25] R. Glowinski. *Finite element methods for incompressible viscous flow*, in: P.G.Ciarlet, J.-L.Lions (Eds), *Handbook of numerical analysis*, volume 9. North-Holland, Amsterdam, 2003.
- [26] P. Hansbo. Nitsches method for interface problems in computational mechanics. *GAMM-Mitt.*, 28(2):183–206, 2005.
- [27] G. A. Holzapfel and R. W. Ogden. Constitutive modelling of passive myocardium: a structurally based framework for material characterization. *Philosophical Transactions of the Royal Society A: Mathematical, Physical and Engineering Sciences*, 367(1902):3445–3475, 2009.
- [28] G. A. Holzapfel, G. Sommer, and P. Regitnig. Anisotropic mechanical properties of tissue components in human atherosclerotic plaques. *Transactions of the ASME-K-Journal of Biomechanical Engineering*, 126(5):657–665, 2004.

- [29] T.J.R. Hughes, W.K. Liu, and T.K. Zimmermann. Lagrangian-Eulerian finite element formulation for incompressible viscous flows. *Comput. Methods Appl. Mech. Eng.*, 29(3):329–349, 1981.
- [30] J. D. Humphrey et al. Mechanics of the arterial wall: Review and directions. *Critical reviews in biomedical engineering*, 23(1-2):1, 1995.
- [31] J.-M. Kim, S.-H. Chang, and C.-B. Yun. Fluid-structure-soil interaction analysis of cylindrical liquid storage tanks subjected to horizontal earthquake loading. *Structural Engineering and Mechanics*, 13(6):615–638, 2002.
- [32] William Layton, Hoang Tran, and Xin Xiong. Long time stability of four methods for splitting the evolutionary Stokes–Darcy problem into Stokes and Darcy subproblems. *Journal of Computational and Applied Mathematics*, 236(13):3198–3217, 2012.
- [33] K. Lee, G.M. Saidel, and M.S. Penn. Permeability change of arterial endothelium is an age-dependent function of lesion size in apolipoprotein e-null mice. *American Journal of Physiology-Heart and Circulatory Physiology*, 295(6):H2273–H2279, 2008.
- [34] M. Lesinigo. *Lumped Mathematical Models for Intracranial Dynamics*. PhD thesis, EPFL, Switzerland, 2013.
- [35] X. Ma, G.C. Lee, and S.G. Wu. Numerical simulation for the propagation of nonlinear pulsatile waves in arteries. *Journal of biomechanical engineering*, 114:490, 1992.
- [36] A. Mikelić and M. Wheeler. Convergence of iterative coupling for coupled flow and geomechanics. *Computational Geosciences*, pages 1–7, 2013.
- [37] L.A. Miller and C.S. Peskin. A computational fluid dynamics of ‘clap and fling’ in the smallest insects. *J. Exp. Biol.*, 208(2):195–212, 2005.
- [38] B. Muha and S. Čanić. Existence of a weak solution to a fluid-multi-layered-structure interaction problem. *Submitted, arXiv:1305.5310*, 2013.
- [39] M. A. Murad, J. N. Guerreiro, and A. F.D. Loula. Micromechanical computational modeling of secondary consolidation and hereditary creep in soils. *Computer methods in applied mechanics and engineering*, 190(15):1985–2016, 2001.
- [40] F. Nobile. *Numerical approximation of uidstructure interaction problems with application to haemodynamics*. PhD thesis, EPFL, Switzerland, 2001.
- [41] F. Nobile and C. Vergara. An effective fluid-structure interaction formulation for vascular dynamics by generalized Robin conditions. *SIAM J. Sci. Comput.*, 30:731–763, 2008.
- [42] M. Prosi, P. Zunino, K. Perktold, and A. Quarteroni. Mathematical and numerical models for transfer of low-density lipoproteins through the arterial walls: a new methodology for the model set up with applications to the study of disturbed luminal flow. *Journal of biomechanics*, 38(4):903–917, 2005.
- [43] S.M.K. Rausch, C. Martin, P.B. Bornemann, S. Uhlig, and W.A. Wall. Material model of lung parenchyma based on living precision-cut lung slice testing. *Journal of the Mechanical Behavior of Biomedical Materials*, 4(4):583–592, 2011.

- [44] A. Robertson, M. Hill, and D. Li. Structurally motivated damage models for arterial walls. Theory and application. In *Modeling of Physiological Flows*, pages 143–185. Springer, 2012.
- [45] L. Shan, H. Zheng, and W. Layton. A decoupling method with different subdomain time steps for the nonstationary Stokes–Darcy model. *Numerical Methods for Partial Differential Equations*, 2012.
- [46] R. Showalter. Poroelastic filtration coupled to Stokes flow. *Lecture Notes in Pure and Applied Mathematics*, 242:229–241, 2010.
- [47] D. Tang, C. Yang, T. Geva, G. Gaudette, and P. Del Nido. Multi-physics MRI-based two-layer fluid–structure interaction anisotropic models of human right and left ventricles with different patch materials: Cardiac function assessment and mechanical stress analysis. *Computers & structures*, 89(11):1059–1068, 2011.
- [48] R. Temam. *Navier-Stokes equations: theory and numerical analysis*, volume 343. Oxford University Press, 2001.
- [49] B. Tully and Y. Ventikos. Coupling poroelasticity and CFD for cerebrospinal fluid hydrodynamics. *Biomedical Engineering, IEEE Transactions on*, 56(6):1644–1651, 2009.
- [50] I.E. Vignon-Clementel, C. Alberto Figueroa, K.E. Jansen, and C.A. Taylor. Outflow boundary conditions for three-dimensional finite element modeling of blood flow and pressure in arteries. *Computer Methods in Applied Mechanics and Engineering*, 195(29-32):3776–3796, 2006.
- [51] R. Vito and S. Dixon. Blood vessel constitutive models-1995-2002. *Annual review of biomedical engineering*, 5(1):413–439, 2003.
- [52] J. Zhou and Y.C. Fung. The degree of nonlinearity and anisotropy of blood vessel elasticity. *Proceedings of the National Academy of Sciences*, 94(26):14255–14260, 1997.

